Copyright Warning & Restrictions

The copyright law of the United States (Title 17, United States Code) governs the making of photocopies or other reproductions of copyrighted material.

Under certain conditions specified in the law, libraries and archives are authorized to furnish a photocopy or other reproduction. One of these specified conditions is that the photocopy or reproduction is not to be "used for any purpose other than private study, scholarship, or research." If a, user makes a request for, or later uses, a photocopy or reproduction for purposes in excess of "fair use" that user may be liable for copyright infringement,

This institution reserves the right to refuse to accept a copying order if, in its judgment, fulfillment of the order would involve violation of copyright law.

Please Note: The author retains the copyright while the New Jersey Institute of Technology reserves the right to distribute this thesis or dissertation

Printing note: If you do not wish to print this page, then select "Pages from: first page # to: last page #" on the print dialog screen

ABSTRACT

HIGH ASPECT RATIO ELECTRODES FOR HIGH YIELD ELECTROPORATION OF CELLS

by

Anil B. Shrirao

Electroporation is a widely used process in cell biology studies. It uses an electric field to create pores on the cell membrane in order to either insert exogenous molecules inside the cells or disrupt the cell membrane to kill the cells. Current micro-fluidic electroporation devices use the planar electrodes situated at the bottom of a microchannel. These planar electrodes i) require a high voltage and ii) generate a nonuniform electric field which result in low yield of the electroporation. The standard silicon microfabrication technologies are not suitable to fabricate non-planar electrodes required to increase the yield of electroporation.

In this research, an electroporation device is fabricated with an array of five pairs of three dimensional (3D) electrodes situated along the sidewalls of a microchannel. These 3D electrodes are fabricated by filling the molten indium inside the chosen microchannels. The indium filling method allows the fabrication of microstructures with planar dimensions larger than ~30 μm regardless of their height, integrated into the PDMS device. The selective electroporation of fibroblast cells is successfully demonstrated using a fabricated device by applying a low voltage (1.67 V). The uniform electric field generated in cross sections of microchannel by 3D electrodes will avoid the limitations of planar electrodes by i) preventing cell death due to an excessive electric field and ii) preventing lack of electroporation due to a low electric field. As a result, these 3D electrodes should be capable of increasing the yield of electroporation.

HIGH ASPECT RATIO ELECTRODES FOR HIGH YIELD ELECTROPORATION OF CELLS

by
Anil B. Shrirao

A Dissertation
Submitted to the Faculty of
New Jersey Institute of Technology
in Partial Fulfillment of the Requirements for the Degree of
Doctor of Philosophy in Electrical Engineering

Department of Electrical and Computer Engineering

August 2012

APPROVAL PAGE

HIGH ASPECT RATIO ELECTRODES FOR HIGH YIELD ELECTROPORATION OF CELLS

Anil B. Shrirao

Dr. Raquel Perez-Castillejos, Dissertation Co-Advisor Professor of Electrical and Computer Engineering, NJIT	Date
Dr. Durgamadhab Misra, Dissertation Co-Advisor Assistant Professor of Biomedical Engineering, NJIT	Date
Dr. Haim Grebel, Committee Member Professor of Electrical and Computer Engineering, NJIT	Date
Dr. Marek Sosnowski, Committee Member Professor of Electrical and Computer Engineering, NJIT	Date
Dr. Cheul H. Cho, Committee Member Assistant Professor of Biomedical Engineering, NJIT	Date

BIOGRAPHICAL SKETCH

Author: Anil B. Shrirao

Degree: Doctor of Philosophy

Date: August 2012

Undergraduate and Graduate Education:

- Doctor of Philosophy in Electrical Engineering,
  New Jersey Institute of Technology, Newark, NJ, 2012

- Master of Technology in VLSI Engineering,
  Shri Ramdeobaba Kamla Nehru Engineering College, Nagpur, India, 2006

- Bachelor of Science in Electronics and Telecommunication Engineering,
  Babasaheb Naik College of Engineering, Pusad, India, 1999

Major: Electrical Engineering

Patent

A. B. Shrirao and R. Perez-Castillejos, "System and Method for Novel Microfluidic Device," U.S. Provisional Application 61/414237, Filed 11/16/2010.

Journal

A. B. Shrirao and R. Perez-Castillejos, Chips and Tips: "Simple Fabrication of Microfluidic Devices by Replicating Scotch-Tape Masters," Lab on a chip, May 2010.

Peer-reviewed Conferences and Symposia

A. B. Shrirao and R. Perez-Castillejos, "Bench-top Fabrication of Microfluidic Devices by Soft-Lithographic Replication of Patterned Tape," 2010 Biomedical Engineering Society Annual Meeting, track: Devices: Nano to Micro, Convention center, university of Texas, Austin, Texas, October 6-9, 2010.

A. B. Shrirao and R. Perez-Castillejos, "Bench-top Fabrication Of Microfluidic Devices By Soft-lithographic Replication Of Patterned Tape," 2010 Metro Area MEMS/NEMS Workshop: NanoManufacturing, Babbio Center, Stevens Institute of Technology, Hoboken, New Jersey, July 26, 2010.

I. Burdallo, A. B. Shrirao, A. Baldi, C. Jimenez-Jorquera, R. Perez-Castillejos, "On-Chip Microfluidics For Advanced Functionalization And Operation Of Microelectrode Arrays," 2010 Metro Area MEMS/NEMS Workshop: NanoManufacturing, Babbio Center, Stevens Institute of Technology, Hoboken, New Jersey, July 26, 2010.

A. B. Shrirao, Y.A. Gharaibeh, and R. Perez-Castillejos, "Hybrid Microfluidic Device with Integrated 3D Electrodes for Live-cell Detection," Gotham-Metro Condensed Matter Meeting, New York Academy of Sciences, New York, November 21, 2009 (Poster).

A. B. Shrirao, Y.A. Gharaibeh, and R. Perez-Castillejos, "Hybrid Microfluidic Device with Integrated 3D Electrodes for Live-cell Detection," BioTechnica 2009, Philadelphia, November 14, 2009 (Poster competitively selected for the Innovation Corridor).

A. B. Shrirao, Y.A. Gharaibeh, and R. Perez-Castillejos, "Hybrid Microfluidic Device with Integrated 3D Electrodes for Live-cell Detection," Graduate Student Association (GSA) research presentation, NJIT, November 11, 2009 (Awarded the Second best poster in the Newark school of Engineering).

A. B. Shrirao and R. Perez-Castillejos, "Development of a hybrid microfluidic device for dielectric spectroscopy of live cells," Dana Knox Student Research Showcase, NJIT, April 8, 2009.

A. B. Shrirao and N. Narkhede, "VHDL design for IEEE-754 floating point ALU," International Conference IFFTOMM PCEA, Nagpur, India, Vol. 3, 2006, pp. 315-323.

A. B. Shrirao and K. Bhurchandi, "RGB reconstruction of RAW image from CCD array," National Conference on Resent trends in Signal Processing at St. Padre Eng. College, Goa, India. 2006, pp. 844 – 852.

A. B. Shrirao and A. Kothari, "Remote Hardware Control Using AT Command Interface," National conference Achieving World Class Excellence: Education & Industry, Nagpur, India, 2005, pp. 712-720.

Invited Talks

A. B. Shrirao, A. Hussain, C. H. Cho, and R. Perez-Castillejos, "Rapid prototyping method for cell patterning: Microfluidic Devices Fabricated by Soft-Lithographic Replication of Adhesive Tape for Patterning Biological Cells," Gotham-Metro

Condensed Matter Meeting, New York Academy of Sciences, New York, November 12, 2010. (Oral presentation)

A. B. Shrirao and R. Perez-Castillejos, "Microfluidics Labs Using Devices Fabricated By Soft-Lithographic Replication of Scotch-Tape Molds," American Society for Engineering Education: Spring 2010 Mid-Atlantic Section Conference, Lafayette College, Easton, Pennsylvania, April 16–17, 2010. (Oral presentation)

Manuscripts in preparation

A. B. Shrirao and R. Perez-Castillejos, "Patterning of Cells Using Adhesive-Tape Soft lithography" submitted to BioTechniques.

A. B. Shrirao and R. Perez-Castillejos, "Vacuum based autonomous metal microstructure fabrication by injection of the molten metal in gas permeable microchannel".

This dissertation is dedicated to my beloved family.

AAI & ANNAJI
PRAJAKTA & ARYA
VILAS DADA & VIDYA WAINI
RAJU DADA & ARCHANA WAINI
MAYUR, ASHUTOSH, VEDANT & VEDIKA

My Mentor

Dr. TONY HOWELL & Ms. MARIA OQUENDO

ACKNOWLEDGMENT

This dissertation would not have been possible without the help of several individuals who contributed their valuable assistance in the preparation and completion of this study. I owe my utmost gratitude to the Department of Electrical and Computer Engineering, NJIT for providing the financial support during this study. I am thankful to my advisor, Dr. Raquel Perez-Castillejos, for her guidance, insight, and encouragement throughout this research. I am truly indebted and thankful to my Ph.D. dissertation committee members: Dr. Haim Grebel, Dr. Durgamadhab Misra, Dr. Marek Sosnowski, and Dr. Cheul H. Cho for actively participating in my dissertation committee and providing valuable advice. I would also like to show my gratitude to the staff in the Electrical Engineering Department: Joan Mahon, Jacinta Williams, Arthur Pereira, Hector Rivas, and Gil Hernandez for their help throughout my stay at NJIT. I am thankful to all the staff members of the Educational Opportunity Program for their support and motivation. I would like to thank to my fellow graduate students: Derek Yip, Nikhil Modi, Vijay Kasi, and Samarth Trivedi for all the help they have provided towards the completion of this dissertation. I wish to express my deepest gratitude to my family for always supporting my academic pursuit and understanding me. I also wish to thank my dear wife Prajakta for her love, patience, understanding, and support throughout my study. I am thankful to all my friends (433, 405 and 623) for supporting and encouraging me all this time. I am thankful to the One Above All of Us, the omnipresent God, for answering my prayers, and giving me the strength to complete this study. Finally, I would like to express my gratitude to everybody who was important to the successful realization of this thesis, as well as express my apology that I could not mention their names one by one.

TABLE OF CONTENTS

TABLE OF CONTENTS
(Continued)

Chapter **Page**

TABLE OF CONTENTS
(Continued)

Chapter **Page**

LIST OF TABLES

LIST OF FIGURES

LIST OF FIGURES
(Continued)

LIST OF FIGURES
(Continued)

LIST OF FIGURES
(Continued)

LIST OF FIGURES
(Continued)

CHAPTER 1

INTRODUCTION

In this chapter, an overview of the theory of electroporation and of conventional electroporation devices is provided. First, living cells and the process of their electroporation are described, which is then followed by applications of electroporation. Then, conventional electroporation methods and currently used devices, along with their limitations, are briefly discussed.

Lastly, a discussion on current microfluidic electroporation devices, their fabrication and limitations is provided. This chapter serves as a background for electroporation, which was prepared by accessing study materials that include electroporation literature, published research, current practices, and market research.

1.1 Electroporation

The cell is the smallest living biological structure in which a lipid bi-layer plasma membrane surrounds the cellular organelles suspended in cytoplasm, as shown in Figure 1.1. The lipid bi-layer is composed of lipid molecules (phospholipids) made of a polar hydrophilic head and non-polar hydrophobic tails, as shown in Figure 1.2. The cell membrane prohibits the release of intracellular organelles and keeps the cell alive. The cell membrane also allows the controlled transport of specific materials such as potassium ions, sodium ions, proteins, etc. across it for the normal functioning of a cell.

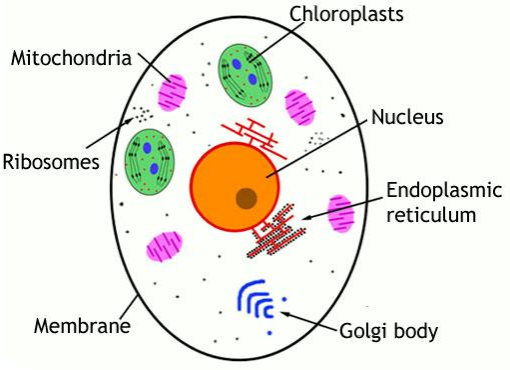

Figure 1.1 Schematic of living cell [1]. The intracellular organelles such as nucleus, Golgi body, etc., are suspended in cytoplasm and surrounded by the cell membrane.

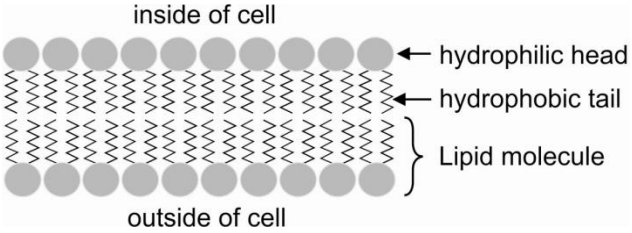

Figure 1.2 The bi-layer of the cell membrane. The bi-layer is composed of lipid molecules. The lipid molecule has a polar hydrophilic head that attracts the water molecules and non-polar hydrophobic tails that repel the water molecules. The self-assembling of the lipid molecules forms the bilayer.

In a living cell, the intracellular concentration of sodium, potassium and calcium ions differs from their extracellular concentration. These ions diffuse from a region of higher concentration to lower concentration through the ion channels present in the cell membrane. The migration of charged ions across the cell membrane makes the intracellular region negative and the extracellular region positive relative to each other. Consequently, the difference between the intracellular and the extracellular ion concentration is responsible for setting up a potential difference across the cell membrane. This potential difference across the cell membrane is called the transmembrane potential.

The transmembrane potential sets up an electric field across the cell membrane that counteracts the diffusion force and eventually stops the diffusion-driven migration of ions across the cell membrane. The system achieves the electrochemical equilibrium when the diffusion of ions across the cell membrane stops due to the opposing electric field. The potential difference across the cell membrane necessary to achieve the electrochemical equilibrium is called the resting membrane potential. Typically, the resting membrane potential varies from -26 mV to -90 mV [2] depending on the type of a cell.

The transmembrane potential controls [3] the transport of sodium, potassium and other ions across the cell membrane through the ion channels embedded in the cell membrane. The external electric field can be used to modulate the transmembrane potential and control the transport of ions across the cell membrane electrically. Schwan's equation [4] describes the relation between the steady state transmembrane potential (V_{tm}) and applied DC electric field (E) derived from the electromagnetic theory and is given in Equation 1.1.

In Equation 1.1, E is the strength of the applied DC electric field in volts per centimeter, θ is the angle between the electric field and the vector perpendicular to a point of interest on the cell membrane, and R is the radius of the spherical cell suspended in a physiological medium. Equation 1.1 is valid under the following conditions: 1) The shape of the cell is spherical 2) The resistivity of the cell membrane is higher than the media inside and outside of the cell and 3) The cell membrane is thin compared to the radius of the cell.

$$V_{tm} = 1.5RE\cos(\theta) \tag{1.1}$$

In cellular biology the need often arises to insert exogenous material/molecules such as DNA or RNA that do not naturally penetrate the cell membrane. Numerous studies in cell biology require the extraction of intracellular organelles [5] such as nucleus, mitochondria, etc., which can be obtained by rupturing the cell membrane. The cell membrane can be made permeable to exogenous materials/molecules that do not naturally penetrate the cell membrane such as DNA or RNA by creating the pores of nano to micro dimension on the cell membrane. These pores of nano to micro dimension on the cell membrane can be created by chemical [6, 7], mechanical [8], optical [9] or electrical stimulation.

Electroporation [10-14] is a process of inducing pores on the cell membrane by applying an external electric field as shown in Figure 1.3 and Figure 1.4. When a lipid bi-layer is subjected to an external electric field, the transmembrane potential across the cell membrane and the columbic force exerted on each lipid molecule increases [15]. The applied external electric field causes an ionic interfacial polarization of the membrane [16] that results in reorientation [17] of the lipid molecules of the cell membrane. This initiates the formation of pores of nano to micro dimensions randomly distributed in the cell membrane, as shown in Figure 1.5.

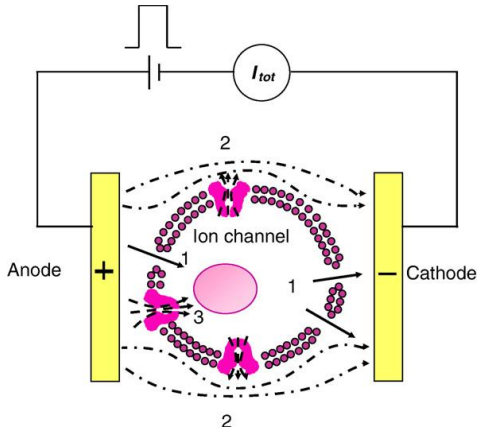

Figure 1.3 Schematic of electroporation [18]. The cell is subjected to the electric field generated between two electrodes. The electric field induces the formation of pores on the cell membrane and opens the ion channels, increasing the permeability of the membrane.

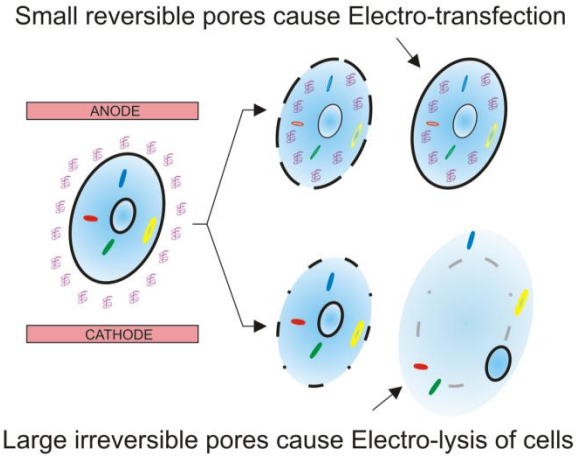

Figure 1.4 Schematic of reversible and irreversible electroporation of a cell. The exogenous materials such as plasmids and drug molecules enter in the cytoplasm of a cell through the small reversible pores induced on the cell membrane by electric pulses. The pores reseal a few seconds after the removal of the electric pulse, and inserted molecules remain trapped inside the cell. Formation of the large irreversible pores on the cell membrane kills (electro-lysis) the cells.

In the initial phase of pore formation, the hydrophobic tail of a lipid molecule is exposed to the liquid inside the pore passage and therefore the pore is initially hydrophobic. The exposed hydrophobic tail of lipid molecules avoids contact with water and induces reorganization of lipid molecules to minimize the exposure of the tail of the

lipid molecules to the water. Consequently, all the lipid molecules along the edge of the initially hydrophobic pore rearrange themselves to minimize the hydrophobic [16] contact. As a result, due to the reorientation of the lipid molecules, the hydrophilic heads of the lipid molecules are exposed in the pore passage, converting the pore hydrophilic, as shown in Figure 1.5.

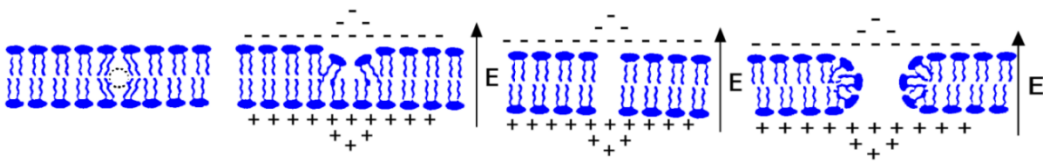

Figure 1.5 The formation of a pore in the cell membrane. The electric field induces pore formation by ionic interfacial polarization of the membrane. The hydrophobic tails reorient lipid molecules to avoid the water, exposing the hydrophilic head in pore passage that makes the pore hydrophilic.

The overall performance of electroporation is quantified using the following parameters:

- Electroporation efficiency: Defined as the percentage of cells electroporated successfully. It is measured by counting those cells in which the molecule to be inserted has been detected after electroporation. The detection of molecules inserted in cells is performed using fluorescent staining and microscopy.

- Cell viability: Defined as the percentage of electroporated cells that remain viable after electroporation. The viability of electroporated cells is measured using live-dead cell staining followed by fluorescent microscopy.

- Electroporation yield [19]: Defined as the product of electroporation efficiency and percentage of viable cells. The electrodes used in electroporation devices generate electric fields with uniform or nonuniform spatial distribution. The magnitude, duration, and the spatial distribution of the applied electric field used for electroporation are instrumental to optimize the yield of electroporation.

The external electric field can increase the transmembrane potential up to several hundreds of mV [20, 21] during electroporation depending on the type of cells. The dynamics of the formation of pores can be controlled by the applied electric field. The pores formed on the cell membrane can either be reversible or irreversible, depending on the strength and the duration of the applied electric field [12, 22, 23]. The magnitude and the duration of the applied electric field also control the pore resealing dynamics [22-24]. Understanding the pore formation and resealing dynamics [23] is important to improve the yield of electroporation.

1.2 Applications of Electroporation

Electroporation is a commonly and widely used method in cell biology studies. Cell transfection is a process of deliberately introducing nucleic acids such as small interfering RNA, DNA or other molecules in a cell through an impermeable lipid membrane. The ability of a transfection agent to stimulate an immune response is called immunogenicity. The ability of a transfection agent to establish an infection in a cell after transfection is called infectivity. The cell transfection process with low immunogenicity and infectivity is desired. Unlike viral cell transfection, electroporation is a non-viral mechanism of cell transfection with no infectivity and absence of immunogenicity [1, 25]. Cell transfection is performed to understand gene function in mammalian cells [26].

Gene therapy is an evolving technique used to treat diseases such as cancer, HIV, etc. Gene therapy [27-29] involves replacing, manipulating, or supplementing nonfunctional genes with new healthy genes. Gene therapy uses the electroporation

method for insertion of new genes [30] into the DNA of a cell in an attempt to correct a genetic defect or a mutation.

Genetic engineering is playing an important role in providing solutions to many life science problems. Genetic engineering [28, 31] studies the modification of the native genome of a cell, which is performed by means of transfection. The electroporation is also used in plant [32, 33] engineering to perform genetic modifications in plant cells for improving their productivity and immunity.

In conventional drug discovery and testing processes, healthy as well as diseased cells are transfected with drug molecules to determine the efficacy of the drug as medicine [34]. Electroporation is used in transdermal drug delivery [35] to increase the transport of drug molecules through the skin. In electro-chemotherapy [36, 37], electroporation is used for the insertion of a controlled dose of drug molecules into a specific cell. Therefore, in the treatment of potentially fatal diseases such as cancer, electro-chemotherapy [38] is used to exterminate the cancer cells by selectively inserting drug molecules into them.

Electroporation is widely used in the food industry in a process called pasteurization [39] that is used to deactivate harmful bacteria without damaging other components of the food. It is also used in the artificial production of proteins [40] for research as well as commercial use.

1.3 Conventional Electroporation Methods

1.3.1 Bulk Electroporation

Conventionally, electroporation is performed in a rectangular cuvette, such as the electroporation cuvettes shown in Figure 1.6. The electroporation cuvette has two parallel sidewalls made of aluminium metal plates as shown in the schematic in Figure 1.7. The metal plates on the two parallel sidewalls are separated by a fixed distance equal to the width of the cuvette varying from 0.1 to 1 cm from cuvette to cuvette. These plates act as electrodes where AC/DC potential is applied to produce an electric field for electroporation.

Figure 1.6 Electroporation cuvette from MIDSCI™ [41]. The commercial electroporation cuvettes are available in different sizes and gaps between the electrodes.

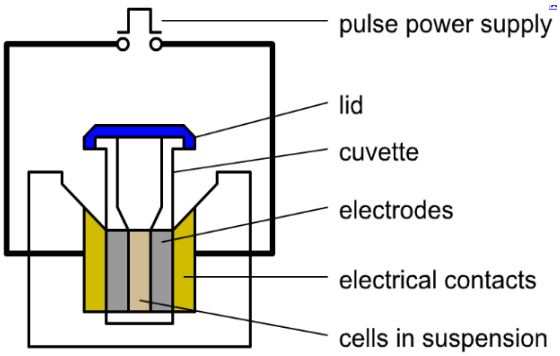

Figure 1.7 Schematic of electroporation cuvette [22]. The suspension containing cells to be electroporated is filled inside the cuvette. The pulses are supplied to the electrodes of the cuvette from the power supply when electrodes make contact with electrical contacts.

In the process of electroporation, harvested cells are first suspended in a solution that contains the molecules to be inserted inside the cells. Then the cell suspension is transferred to the electroporation cuvette and electrodes are connected to a power supply that applies electroporation pulses as shown in Figure 1.8. The electroporation power supply is designed to produce the electric field necessary for electroporation of a cell by selecting desirable pulse shape, magnitude, width and pulse repetition frequency. This method of electroporation shown in Figure 1.8 is called bulk electroporation [42].

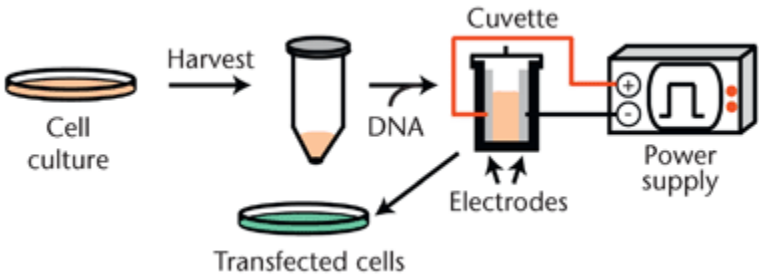

Figure 1.8 Schematic of cuvette based bulk electroporation process [43]. The cells are harvested, suspended in solution containing molecules to be inserted, and filled in the electroporation cuvette. The power supply applies electric pulses to the cuvette to perform electroporation.

According to Schwann's equation given in Equation 1.1, an increase in transmembrane potential, which is responsible for electroporation of cells, depends on the applied electric field and the size of the cell. The intensity of the electric field needed to increase the transmembrane potential above the threshold for electroporation of cells varies from 10^3-10^4 V/cm [44]. The magnitude and duration of applied potential using a power supply are adjusted to optimize the yield of electroporation.

1.3.2 Disadvantages of Bulk Electroporation

Although the cuvette-based electroporation is easy to perform and widely used, it has low electroporation efficiency and cell viability [45]. The electric field of a magnitude of 1 to 10 kV/cm [12, 45] is commonly used for the electroporation of cells. In electroporation cuvettes, the electric field (E) generated by voltage (V) applied between two electrodes separated by a distance (d) is given by Equation 1.2.

$$E = \frac{V}{d} \tag{1.2}$$

In conventional electroporation cuvette, electrodes are separated by a distance of 0.1 to 1 cm. According to Equation 1.2, the voltage required to generate an electric field with a magnitude of 10 kV/cm between the two electrodes of a cuvette separated by 0.1 to 1cm is 1 to 10 kV. This shows that cuvette-based bulk electroporation requires very high voltage in the range of 10^4-10^5 V to produce the electric field in the range 10^3-10^4 V/cm necessary for electroporation [12, 46, 47]. The need for very high voltage arises due to the large separation between the two electrodes of the electroporation cuvettes

used for bulk electroporation. The high voltage supply in bulk electroporation hampers the portability of the technique and increases the cost of the electroporation equipment. Special safety precautions are also required while handling high voltage electroporation device.

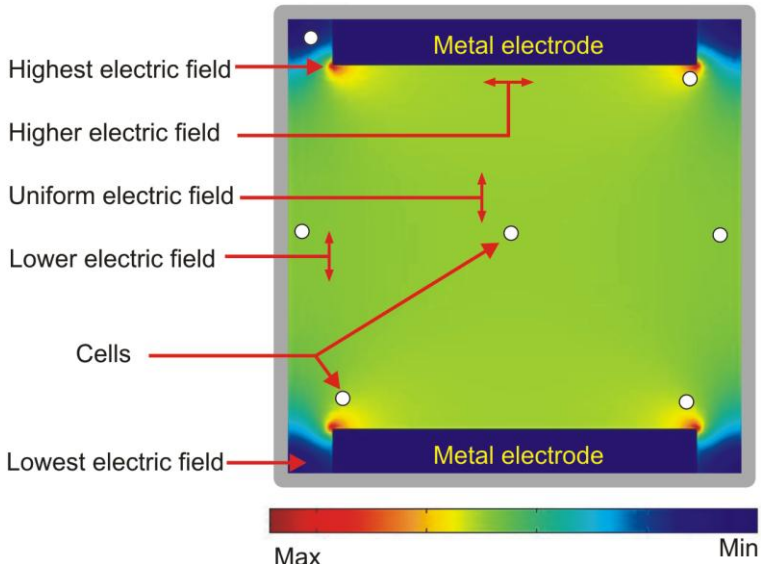

Figure 1.9 The electric field generated in a cross section of an electroporation cuvette. The cells indicated by white circles are very small compared to the aluminum electrodes and the area of the cuvette. The intensity of the electric field in various regions of the cuvette indicated by double head arrows is nonuniform. The cells close to the walls of the cuvette remain un-electroporated due to insufficient electric field intensity while the cells near the corners of the electrode are damaged due to very high electric field. The nonuniform electric field generated in the cuvette decreases electroporation yield.

In the case of cuvette-based electroporation, two parallel electrodes generate an electric field that is not uniform throughout the electroporation cuvette, as shown in Figure 1.9. The electric field at the edges of the electrodes is very high compared to other places. The dimension of the electrodes and the gap between them is very large compared to the size of a cell. Therefore, each cell is subjected to different electric fields depending on their position between the two parallel plate electrodes. The nonuniform electric field

results in unequal electroporation [12] in which some cells are damaged due to a strong electric field, while others are not electroporated.

When an electric current is passed through an electrolyte solution, the electrodes and electrolytes undergo oxidation and reduction, and decompose into positive and negative ions that migrate to opposite electrodes. This process is called electrolysis. In cuvette-based electroporation, high voltage results in electrolysis of the cell suspension. The generation of bubbles due to the electrolysis of the aqueous cell suspension [48] disrupts and damages the electroporated cell. The electrolysis also alters the pH of the cell suspension [49] causing adverse effects on the health of the electroporated cells. Therefore, the overall yield of bulk electroporation is low [50], in the range of 20-50%.

After electroporation, cells become fragile and are susceptible to damage while they are transferred from cuvette to culture plate for further processing. The cuvette-based electroporation also requires a large volume of cell suspension and molecules/DNA/plasmid/SiRNA resulting in an increase in the cost of operation.

1.3.3 Types of Microfluidic Devices for Electroporation

Microfluidic devices used for electroporation consist of microchannel and microelectrodes integrated on the same device. The microchannels in a microfluidic device are typically rectangular channels of several tens of micrometers in width and height. The microchannels are used to deliver cells to a specific point in the device for electroporation. The microelectrodes are situated at the bottom of the microchannel and generate an electric field for the electroporation of cells. The microchannels and microelectrodes are fabricated by using a semiconductor microfabrication process.

The microscale electroporation [50, 51] performed using microfluidic devices with integrated electrodes can be categorized based on the state of cells during electroporation. The electroporation of cells as they flow along a microchannel has been defined as “Flow-through cell electroporation” [51]. In flow-through cell electroporation, cells go through a region of high electric fields while they flow from one end of the microchannel to the other.

The flow-through cell electroporation device [52] shown in Figure 1.10 generates the electric field necessary for electroporation by applying very high voltage between the two ends of the microchannel. Although the width of the channel has been changed from W_1 to W_2 in section L_2 of this device to increase the electric field, it requires very high voltage for electroporation due to the large separation between the two electrodes shown in Figure 1.10. In another flow-through cell electroporation device [51] shown in Figure 1.11, the high electric field required for electroporation is generated by a pair of platinum microelectrodes integrated into the microchannel. The height of these microelectrodes is ~1 μm and they are called planar microelectrodes. These conventional flow-through cell electroporation devices use planar electrodes and also require high voltage for electroporation.

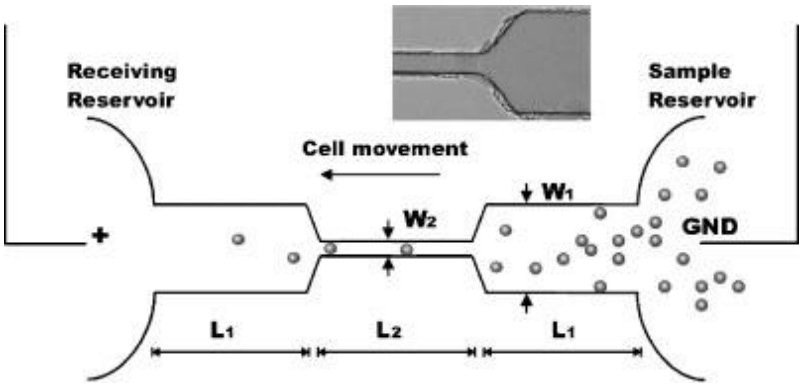

Figure 1.10 Schematic of Flow-through cell electroporation device [52]. The electrodes are at opposite ends of the channel separated by a large distance ($2L_1+L_2$) and require high voltage (500 V) for electroporation. The cells are electroporated when they flow through the channel of width W_2. The width of the channel is decreased from W1 to W2 to increase the electric field for electroporation.

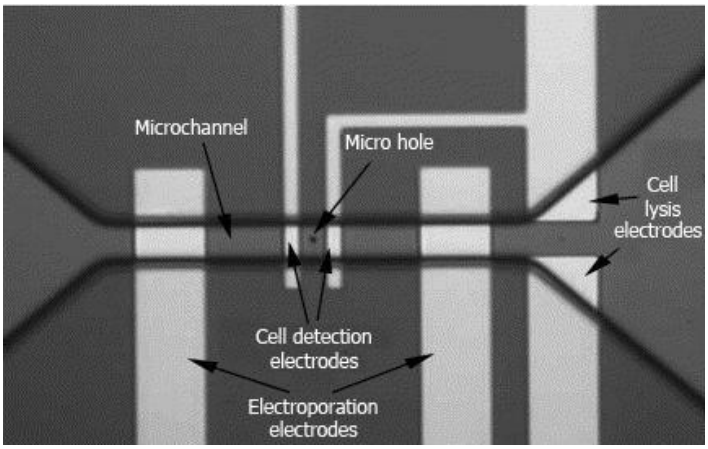

Figure 1.11 Optical image of the Flow-through cell electroporation device [51]. The planar microelectrodes present at the bottom of the microchannel perform the cell detection and the electroporation.

The electroporation of cells adhered to the base of the microchannel has been defined as "Adherent Cell Electroporation" [13, 53]. In the case of Adherent Cell Electroporation, cells are first cultured on a transparent conductive electrode substrate such as indium tin oxide. The cells are allowed to grow and adhere to the electrode substrate. The cells are electroporated while they are attached to the bottom electrode.

The high voltage is applied between the bottom and top electrode, which is either a plate electrode or an array of planar electrodes for electroporation. In this electroporation method, very high voltage is required for electroporation due to the large separation between the two electrodes of the device. Figure 1.12 shows the schematic of a device [13] used for adherent-cell electroporation. The device is used to insert plasmids into human embryonic kidney cells.

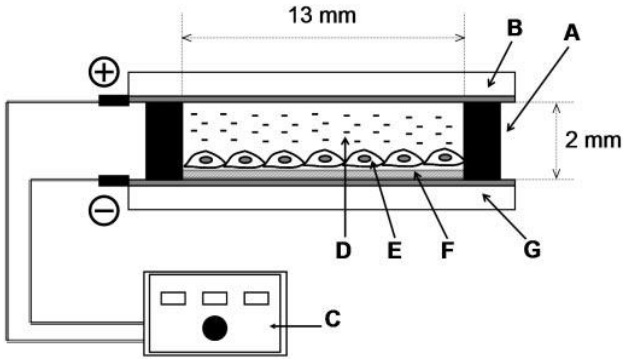

Figure 1.12 Schematic illustration of adherent cell electroporation device [13]. Silicone frame (A), top electrode (B), electric pulse generator (C), PBS (D), cell (E), plasmid (F) bottom electrode (G). The cells are allowed to grow and attach to the bottom electrode. The electroporation is performed while the cells are attached to the bottom electrodes by applying electric pulses to the top and bottom electrodes using an electric pulse generator.

The flow-through cell or adherent cell electroporation can be performed either one cell at a time, called single cell electroporation, or multiple cells at the same time, called bulk electroporation. The single cell electroporation can also be performed by trapping the cell during electroporation and then releasing it. The device used to perform the flow-through cell electroporation by cell-trapping [24] is shown in Figure 1.13. The microfabricated device consisting of an array of the patch clamp electrodes that perform the electroporation by cell-trapping is shown in Figure 1.13a. The cell-trapping

mechanism used in the device to trap a single cell during electroporation is shown in Figure 1.13b.

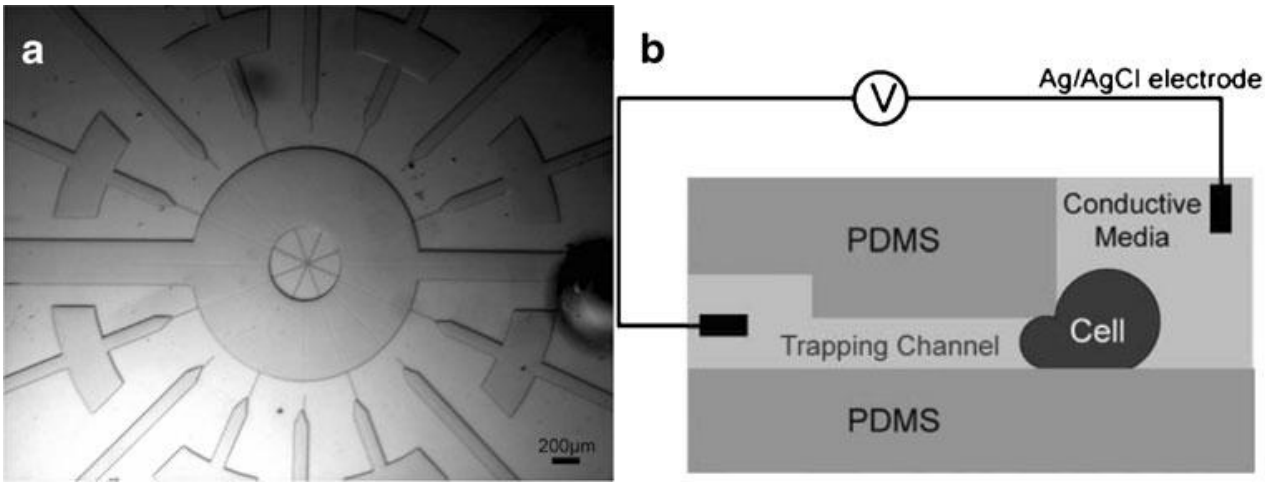

Figure 1.13 Multiple cell electroporation by cell-trapping [24] using a microfluidic device. a. Microfabricated multiplexed patch clamp array device for high-throughput Flow-through cell electroporation. b. Schematic of the cross-section of the chip illustrating the mechanism of cell-trapping during electroporation. The device performs the electroporation of multiple cells by trapping them while they are flowing through the device. A pressure gradient is applied between the two ends of the trapping channel in order to trap the cell. After electroporation, cells are released and new cells are trapped reusing the trapping channel for high-throughput electroporation.

1.3.4 Advantages of Microfluidic Devices for Electroporation

The fabrication of microfluidic devices with integrated electrodes became feasible due to semiconductor microfabrication technologies [11, 12, 23, 50]. Integrated microfluidic devices are used for electroporation due to the following merits: Microfluidic devices that perform the electroporation of one cell at a time are called microscale electroporation [50, 51]. The microscale electroporation provides better control of the electroporation of each cell than bulk electroporation.

Microfabrication technologies allow fabricating an array of electrodes with dimensions comparable to the size of a single cell (10-30 μm). An array of individually addressable microelectrodes can be used to generate a customized electric field depending upon the size of individual cells being electroporated by the electrodes. Electroporation using microfluidic devices is suitable for enhancing the yield of electroporation due to their ability to provide control of the electric field and the size of the electrodes for the size of the cell being electroporated.

Unlike electrodes in bulk electroporation devices, the separation between the microelectrodes is a few tens of micrometers (three orders of magnitude smaller than bulk electroporation). Therefore, the microfluidic device requires a voltage three orders of magnitude smaller than bulk electroporation. The small voltage supply not only allows the portability of the device but also avoids the requirement for special safety precautions required during the operation. The decrease in voltage reduces the power consumption and heat generation as compared to bulk electroporation devices.

Microfluidic electroporation requires only a small volume (pico-liter to microliter) of difficult-to-produce reagents and biomolecules such as specific plasmids or DNA. The time to process the small volume of reagents [54] and its cost are significantly lower in microfluidic electroporation than the bulk electroporation. In microfluidic devices, the width and height of the microchannel is a few tens of micrometers, whereas the volume of the reagents used varies from pico-liter to several microlitres. Therefore, the surface area-to-volume ratio in the case of microfluidic devices is very large [55] as compared to the bulk electroporation system.

The large surface area-to-volume ratio in microfluidic devices removes excess heat rapidly and provides faster heat dissipation [56, 57]. The fast dissipation of generated heat makes it possible to distinguish the heating effects and the electric field effects during electroporation [12]. Microfluidic devices are able to perform flow-through, single-cell and adherent-cell electroporation required in cell biology research. Microfluidic systems are very effective in handling the cell and support cell manipulation such as cell detection, separation, trapping, and sorting.

Microfluidic devices allow in-situ observation [12] of molecular uptake during the electroporation process. In addition to electroporation, the microfluidic systems are capable of integrating the module for post-electroporation [58, 59] processing that includes viable cell separation and detection or quantification of molecules inserted into a cell by electroporation called internalization measurement.

CHAPTER 2

CURRENT STATE OF THE ART IN ELECTROPORATION DEVICES

This chapter provides the rationale behind investigating the conventional electroporation devices and their fabrication methods in order to design high-yield electroporation devices. In this chapter, electrodes used in current electroporation devices are highlighted along with their fabrication methods. First, the problems associated with currently used planar electrodes are discussed with the help of simulations of these electrodes using the Finite Element Modeling (F.E.M) tool COMSOL 3.5a. Then the standard microfabrication technologies used in the fabrication of conventional electroporation devices are discussed, and then an explanation of how these technologies are incapable of fabricating electroporation devices with non-planar electrodes is provided. Lastly, a summary of conventional electroporation devices is provided to justify the need for further research on electroporation devices in order to fabricate them with greater ease and to increase their performance.

2.1 Current Electroporation Devices Typically Use Planar Electrodes

Most of the microfluidic electroporation devices use either an array or a pair of planar microelectrodes integrated into the microfluidic devices [10, 46, 53, 59-61]. The planar microelectrodes became the common trend due to ease-of-fabrication and the challenges in fabrication of high aspect ratio non-planar microelectrodes. These planar microelectrodes are located at the bottom of a microchannel in a microfluidic device such as that shown in Figure 1.11. The thickness of the planar electrode is up to ~1 μm and the

schematic of the cross section of a device with planar electrodes is shown in Figure 2.1a. An example of the position and dimensions of planar microelectrodes with respect to a suspended cell being electroporated is shown in Figure 2.1a. Although the fabrication of planar electrodes is easy, it is not an ideal choice for electroporation.

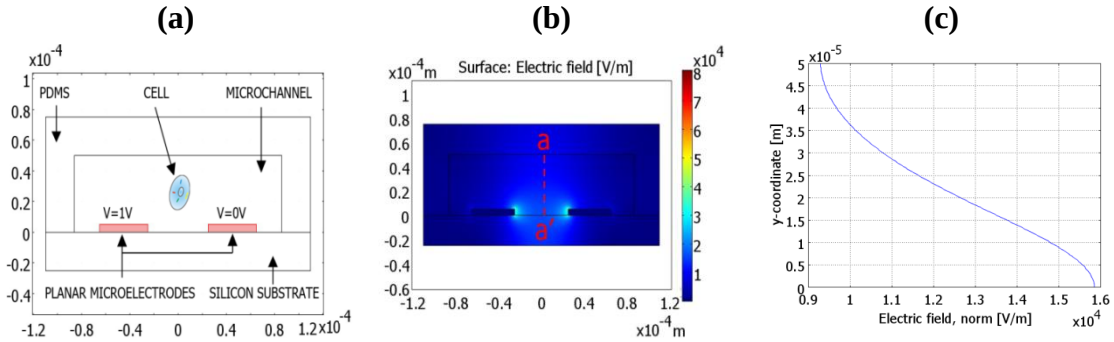

Figure 2.1 The electric field generated by the planar electrodes. a) Schematic of cross section of a microchannel device with planar electrodes. b) The electric field generated by planar electrodes in a microchannel, which shows that the intensity of the electric field is high near electrodes and low at the corners of the microchannel. c) The graph of the magnitude of the electric field along the a-a'axis of the microchannel, which shows that the electric field resulting from the planar electrodes is nonuniform and decays exponentially away from the electrodes, from the bottom to the top of the microchannel.

In order to understand the problems associated with planar electrodes for electroporation, a model of the electroporation device with planar electrodes is simulated using the Finite Element Modeling (F.E.M.) tool COMSOL 3.5a. The schematic of the PDMS/Glass device used in this simulation is shown in Figure 2.1a. The PDMS/Glass device has a pair of 5 µm x 40 µm planar metal electrodes located at the bottom of a 160 µm x 50 µm PDMS/Glass microchannel. The planar electrodes were excited by applying a DC voltage of 1 V between two electrodes. The electric field generated by planar electrodes in the microchannel of a device as observed in the simulation is shown in Figure 2.1b and Figure 2.1c.

It can be seen from Figure 2.1b that the intensity of the electric field is high at the edges of the planar electrodes facing each other and decreases as the distance from the electrodes increases. The magnitude of the electric field along the vertical axis of the microchannel indicated by dotted red line a-a' in Figure 2.1b is plotted in Figure 2.1c. The plot in Figure 2.1c shows that the magnitude of the electric field resulting from the planar microelectrodes is a maximum near the bottom of the microchannel and decays exponentially away from the surface of the electrodes towards the top of the microchannel. Figure 2.1c clearly shows that the electric field produced by planar electrodes is nonuniform throughout the cross section of the microchannel, which is also consistent with the visual representation of the electric field in Figure 2.1b. Therefore, this modeling reveals that the planar electrodes generate a nonuniform electric field in a cross section of the microchannel.

In electroporation devices with planar electrodes, the cells flow through the region over the electrodes where the electric field is lower than the region between the two electrodes with maximum electric field intensity. As a result, the electroporation of the cells away from the electrodes requires higher voltage than the cells between the two electrodes of the electroporation device with planar electrodes. When the cell flows through the region of nonuniform electric field, it is subjected to a dielectrophoretic motion [62] induced by a nonuniform electric field. The dielectrophoretic motion depends on size, shape and weight of an individual cell. The cells are different in shape, size and weight and hence, accordingly, they levitate at different heights above the electrodes. The cells near the bottom and close to the region between the two electrodes are subjected to a stronger electric field than other cells.

The cells in a region where the electric field is optimum for their electroporation are electroporated successfully. On the other hand, the cells close to the electrodes are disrupted due to an excessive electric field and cells far from electrodes remain un-electroporated due to an insufficient electric field. The position of cells in a microchannel is uncertain and therefore, generating an optimal electric field for electroporation at every place in a microchannel using planar electrodes is impossible. This makes the determination of voltage required to successfully electroporate all the cells very difficult. As a result, electroporation devices with planar electrodes suffer from the consequences of a very high electric field such as cell death and of a low electric field such as no electroporation. Therefore, the efficiency of the electroporation process and cell viability using planar electrodes is low, resulting in low electroporation yield.

In order to improve the yield of electroporation, it is necessary to replace the planar electrodes with electrodes capable of providing a uniform electric field throughout the cross section of the microchannel for electroporation. Therefore, this research investigates the non-planar electrodes that can generate a uniform electric field inside the cross section of electroporation device in order to perform the electroporation.

2.2 Standard Microfabrication Processes to Fabricate Electroporation Electrodes

Silicon microfabrication technologies are widely used to fabricate conventional microfluidic electroporation devices with integrated microelectrodes. The silicon microfabrication processes include photoresists spin coating, photolithography, sputtering, chemical vapor deposition, etching, polishing etc. These techniques are well

studied and have been popular for fabricating the microstructure for more than the last three decades. The fabrication cost of devices using the standard microfabrication process is high due to the use of expensive chemical reagents, tools and metals. Consequently, the existing microfabrication processes are suitable only for mass production.

A microfluidic electroporation device has two components 1) Microelectrodes to generate the electric field for the electroporation of cells and 2) Microchannels to deliver the cells to be electroporated between the electroporation electrodes. To fabricate electroporation devices, first the metal layer of gold/platinum is deposited on an insulating substrate such as glass or silicon. Second, the metal layer is then patterned according to the layout on a mask by using photolithography. This patterned metal layer acts as the electrode layer of the device. Third, fluidic microchannels are patterned in an elastomeric substrate such as PDMS using soft-lithography. Finally, both the electrode layer and the microchannel substrate are aligned and bonded together by using a suitable bonding method such as adhesive or anodic bonding.

The multi-step microfabrication protocol described above is extremely challenging. The process allows the fabrication of electrodes situated at the bottom of the microchannel. These electrodes obstruct light and do not support the monitoring and the recording of the electroporation process using a phase contrast microscope. The misalignment between two layers leads to leakage in the microchannel, ruining the device. The bonding between two non-planar layers is weak due to raised metal patterns. The variation in fluid pressure in microchannels during the operation of the device due to flow switching disrupts the weak bonding between the two layers of the device, causing leakage in the device. In addition to microfabrication technologies, the precision

alignment and bonding technique play an important role in the fabrication of the final device without any leakage. Therefore, the multi-step fabrication process is not only complex, but also has a high device failure rate.

Standard silicon technologies are suitable for fabricating the metal microstructures with a thickness up to ~10 μm. The fabrication of metal microstructures of thickness higher than 10 μm is challenging. The fabrication of non-planar electrodes [18, 63, 64] integrated in microfluidic devices demonstrated by other researchers uses complex, time-consuming and expensive methods. LIGA (LIthografie Galvanoformung Abformung) is a microfabrication process that allows the fabrication of a high aspect ratio metal structure using lithography, electroplating, and molding. The flowchart of the LIGA microfabrication process is shown in Figure 2.2, which highlights the complicated procedure involved in the fabrication of high aspect ratio microstructures using the LIGA process.

The LIGA process requires very expensive and rare X-ray synchrotron radiation photolithography tools to pattern the photoresist due to high aspect ratio requirements. The high aspect ratio microstructures are very susceptible to damage during the development process and hence require a controlled development process and equipment. Electroforming is a very slow process that deposits metal by electroplating in a region not covered with photoresist, and takes a very long time to deposit a thick metal layer. Therefore, LIGA is not only complex and time-consuming, but also limited due to the requirement of expensive equipment and rare X-ray synchrotron radiation photolithography tools. Consequently, the fabrication of high aspect ratio microstructures is a bottleneck to the existing standard microfabrication technologies.

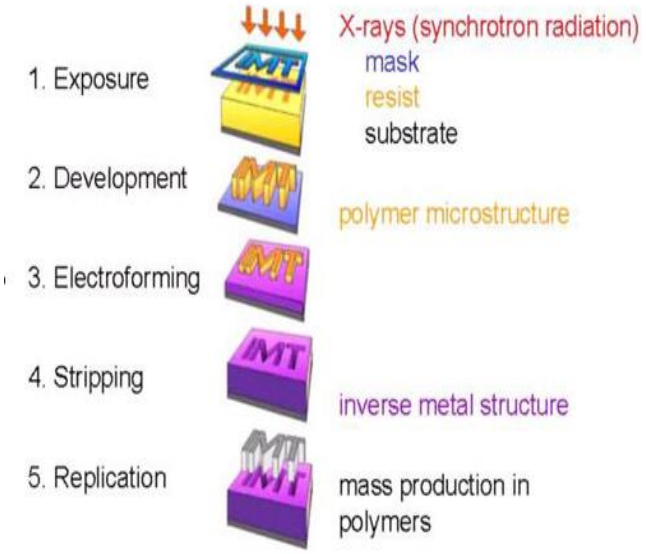

Figure 2.2 Fabrication flow chart of the LIGA process. LIGA is a complex process and the only process to fabricate high aspect ratio microstructures using very expensive X-ray photolithography tools.

Standard microfabrication processes use harmful chemicals, which not only require safe handling but also limit the usability of the device due to its biocompatibility issues. These microfabrication processes use silicon wafers as a substrate since they have very good surface properties and the ability to withstand process parameters such as high temperature. However, the electroporation device should be transparent to the light in order to monitor and record the process of electroporation under a phase contrast microscope as required. Silicon, being an optically non-transparent substrate, is not suitable for such transparent micro devices and does not allow the inspection of ongoing process in electroporation devices using a phase contrast microscope.

This has created the need to use transparent and biocompatible materials such as polymer Poly (dimethylsiloxane) to construct transparent electroporation devices. However, transparent materials such as polymers are not compatible with conventional microfabrication technologies. Polymers are either not able to withstand processing

parameters such as high temperatures, or their surface properties are not suitable for photoresist or metal adhesion. Therefore, the microfabrication processes compatible with polymeric materials such as PDMS have been investigated for the last decade.

Cell biology, medicine and biochemistry require hybrid microdevices with different components (optical, electrical, mechanical, chemical, etc.) integrated on the same device. Such hybrid microdevices require that the final assembly of their components be built from the different platforms. The standard silicon microfabrication techniques do not readily permit cross-platform integration to fabricate hybrid microdevices that would be useful in life science studies. In addition, the silicon microfabrication techniques require specialized operating skills not often required by the users from a molecular biology, biochemistry or medicine background. The user of electroporation devices cannot customize or modify devices as per the need of an application due to a lack of knowledge of the microfabrication processes. Therefore, rapid prototyping is not feasible, which is an important requirement in the experiments of scientific research.

The need for low cost, biocompatible, transparent, disposable and safe electroporation devices for research is the collective conclusion of the reviews published on electroporation [12, 23]. Research in other fabrication techniques is necessary and it is the topic of current scientific studies. Consequently, microfabrication technologies other than silicon technologies are being investigated to cover the broader range of applications and new materials. These techniques include microcontact printing [65], micro transfer molding [20], soft-lithography [66], CD injection molding [67], and microsolidics using soft-lithography [68]. The aim of this research is to design a user-friendly

microfabrication protocol that supports the fabrication of hybrid PDMS microfluidic devices with integrated non-planar electrodes for high yield electroporation.

2.3 Conclusions of the Chapter

Conventional electroporation devices with planar electrodes generate nonuniform electric fields for electroporation. The use of nonuniform electric fields decreases the yield of electroporation since it causes cell damage due to high electric field and no electroporation due to weak electric field. There is a need for investigating other electrodes to replace the planar electrodes in order to increase the yield of electroporation.

Standard microfabrication technologies are complex and do not support the fabrication of electroporation devices with non-planar electrodes. These techniques are not compatible with biocompatible materials such as PDMS polymers and use hazardous chemicals that hamper the biocompatibility of fabricated devices. These techniques do not support the fabrication of transparent devices suitable for phase contrast microscopy.

In addition, expensive tools, materials and the complex procedures of standard microfabrication methods are challenges for users from a biology background. Therefore, it is clear that there is a need to design a user-friendly fabrication protocol that supports fabrication of transparent and biocompatible electroporation devices with non-planar electrodes. This research investigates non-planar microelectrodes and methods to fabricate them in order to realize an electroporation device capable of providing high yield electroporation.

CHAPTER 3

PROPOSED DEVICE FOR HIGH YIELD ELECTROPORATION

This chapter explains the performance of conventional microfluidic electroporation and highlights two main problems which limit the performance of the device. These problems are 1) use of planar electrodes and their nonuniform electric field and 2) complexity in fabrication of the non-planar electrodes using standard microfabrication technologies. The objective of this research is to improve the performance of the electroporation process. Thus, this research aims to devise an electroporation device that has a high electroporation yield, that is easy to fabricate, that could operate using a low voltage supply, and that could be reliable, easy to use, efficient, and safe.

In this chapter, the proposed solution in order to improve the performance of electroporation is described in detail. First, non-planar electrodes such as three-dimensional (3D) electrodes and the electric field generated by them are explained. Then a description of the proposed electroporation device using 3D electrodes in order to increase the yield of electroporation is provided. Lastly, a new fabrication approach in order to fabricate the proposed electroporation device is discussed.

3.1 3D Electrodes to Generate Uniform Electric Field for Electroporation

In chapter 2, it is described that the planar electrodes generate a non-uniform electric field inside the microchannels such as shown in Figure 2.1. The non-uniform electric field decreases the yield of electroporation. As a result, planar electrodes are not ideal for electroporation despite their easy fabrication.

In this research, non-planar electrodes are examined in order to generate a uniform electric field inside the microchannel of the electroporation device. The main hypothesis of this research is that electrodes with a thickness greater than that of planar electrodes can be used to generate a uniform electric field inside the microchannel. This hypothesis is tested by studying the electric field generated by the thick electrodes inside the microchannel of the electroporation device and comparing it with planar electrodes. The differences between the electroporation device with the planar electrodes and the thick electrodes are explained with the help of Figure 3.1.

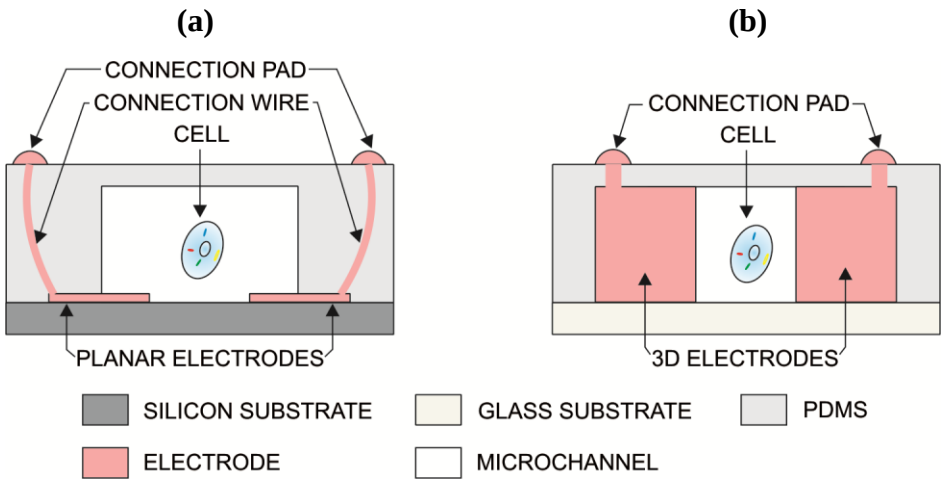

Figure 3.1 Schematic of the cross section of the microfluidic electroporation devices. a) Conventional electroporation device with planar electrodes. The planar electrodes with a height smaller than the dimensions of the cell are present on the bottom of the microchannel b) Proposed electroporation device with 3D microelectrodes. Unlike the planar electrodes, the 3D electrodes with a height greater than the dimensions of the cells are present along the sidewalls of the microchannel of the device.

The height of the planar electrodes in a conventional electroporation device is smaller than the dimensions of the cell. The planar electrodes are present on the bottom of the microchannel as shown in Figure 3.1a. Unlike the planar electrodes, the proposed

thick electrodes are present along the sidewalls of the microchannel and their height is greater than the dimensions of the cell as shown in Figure 3.1b.

It is important to note that unlike the planar electrodes, the thick electrodes do not obstruct light in the vertical direction as they are situated along the sidewalls of the microchannel. The thick electrodes with a height equal to the height of the microchannel extend vertically from the top to the bottom of the microchannel, and are referred to as 3D electrodes.

The electroporation device with 3D electrodes is modeled by using the Finite Element Modeling (F.E.M.) tool COMSOL3.5a. In this modeling, the electric field generated by these 3D electrodes inside the microchannel of the electroporation device is studied. The results of the simulation of the electroporation device with 3D electrodes are shown in Figures 3.2 and 3.3.

Figure 3.2a shows the schematic of the electroporation device with the 3D electrodes used in this simulation. The electric field generated by the 3D electrodes is uniform inside the cross section of the microchannel of the electroporation device, which can be seen from Figure 3.3b. The intensity of the electric field generated by the 3D electrodes is constant along the x and y axes of the microchannel, which can be seen from the Figure 3.3.

From the results of the simulations, it is clear that unlike planar electrodes, the 3D electrodes generate the uniform electric field inside the microchannel. As a result, the cells experience a uniform electric field regardless of their position anywhere between the two 3D electrodes.

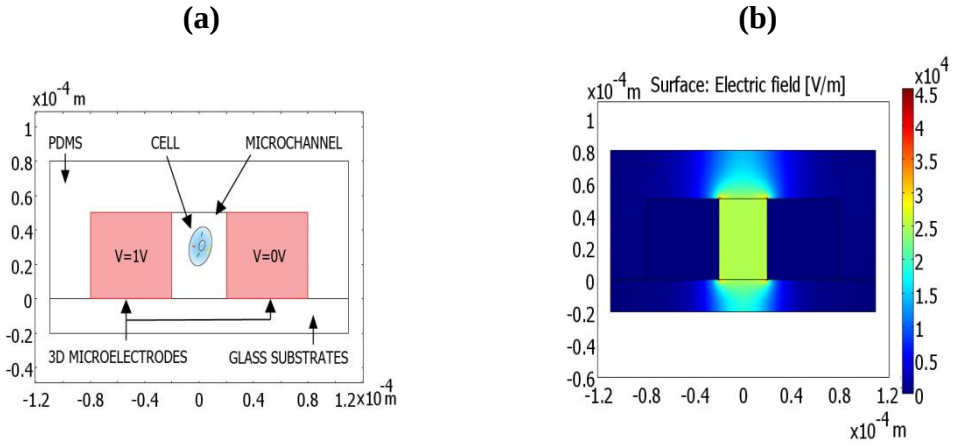

Figure 3.2 Electric field generated by the 3D electrodes inside the microchannel. a) Schematic of the cross section of the electroporation device with 3D electrodes. b) Spatial distribution of the electric field generated by 3D electrodes inside the microchannel, which shows that the electric field is high, focused and uniform inside the microchannel.

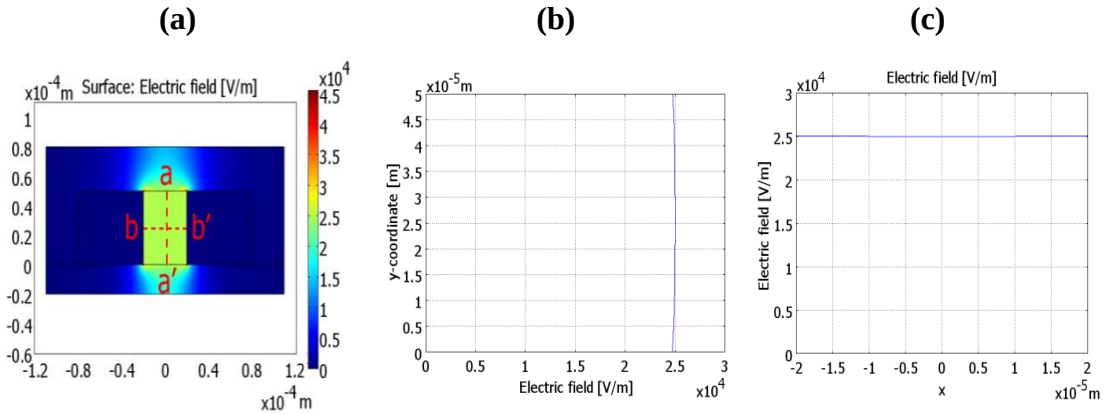

Figure 3.3 Intensity of the electric field generated by the 3D electrodes inside the microchannel. a) Spatial distribution of the Electric field generated by the 3D electrodes inside the microchannel showing the vertical a-a’ and horizontal b-b’ axes of the microchannel of the device. b) Electric field along the line a-a’, which shows that the intensity of the electric field in the vertical direction between the two 3D electrodes is constant. c) Electric field along the line b-b’, which shows that the magnitude of the electric field in the horizontal direction between the two 3D electrodes is constant. Unlike the planar electrodes, the 3D electrodes generate a uniform electric field inside the microchannel in both vertical and horizontal direction.

3.2 Proposed Electroporation Device with 3D Electrodes

This research hypothesizes that the uniform electric field generated by the 3D electrodes can be used to perform the electroporation of cells inside microfluidic electroporation devices. The use of a uniform electric field avoids the creation of regions of very low and very high electric field inside the microchannel. Electroporation using a uniform electric field avoids cell death resulting from a very high electric field and no-electroporation of the cells resulting from a very low electric field. As a result, the yield of electroporation by using a uniform electric field would be greater than by using a non-uniform electric field. This research proposes the use of a uniform electric field as opposed to the conventional nonuniform electric field to perform electroporation in order to improve the yield of electroporation. Some earlier research [23, 69] used a uniform electric field to stimulate cells, but none of them demonstrated its use for the electroporation of the cells.

In electroporation devices with planar electrodes, the cell is subjected to the electric field that depends on its position between the electrodes, which was explained earlier in chapter 2. The cells are also subjected to dielectrophoresis due to a nonuniform electric field. In some electroporation devices, cell traps [23, 24, 46] are used to hold the cell at a fixed point in order to impart the same electric field on each cell being electroporated. These cell traps consist of micro pores or microchannels connected to negative pressure in order to hold the cell in a region between the two electrodes for electroporation, which can be seen in Figures 1.11 and 1.13 in chapter 1. However, the negative pressure applied to trap the cell exerts an additional mechanical force on the cell, which interferes with the process of electroporation.

The region between the two electrodes of the same pair, where electrodes generate the electric field is referred to as electroporation region. 3D electrodes generate a uniform electric field in a volume larger than the volume of the cell inside the electroporation region. As a result, a cell would experience the same electric field regardless of its position in the electroporation region. The uniform electric field in the electroporation region avoids the need for cell trapping. The dielectrophoresis, and hence movement of the cells due to it, does not occur in a uniform electric field. As a result, electroporation is reliable and free from the interference of mechanical force that occurs due to cell trapping. Therefore, this research proposes the use of 3D electrodes to generate a uniform electric field for electroporation of the cell in the microchannel device.

The schematic of the proposed electroporation device in this research is shown in Figure 3.4. In this device, an array of individually addressable 3D microelectrodes is proposed. The individually addressable electrodes provide an ability to control the electric field generated by each pair of electrodes independently. The isolation between the neighboring pair of electrodes and the ability to control them independently will allow applying the electric field to a specific cell without affecting neighboring cells.

Some cells such as HUVEC, JURKAT are considered difficult to transfect [70] because either correct parameter for transfection of these cells are not known or have low yields. An array of pair of electrodes will allow performing the re-electroporation of the cell under the same condition in order to facilitate the transfection of difficult to transfect cells [71, 72].

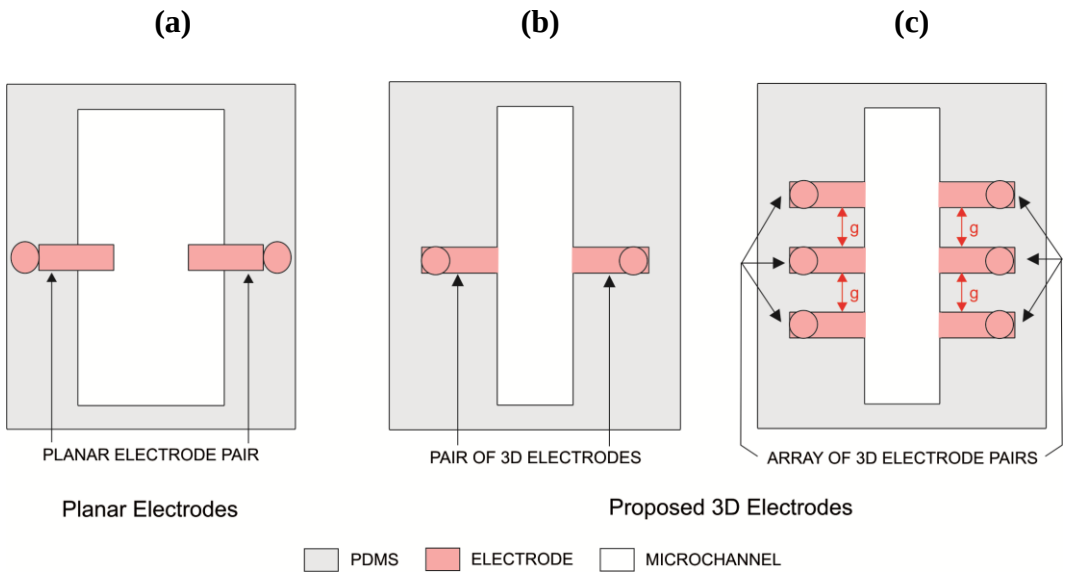

Figure 3.4 Schematic of the top view of the conventional and proposed microfluidic electroporation devices. a) Top view of the conventional device with a pair of planar electrodes, in which the cells flow over the electrodes. b) Top view of the proposed pair of 3D electrodes. c) Top view of the proposed array of 3D electrode pairs for electroporation. Each pair of electrodes in an array can be controlled independently during electroporation.

In the proposed device, the gap between the two 3D microelectrodes of one pair will be equal to 2 - 5 times the diameter of the cell being electroporated. This gap is significantly smaller than the gap between the electrodes in a commercial electroporation cuvette. Consequently, the proposed device requires a low voltage that can be produced by a portable voltage supply such as a battery. This will make the device portable and safe to operate in clinical use without any additional precautions.

3.3 Method to Fabricate 3D Electrodes

Conventional microfabrication technologies have difficulty fabricating a metallic microstructure taller than 5 µm above the substrate. Standard silicon microfabrication technologies are not suitable for fabricating 3D electrodes of thickness equal to the height

of the microchannels, which is of the order of ~50 µm and above in proposed device as shown in Figure 3.1b. The fabrication of the proposed 3D electrodes using the LIGA process explained in chapter 2 is impractical due to the difficult access to a synchrotron radiation tool for photolithography.

The non-metal thick electrodes of the highly doped silicon [69] can be used as 3D electrodes but they are limited by their high impedance. The electroplating [73] and electroforming [64] processes are the only accessible methods to fabricate the thick metal electrodes. These processes are very slow and use hazardous chemicals. The fabrication of 3D electrodes using these methods is complex and time consuming due to multiple steps involved. So far, thick microstructures are fabricated by using a complex microfabrication protocol that includes multistep photolithography, electrodeposition and use of precision alignment tools.

The co-fabrication method [68, 74] was introduced to fabricate metallic microstructures. In the co-fabrication method, a low melting point metal such as indium is injected into PDMS microchannels, as shown in Figure 3.5. This method requires microchannels to have both an inlet and an outlet. In this method, the PDMS microchannels are exposed to the vapors of the solution of 3-mercaptopropyltrimethoxysilane in acetonitrile. This process is referred to as silanization.

The silanization facilitates the insertion of the molten indium into the PDMS microchannels. The silanized microchannels can be filled with the molten indium using two different methods. First, the molten indium can be pushed into the microchannel until it comes out of the microchannel through an outlet, by using a syringe filled with the molten indium. This is shown in figure 3.5 and is called here the pressure-based injection.

Second, the molten indium on the inlet can be inserted into the microchannel until it comes out of the outlet by applying a vacuum at the outlet. This is also shown in Figure 3.5 and is called here the vacuum-based injection.

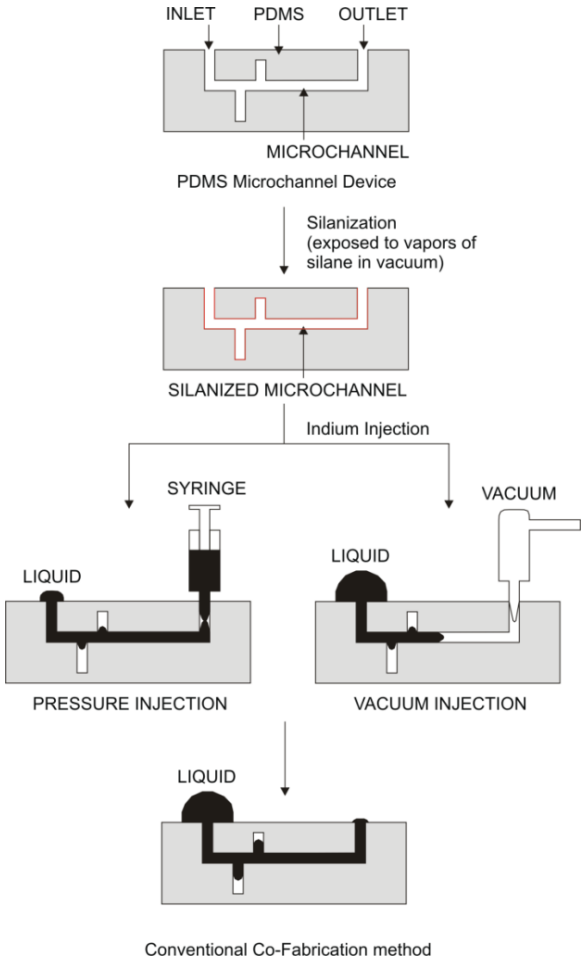

Figure 3.5 Illustration of the co-fabrication [68, 75] method. The method injects indium inside the PDMS microchannels either by pulling indium with a vacuum or by pushing indium with pressure. The method requires silanization and does not completely fill the dead-end microchannels.

Co-fabrication has three limitations. First, it cannot inject the molten indium inside microchannels without an outlet. The requirement of an inlet and an outlet for each microchannel increases the area consumed by the microchannels and decreases the

density of the microchannels. As a result, co-fabrication is not suitable to fabricate electrodes with a high packing density.

Second, it requires silanization in order to lower the surface free energy of the PDMS and make it wettable by liquid indium. The silanization is performed by using highly toxic and hazardous chemical 3-mercaptopropyltrimethoxy silane. The use of toxic and hazardous chemicals not only makes device fabrication unsafe, but also makes the device unsuitable to use with biological cells due to biocompatibility issues.

Third, in co-fabrication each channel has to be filled manually by applying positive/negative pressure at the inlet/outlet. Therefore, it is a serial process, not easily scalable to mass fabrication. In addition, co-fabrication only fills the indium in straight microchannels and does not fill the indium in a complex network of the interconnected microchannels.

This research proposes a new fabrication method to fabricate the proposed electroporation device based on the following hypotheses. The first hypothesis is that the molten indium can be injected inside the microchannel by generating a negative pressure inside the microchannel. Based on this, the second hypothesis is that microchannel injection can be used as a method to fabricate high aspect ratio 3D electrodes. The third hypothesis is that the high aspect ratio 3D electrodes embedded inside the microchannel device can be fabricated in order to generate a uniform electric field for electroporation.

The proposed new method of fabricating the electroporation device with integrated 3D electrodes is as follows. In this method, first the microfluidic device with microchannels made of glass and PDMS will be fabricated by using soft lithography. Then the electrode microchannels of the device will be filled with the molten indium in

order to fabricate the 3D electrodes. The indium injection process will use the vacuum in order to inject the molten indium inside microchannels, even if they are dead-end channels. The proposed method will be explained in detail later, in chapter 6. The differences between the proposed method and the current co-fabrication method are illustrated with the help of Figure 3.6.

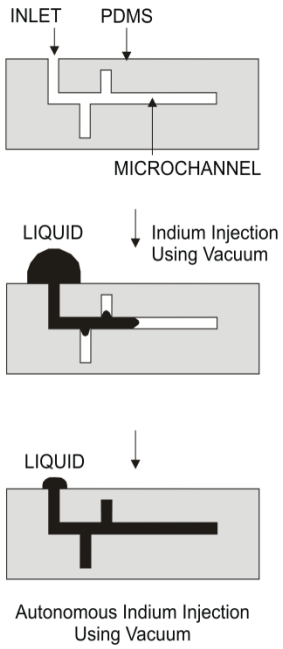

Figure 3.6 Illustration of the proposed vacuum-based Indium Injection method. The method fills high aspect ratio and even dead-end microchannels without silanization.

This figure highlights that the proposed method can inject the indium in dead-end microchannels completely without silanization. Unlike co-fabrication, the proposed method does not require an outlet to the microchannel. The method does not require manual interaction to push or pull the molten indium inside the microchannel by applying the vacuum/pressure manually at inlet/outlet using a syringe. Therefore, this method is called Autonomous Indium Injection.

3.4 Conclusions of the Chapter

The main features of the proposed electroporation device and its fabrication using the proposed autonomous indium injection are as follows;

- The height of the 3D electrode will be higher than the size of the cells.
- The 3D electrodes will be able to generate a high and uniform electric field inside the cross section of microchannel using low voltage.
- The 3D electrodes will generate a uniform electric field in a volume greater than the volume of the cell.
- The 3D electrode will avoid the creation of regions with a very low and very high electric field inside the microchannel.
- The absence of regions with a very high electric field will increase the cell viability by preventing cellular and intracellular damage due to electric field.
- The absence of regions with low electric field will increase the electroporation efficiency by avoiding no-electroporation due to the weak electric field.
- The fabrication is simple and does not require hazardous chemicals, costly microfabrication equipment and operating skills.
- The method is capable of filling high aspect ratio microchannels with the molten indium.
- This method is compatible with PDMS and glass, and therefore it allows the fabrication of transparent electroporation devices that support the use of phase contrast microscopy in order to monitor the process.
- Therefore, the devices will not have a biocompatibility issue and would be acceptable in a biological application.

CHAPTER 4

DESIGN OF HIGH YIELD ELECTROPORATION DEVICE

In this chapter, the design of a proposed electroporation device to increase the yield of electroporation is described. In the previous chapter, the fabrication of 3D electrodes is proposed by injecting the molten indium into microchannels. The proposed electroporation device has two types of microchannels as shown in Figure 4.1. 1) Electroporation microchannel, which will carry the cells to be electroporated, and 2) Electrode microchannels, which will be filled with the molten indium in order to fabricate 3D electrodes.

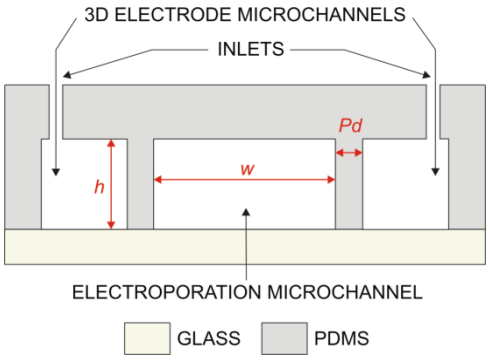

Figure 4.1 Schematic of the cross sectional view of the microchannel device used to fabricate the proposed device. The electrode microchannels and the electroporation microchannels are separated by the PDMS sidewalls.

In this chapter, first the design of an electroporation microchannel is explained. Then, the design of the 3D electrodes that later on will be fabricated by injecting the molten indium in electrode microchannels is explained. The effects of various design parameters of electrodes on the electric field generated by electrodes are modeled in Finite Element Modeling tool COMSOL 3.5a. The results of the simulation are then used

to determine the values of the design parameters of electrodes and electrode microchannels.

4.1 Design of Electroporation Microchannel

This section describes the design of electroporation channel, which is used to deliver the cells for electroporation. While the cells flow in the electroporation microchannel, they pass through the electroporation region between the pair of electrodes. In this region, the cells are electroporated due to the electric field generated by the pair of electrodes connected to a voltage supply.

The design of the electroporation microchannel depends on the dimensions of the cells being electroporated. The diameter (Φ) of the cells varies from 5 μm to 30 μm depending upon the type of cell. In order to avoid cell damage due to squeezing or excessive shear stress, the height and width of the electroporation microchannel should be greater than the size of the cells. Therefore, the height of the electroporation microchannel is selected as 50 μm, which is greater than the size of the cell (Φ = ~ 30 μm).

In the proposed electroporation device, shown in Figure 4.2, 3D electrodes are situated along the left and right sidewalls of the electroporation microchannel. The 3D electrodes of height greater than or equal to the height of the electroporation channel generate a uniform electric field inside the cross section of the electroporation microchannel. The cells are subjected to a uniform electric field irrespective of their position between the two electrodes, if the height of the electrodes is greater than or equal to the height of the electroporation microchannel.

In order to generate a uniform electric field inside the electroporation microchannel, the electrodes and the electroporation microchannel have the same height, and are selected as 50 µm.

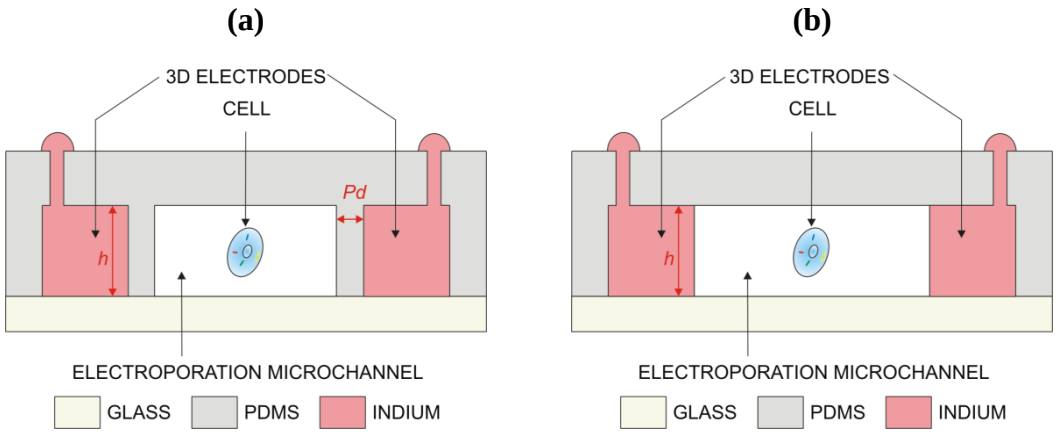

Figure 4.2 Schematic of the cross section of the proposed high yield electroporation device. a) Device with PDMS sidewalls b) Device without PDMS sidewalls between electrodes and electroporation microchannel. 3D electrodes with a height greater than the size of a cell are situated along the sidewalls of the microchannel. These 3D electrodes have the same height as the microchannel.

In proposed electroporation device, the separation between two 3D electrodes (D_E) depends on the width of the electroporation microchannel (w) as shown in Figure 4.3. According to Equation 1.2 in chapter 1, the voltage required to generate the electric field necessary for electroporation is directly proportional to the separation (D_E) between the two electrodes. In order to operate the device with a low voltage, the separation (d) between the electrodes should be small. The width of the electroporation microchannel is selected as 100 µm, which is sufficiently greater than the size of the cells and allows them to flow without squeezing.

3D electrodes situated along the sidewalls of the electroporation microchannel, as shown in Figures 4.2 and 4.3, will be fabricated by filling the electrode microchannels with the molten indium. The molten indium which will be injected into the electrode microchannels should not fill the electroporation microchannel. Therefore, it is necessary to isolate the electrode microchannels from the electroporation microchannel in order to fabricate the 3D electrodes by the proposed Autonomous Indium Injection Method.

The isolation between the electrode and electroporation microchannels increases the separation (D_E) between two electrodes. In order to minimize the separation (D_E), the electrode and the electroporation microchannels should be separated by PDMS sidewalls with the smallest width possible (*Pd)* as shown in Figure 4.1. Based on the resolution of the photolithography equipment used in fabrication, PDMS sidewalls with a width of ~15-20 µm on each side of the electroporation microchannel are used in order to separate the electrode and electroporation microchannels.

A separation of ~15-20 µm between the electrode and electroporation microchannels gives a distance of 130-140 µm between the two 3D electrodes. The PDMS sidewalls of a small width (*Pd*) will be easy to remove after the fabrication electrodes in order to expose the electrodes inside the electroporation microchannel, if needed. In this way, the electroporation microchannel is designed by considering factors such as the size of the cells, operating voltage requirement, and the resolution of the equipment required for fabrication.

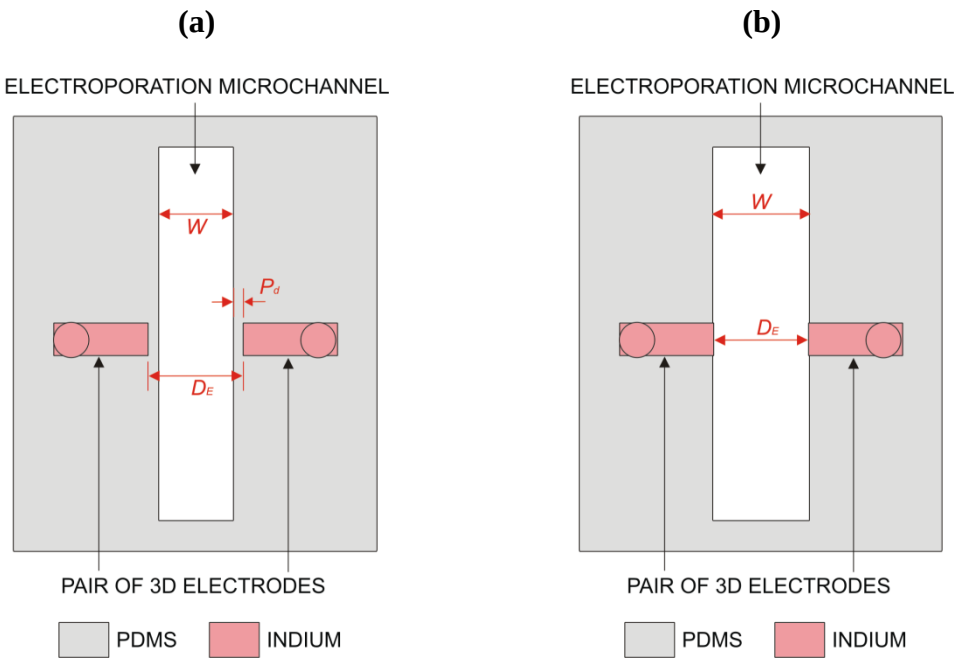

Figure 4.3 Schematic of top view of the proposed high yield electroporation device. a) Device with PDMS sidewalls b) Device without PDMS sidewalls. The device shows the pair of electrodes separated by a distance (d) equal to the sum of the width of a channel (w) and the thickness of PDMS sidewalls. The electric field is produced between the two electrodes to electroporate the cells by applying voltage to the electrodes.

4.2 Design of Electrode Microchannels for High Aspect Ratio 3D Electrodes

In this section, the design of high aspect ratio 3D electrodes that generate the uniform electric field for increasing the yield of electroporation of the cells is discussed. The electric field plays a critical role in electroporation [76], therefore the effects of different parameters of electrodes on the electric field produced by them are studied. In this study, two parameters of high aspect ratio 3D electrodes are emphasized. These parameters are 1) shape of the tip of the 3D electrodes and 2) gap between the neighboring electrode pairs in an array of electrode pairs.

The simulation of a single pair of electrodes with different shapes and array of such electrode pairs is performed using Finite Element Modeling (F.E.M.) tool COMSOL3.5a. The simulation visualized the spatial distribution of electric field generated by the electrodes in the electroporation microchannel. The results of the simulation helped to determine the shape of the electrodes necessary for generating the desired electric field distribution.

4.2.1 Shape of the Tip of 3D Electrodes

The shape of the tip of the electrodes governs the electric field distribution near the electrodes. The electric field near the corners of the metal electrodes is higher than near flat edges [76]. The electric field decreases on both sides of the electrodes away from the tips and it depends on the sharpness of the corner present on the tip of the electrodes. In order to determine the shape of the tip of the 3D electrodes that generate a uniform electric field in a cross section of the electroporation microchannel, the electrodes with and without corners on the tip are modeled and the electric field near the electrodes is observed.

The electroporation devices with a pair of electrodes of different shapes of the tip simulated using Finite Element Modeling (F.E.M.) tool COMSOL 3.5a are shown in Figure 4.4. In this simulation, the electric field generated inside the electroporation microchannel by the electrodes of different shapes is studied. The electric field near the electrode is also plotted in order to examine the electric field exerted on the cell when it is close to the tip of the electrodes. The results of the simulation are shown in Figures 4.5 to 4.9.

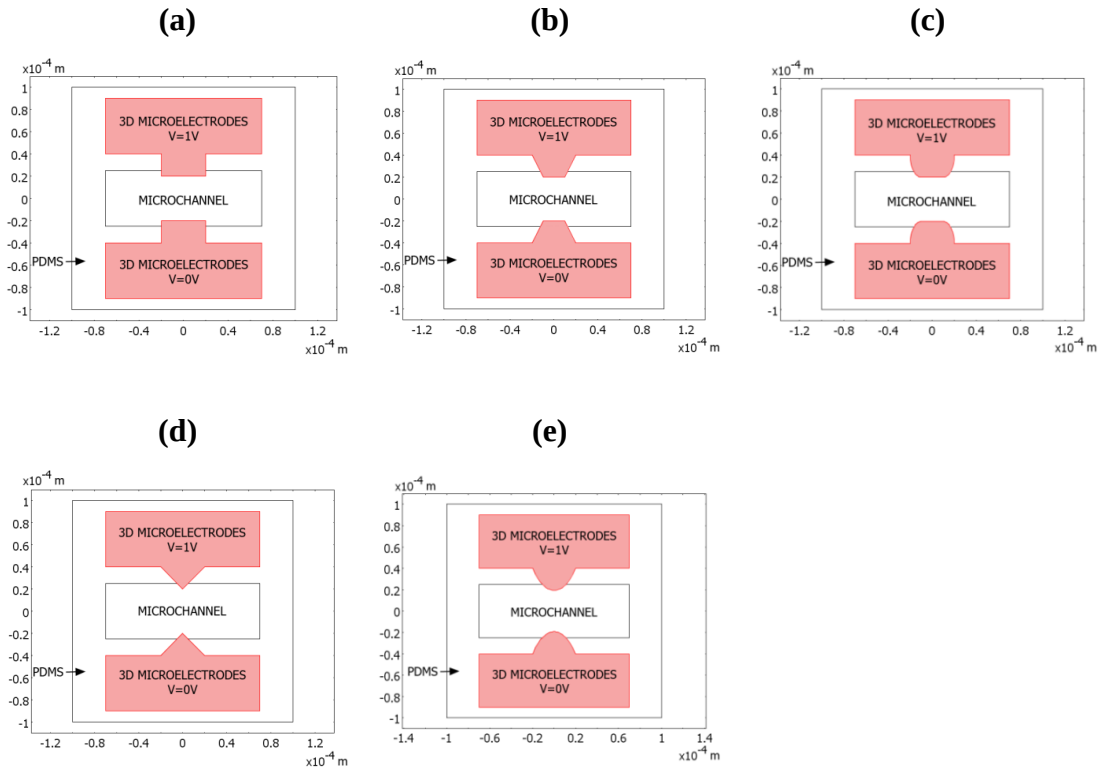

Figure 4.4 Schematics of the top view of the electroporation devices with a pair of electrodes of different shapes of tip. a) Rectangular tip electrodes b) Tapered tip electrodes c) Rounded tip electrodes d) Triangular tip electrodes e) Circular tip electrodes. The electrodes with corners present on their tip (rectangular, tapered and triangular tip) and smooth tips such as rounded corners and circular tip are modeled.

The electric fields generated inside the electroporation microchannel by the electrodes of different shapes of the tip are shown in Figures 4.5b to 4.9b. These figures show that the electric field is high near the corners on the tip of the electrodes. The plots in Figures 4.5c to 4.9c also show that the electric field peaks near the corners on the tip of the electrodes and that the electric field decays on both sides.

The plots in Figures 4.5c, 4.6c, and 4.7c show the electric field generated by the pair of electrodes with rectangular, tapered, and rounded tips, respectively. These figures show that the electric field near the tip of the electrodes has two peaks due to the two corners present on the rectangular, tapered and rounded tip of the electrodes. The electric

field near the tip of the electrodes becomes nonuniform if it has more than one peak. The electrodes with rectangular, tapered, and rounded tips generate nonuniform electric field near the electrodes due to more than one corner on the tip of these electrodes. Therefore, the electrodes with more than one corner on the tip such as rectangular, tapered, and rounded tips are not suitable for the proposed electroporation device.

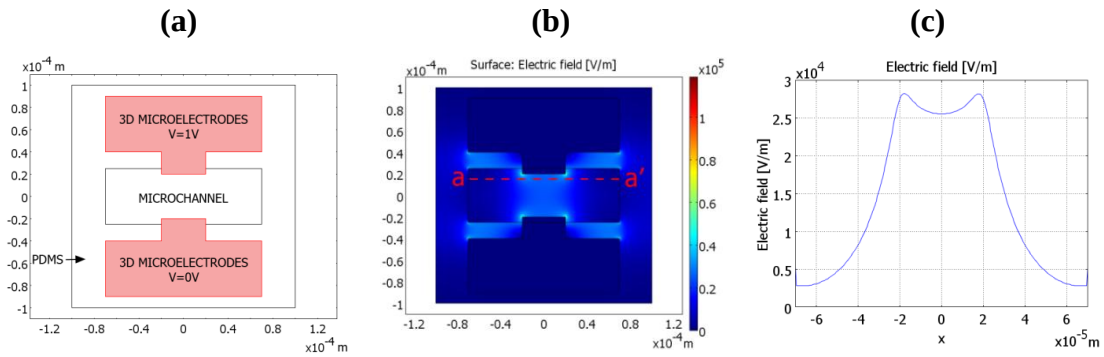

Figure 4.5 Electric field generated by a pair of rectangular tip electrodes in a microchannel. a) Schematic of the top view of the device with a pair of rectangular tip electrodes. b) Electric field inside the microchannel showing that the electric field is high near the corners on the tip of the electrodes and focused in a region between the two tips. c) Electric field along the red dotted line a-a', 10 µm below the tip of the top electrode. The plot shows that the electric field has two peaks due to the two corners present on the rectangular tip of the electrodes. The pair of rectangular tip electrodes generates a nonuniform electric field between the electrodes with more than one peak value.

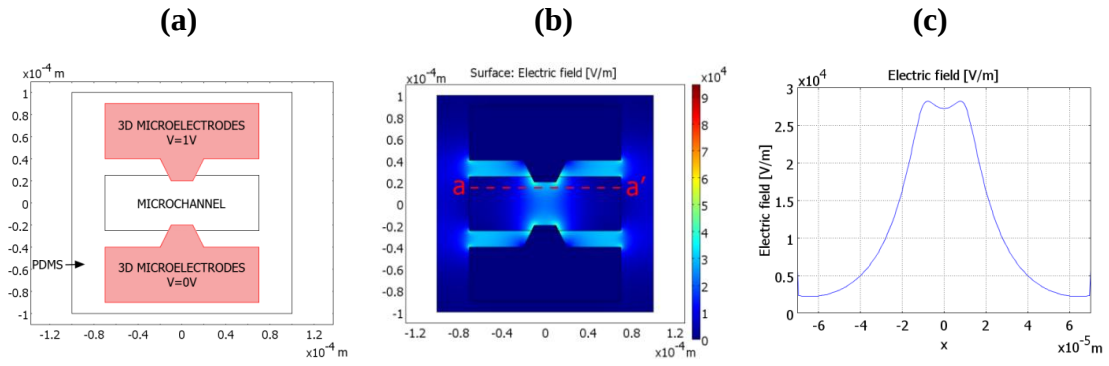

Figure 4.6 Electric field generated by a pair of tapered tip electrodes in a microchannel. a) Schematic of the top view of the device with a pair of tapered tip electrodes. b) Electric field inside the microchannel showing that the electric field is high near the corners on the tip of the electrodes and focused in a region between the two tips. c) Electric field along the red dotted line a-a', 10 μm below the tip of the top electrode. The plot shows that the electric field has two peaks due to the two corners present on the tapered tip of the electrodes. The pair of tapered tip electrodes generates a nonuniform electric field between the electrodes with more than one peak value.

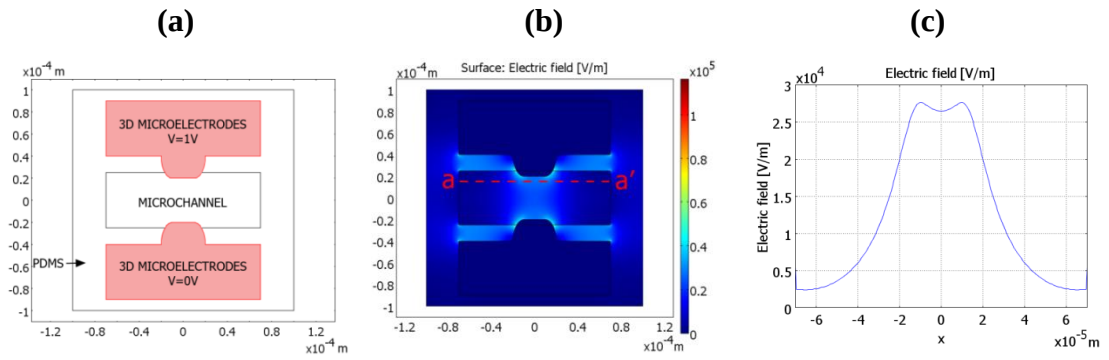

Figure 4.7 Electric field generated by a pair of rounded tip electrodes in a microchannel. a) Schematic of the top view of the device with a pair of rounded tip electrodes. b) Electric field inside the microchannel showing that the electric field is high near the corners on the tip of the electrodes and focused in a region between the two tips. c) Electric field along the red dotted line a-a', 10 μm below the tip of the top electrode. The plot shows that the electric field has two peaks due to the two corners present on the rounded tip of the electrodes. The pair of rounded tip electrodes generates a nonuniform electric field between the electrodes with more than one peak value. The magnitude of the peak is smaller than the rectangular and triangular tips.

Figure 4.8 shows the electric field generated by a pair of triangular tip electrodes. The triangular tip has a sharper corner than the rectangular tip. The plot in Figure 4.8c shows that the electric field generated by the triangular tip electrodes has a peak near the corner on the tip. The electric field generated by a triangular tip is focused in a narrow region and decreases abruptly on both sides of electrodes due to the sharp corners of the triangular tip.

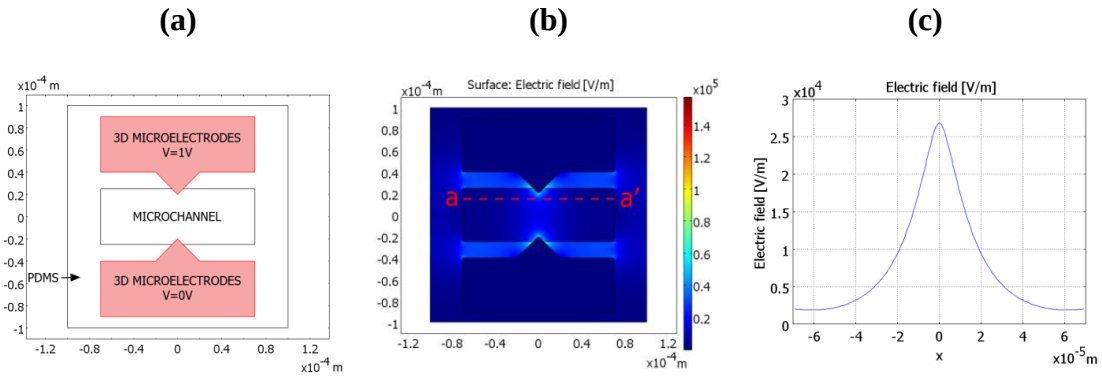

Figure 4.8 Electric field generated by a pair of triangular tip electrodes in a microchannel. a) Schematic of the top view of the device with a pair of triangular tip electrodes. b) Electric field inside the microchannel showing that the electric field is high near the corners on the tip of the electrodes and focused in a region between the two tips. c) Electric field along the red dotted line a-a', 10 µm below the tip of the top electrode. The plot shows that the electric field has the peak due to the corner present on the triangular tip of the electrodes. The electric field decreases abruptly on both sides of the electrodes. The pair of electrodes with triangular tip generates an electric field focused over a narrow region and varies abruptly away from the tips.

The electric field generated by a pair of circular tip electrodes is shown in Figure 4.9. The circular tip has a smooth edge without any corners. The plot in Figure 4.9c shows that the electric field generated by the circular tip electrodes has peak intensity near the tip, which is similar to the triangular tip electrodes. However, the electric field generated by the circular tip is focused in a wider region than the triangular electrodes

and decreases gradually on both sides of the electrodes due to the smooth edge of the circular tip.

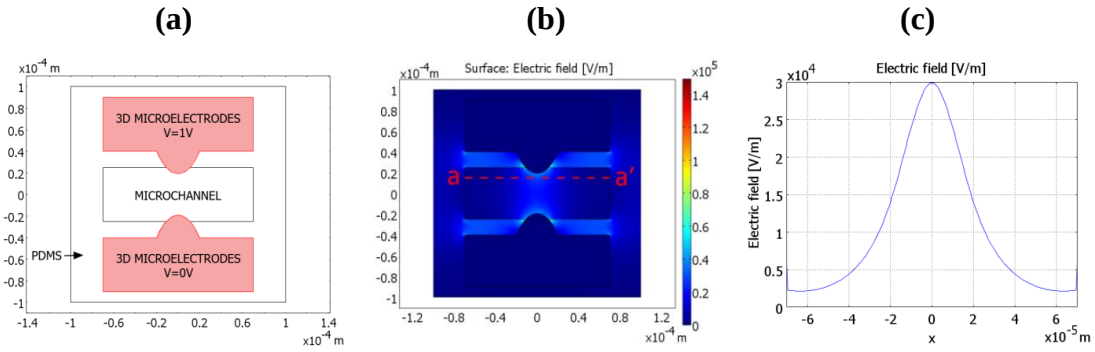

Figure 4.9 Electric field generated by a pair of circular tip electrodes in a microchannel. a) Schematic of the top view of the device with a pair of circular tip electrodes. b) Electric field inside the microchannel showing that the electric field is high near the tip of the electrodes and focused in a region between the two tips. c) Electric field along the red dotted line a-a', 10 µm below the tip of the top electrode. The plot shows that the electric field has the peak and decreases gradually on both sides of electrodes. The pair of circular tip electrodes generates an electric field focused over a wide region and varies gradually away from the tips.

The electric field with uniform intensity in a wide region (volume larger than volume of cell) and gradual variation on both sides of electrodes is desirable for electroporation of cells. Electrodes with circular tips are easy to fabricate compared to electrodes with sharp tips. The fabrication of sharp tips such as triangular tips or rectangular tips is uncertain due to the rounding of the sharp corners of the tips during the fabrication process. As a result, the electrodes with a circular tip as shown in Figure 4.9 are selected for high yield electroporation of cells due to their ability to generate the uniform electric field inside the cross section of the electroporation microchannel.

4.2.2 Array of Electrode Pairs

The experiments in cell biology require the electroporation of hundreds of cells. The single cell electroporation performed on one cell at a time using the high aspect ratio 3D electrodes will take a long time to electroporate hundreds of cells. The array of electrode pairs allows the electroporation of more than one cell simultaneously. It reduces the electroporation time despite the single cell electroporation. Therefore, instead of one pair of electrodes such as those shown in Figure 4.3, the electroporation device is instead designed with an array of electrode pairs.

An array of electrode pairs allows electroporation to repeat with or without changing the electric field. The isolated pairs of electrodes in an array can be independently turned ON and OFF. The electric field generated by each isolated pair of electrodes can be controlled independently, according to the requirements of the cells being electroporated.

The isolation between the neighboring pair of electrodes and the ability to control them independently will allow application of the electric field to a specific cell without affecting neighboring cells. This avoids cell death due to a strong electric field and exclusions of the cells from the electroporation due to a low electric field. Therefore, an array of isolated pairs of electrodes is desirable to increase the yield of electroporation.

An array of electrode pairs with different shapes of the electrode tips are modeled using Finite Element Modeling (F.E.M) tool COMSOL 3.5a. In this modeling, the electric field generated by the array of electrode pairs of different shape, of the electrode tips, and interference between the neighboring electrode pairs are studied. The results of the simulation are shown in Figures 4.10 to 4.14 and each figure has panels a, b, and c.

Figures 4.10a to 4.14a show the top view of the electroporation device with an array of electrode pairs of rectangular, tapered, rounded, triangular, and circular tips. The spatial distribution of the electric field generated in a microchannel by the array of electrode pairs with different shapes of the tips is shown in panel b of Figures 4.10 to 4.14. The intensity of the electric field along the horizontal line 10 µm below the top electrodes of the array is plotted in panel c of Figures 4.10 to 4.14.

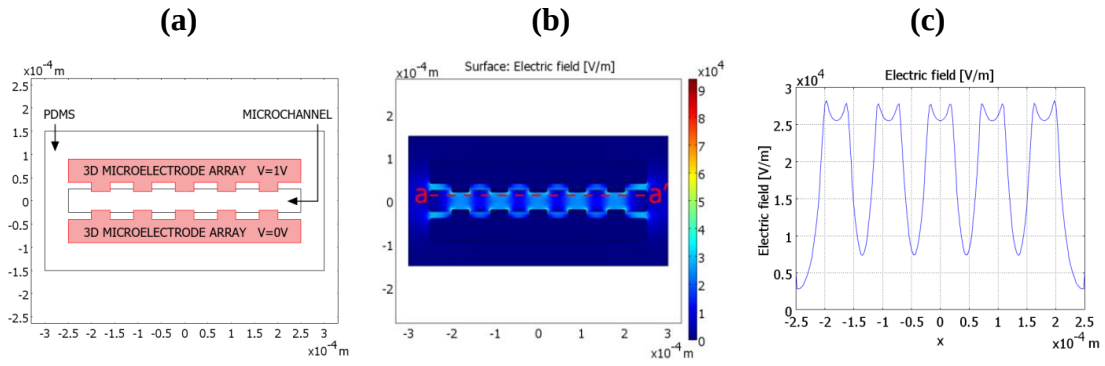

Figure 4.10 Electric field generated by the array of electrode pairs with rectangular tips in a microchannel. a) Schematic of the top view of device with array of electrode pairs of rectangular tip electrodes. b) Electric field in a microchannel showing that the electric field is high and focused in a region between the two electrodes of the pair. c) Electric field along the red dotted line a-a', 10 µm below the tips of the top electrodes. The plot shows that the electric field near the electrodes is nonuniform since it has two peaks corresponding to the two corners present on the rectangular tip. The magnitude of the electric field in a region between the neighboring electrode pairs, due to their interference is ~0.75×10^4 V/m.

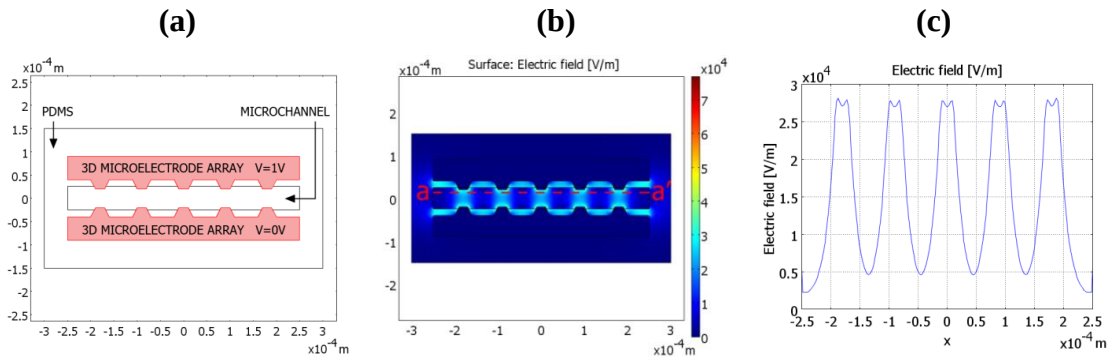

Figure 4.11 Electric field generated by the array of electrode pairs with tapered tips in a microchannel. a) Schematic of the top view of device with array of electrode pairs of tapered tip electrodes. b) Electric field in a microchannel showing that electric field is high and focused in a region between the two electrodes of the pair. c) Electric field along the red dotted line a-a', 10 µm below the tips of the top electrodes. The plot shows that the electric field near the electrodes is nonuniform since it has two peaks corresponding to two corners present on the tapered tip of the electrodes. The magnitude of the electric field in a region between the neighboring electrode pairs, due to their interference is ~0.5×10^4 V/m.

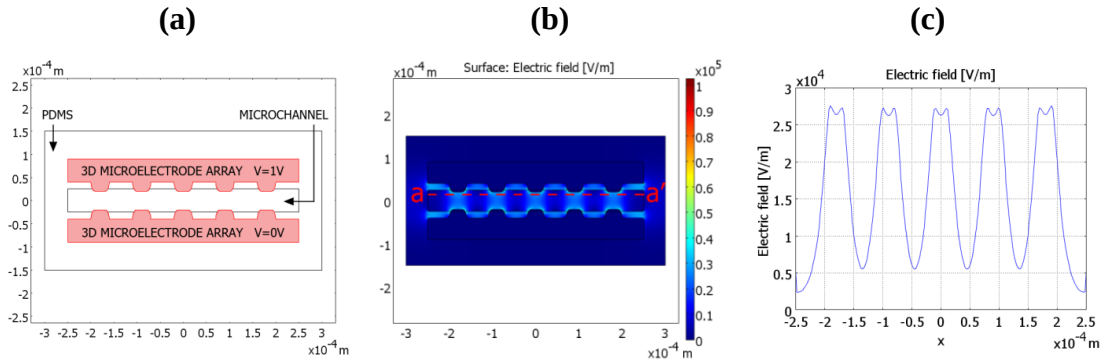

Figure 4.12 Electric field generated by the array of electrode pair with rounded tips in a microchannel. a) Schematic of the top view of device with array of electrodes pairs of rounded tip electrodes. b) Electric field inside the channel showing that electric field is high and focused in a region between the two electrodes of the pair. c) Electric field along the red dotted line a-a', 10 µm below the tips of the top electrodes. The plot shows that the electric field near the electrodes is nonuniform since it has two peaks corresponding to the two corners present on the rounded tip of the electrodes. The magnitude of the electric field in a region between the neighboring electrode pair, due to their interference is ~0.55×10^4 V/m.

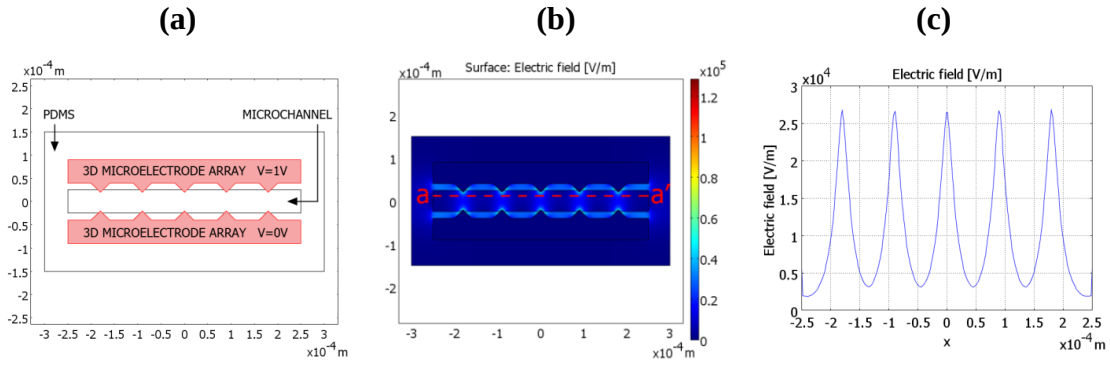

Figure 4.13 Electric field generated by the array of electrode pairs with triangular tips in a microchannel. a) Schematic of the top view of device with array of electrode pairs of triangular tip electrodes. b) Electric field inside the channel showing that electric field is high and focused in a region between the two electrodes of the pair. c) Electric field along the red dotted line a-a', 10 µm below the tips of the top electrodes. The plot shows that the electric field is focused in a narrow region with the peak magnitude near the tip of electrodes and varies abruptly on both sides of the electrodes. The magnitude of the electric field in a region between the neighboring electrode pairs, due to their interference is ~0.3 x 10^4 V/m.

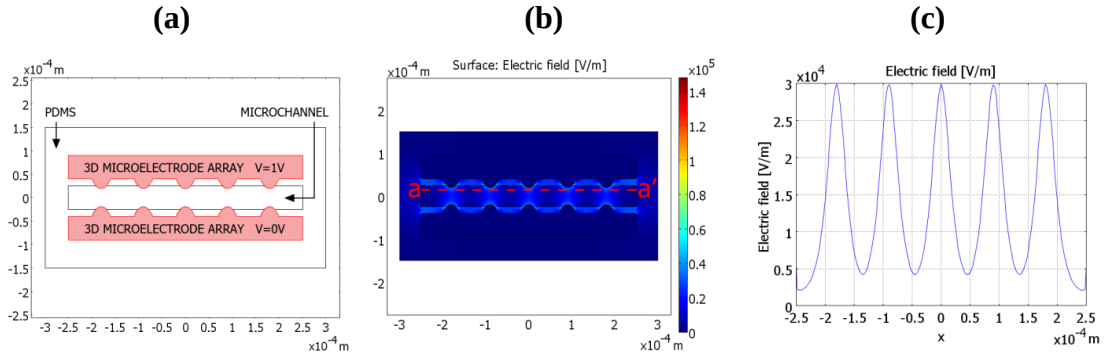

Figure 4.14 Electric field generated by the array of electrode pairs with circular tips in a microchannel. a) Schematic of the top view of device with array of electrode pairs with circular tip electrodes. b) Electric field inside the channel showing that electric field is high and focused in a region between the two electrodes of the pair. c) Electric field along the red dotted line a-a', 10 µm below the tips of the top electrodes. The plot shows that the electric field is focused in a wide region with the peak magnitude near the tip of the electrodes and varies gradually on both sides of the electrodes. The magnitude of the electric field in a region between the neighboring electrode pairs, due to their interference is ~0.4 x 10^4 V/m.

The results of these simulations are consistent with the simulation of a single pair of electrodes with the same tips. The comparison of Figures 4.10c to 4.14c shows that the array of electrode pairs with triangular and circular electrode tips generates an electric field of lower intensity in a region between the two neighboring electrode pairs than any other array of electrode pairs. An array of electrode pairs with circular tips is selected for the proposed electroporation device due to the uncertainty of fabricating an array of electrode pairs with triangular tips.

4.2.3 Gap Between the Neighboring Electrode Pairs in an Array of Electrode Pairs

In an array of isolated electrode pairs, the electric field generated by the neighboring electrode pairs may interfere with each other. As a result, the electric field in a region between the neighboring pair of electrodes may not be zero as it is the result of adding the electric fields generated by each of the two neighboring electrode pairs. To obtain an array of isolated electrode pairs, the separation between the neighboring electrode pairs should minimize the interference of the electric field between them. The neighboring pair of electrodes should be separated by a distance that minimizes the interference between them.

Ideally, the neighboring electrode pairs in an array should be separated by infinite distance to obtain an array of isolated electrode pairs, which is impractical. It is also important to note that the large separation between the neighboring electrode pairs decreases the density of the electrode pairs. Thus, the separation between neighboring electrode pairs is obtained by trade-off between the electric field interference and density of pair of electrodes. The optimum value of separation between the neighboring electrode

pairs should decrease the interference of their field and increase the density of electrode pairs in an array.

The proposed electroporation device is designed to electroporate the cell when it is inside the microchannel and between two electrodes of the same electrode pair as shown in Figure 4.15. Such a design will allow selective electroporation of the cell between the electrodes of the same pair without affecting the adjacent cells. This design requires that the intensity of the electric field in a region between neighboring electrode pairs to be less than the threshold electric field necessary to electroporate the cell.

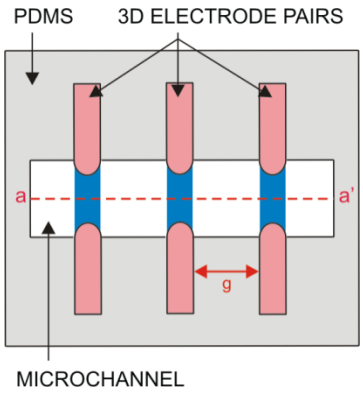

Figure 4.15 Schematic of the proposed device showing neighboring electrode pairs and the electroporation regions. The device electroporates the cell in a region indicated using the blue color between a pair of electrodes without affecting neighboring cells in a region indicated using the white color by applying a voltage to the electrodes.

The reversible electroporation of cells occurs above a threshold electric field of intensity 365 V/cm [77], whereas the electric field of intensity above 700 V/cm is necessary to perform the irreversible electroporation of cells [77]. Therefore, in order to perform selective electroporation, the gap between neighboring electrode pairs should be selected to obtain an electric field with intensity less than 365 V/cm in a region between the neighboring electrode pairs.

In this research, the maximum intensity of the electric field between the two electrodes of the same pair will be less than or equal to 5 kV/cm. In order to determine the gap between the neighboring electrode pairs, the electroporation devices with three pairs of electrodes and varying gap (g) between them, as shown in Figure 4.15, are studied using finite element analysis tool COMSOL 3.5a. The values for the gap between neighboring electrode pairs used for this modeling are 50 µm, 60 µm, 75 µm, 100 µm, 110 µm, 125 µm, 150 µm, and 250 µm. All electrode pairs are connected to the same potential difference of 15 V to generate an electric field with an intensity 5 kV/cm between the two electrodes of the same pair. The results of the simulation are used to determine the minimum intensity of the electric field in a region between neighboring electrode pairs along red dotted line a-a' as shown in Figure 4.15 which are given in Table 4.1.

Table 4.1 The Minimum Intensity of an Electric Field in a Region Between Neighboring Electrodes Separated by Varying Gap

Gap (µm)	**Electric Field between neighboring electrodes (V/cm)**
50	549
60	445
75	343
100	250
110	230
125	210
150	192
250	177

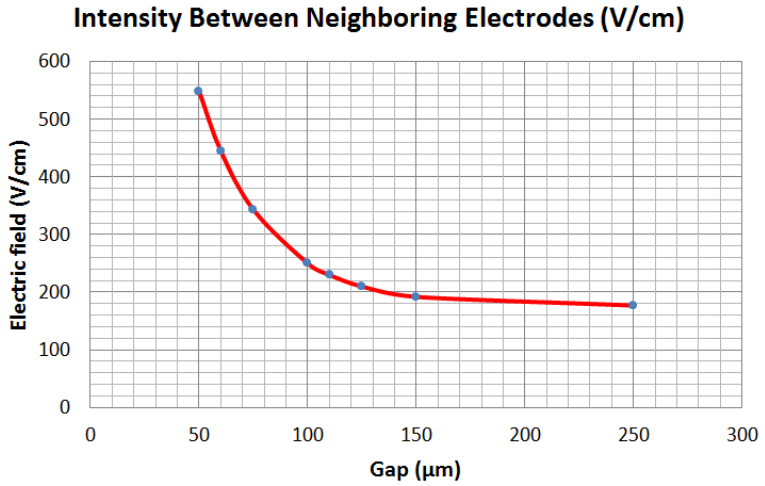

Figure 4.16 Minimum intensity of electric field in a region between neighboring electrodes separated by varying gap. A large gap does not significantly decrease the electric field.

The variation of the intensity of the electric field in a region between neighboring electrodes with respect to the gap as given in Table 4.1 is plotted and shown in Figure 4.16. This plot shows that the intensity of the electric field in a region between neighboring electrode pairs is less than the threshold electric field required for the reversible electroporation if the gap is more than 75 µm. The electric field along the red dotted line a-a' as shown in Figure 4.15 in devices with a gap 50 µm, 100 µm and 150 µm are plotted and shown in Figure 4.17.

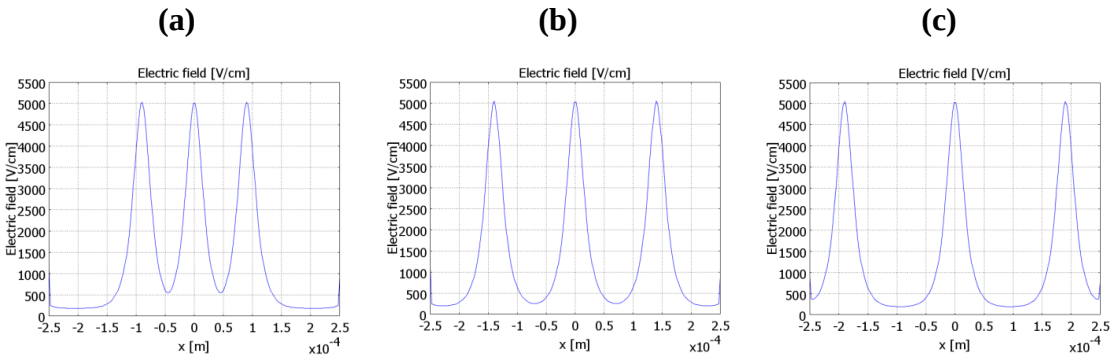

Figure 4.17 Electric field inside microchannel generated by electrode pairs separated by varying gap. The electric field is plotted along the red dotted line shown in Figure 4.15. The gap is a) 50 µm b) 100 µm and c) 150 µm. The intensities of the electric field in a region between the neighboring electrode pairs of the device with a gap 100 µm and 150 µm differ by a small value.

These plots show that a large value for the gap between neighboring electrodes does not significantly decrease the electric field. In this design, an electrode pair is considered isolated from another, if the intensity of the electric field in a region between two pairs is less than the threshold electric field required for the reversible electroporation. As a result, the gap between neighboring electrode pairs in an array is selected 50 µm and 100 µm. The neighboring electrode pairs are isolated from each other in a device with a 100 µm gap between the neighboring electrode pairs, whereas they are not isolated in a device with a 50 µm gap. In this way, the devices with isolated and not isolated neighboring electrode pairs are designed.

4.2.4 Advantages of an Array of Electrode Pairs

In the proposed electroporation device, an array of isolated circular electrode pairs is selected. An array of electrodes allows the simultaneous single cell electroporation of more than one cell in order to reduce the electroporation time. In addition, isolated

electrode pairs in an array can be controlled independently to generate the required electric field inside the electroporation microchannel. This can be used to generate an electric field of a desired configuration inside the electroporation microchannel. This is demonstrated with the help of finite element analysis of the designed electroporation device as shown in Figure 4.18a using COMSOL 3.5a.

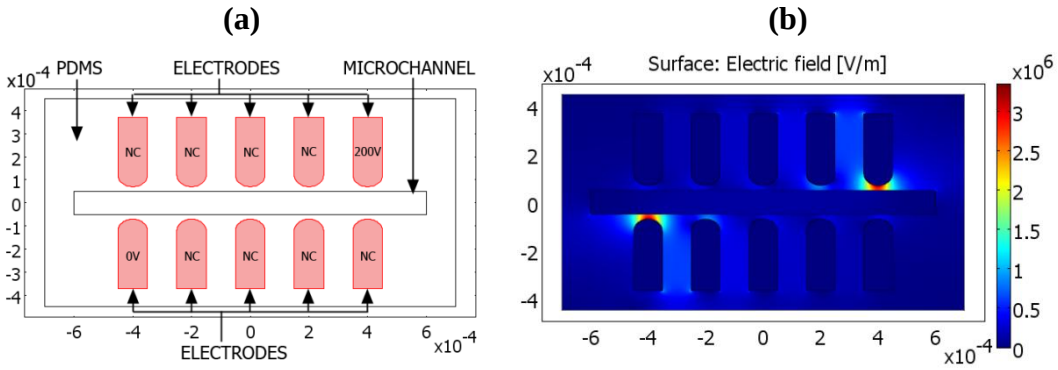

Figure 4.18 Proposed device with selected electrodes of an array connected to voltage source. a) Schematic of top view of proposed electric field indicating the voltage applied to each of the electrodes of the device (NC indicates no connection). b) Electric field inside the device generated by excitation of selected electrodes of the device.

In this study, the generation of a uniform electric field inside the microchannel over some finite length is demonstrated by applying the voltage to the selected electrodes of the device. In this study, the device with an array of isolated circular electrode pairs with tip radius of 50 µm and gap of 100 µm between the neighboring electrode pairs is used. The width of the electroporation microchannel is 100 µm and the electrode pairs are separated from this microchannel by the PDMS sidewalls of thickness 20 µm. The rightmost electrode of the top row of electrodes is connected to 200 V and the leftmost electrode of the bottom row of electrodes is connected to 0V as shown in Figure 4.18a. The electric field generated by excitation of selected electrodes is shown in Figure 4.18b.

In order to carefully analyze the electric field generated inside the microchannel, only the electric field inside the microchannel is visualized as shown in Figure 4.19a.

This figure clearly shows that the electric field inside the microchannel over a region between two excited electrodes is uniform. Also, the electric field along the axis of the microchannel indicated by the red dotted line is plotted in Figure 4.19b. This plot confirms that the electric field inside the microchannel over the region between two excited electrodes from x=-200 µm to 200 µm is constant. The plot of the x and y components of the electric field shown in Figure 4.19b also clearly indicates that the electric fields in the x and y directions are constant. These results show that the selective excitation of individually addressable electrodes of an array can be used to generate a uniform electric field in a selected region inside the microchannel. In this way, an array of individually addressable electrode pairs can be used to generate the desired electric field inside the microchannel by applying different voltages to the electrodes.

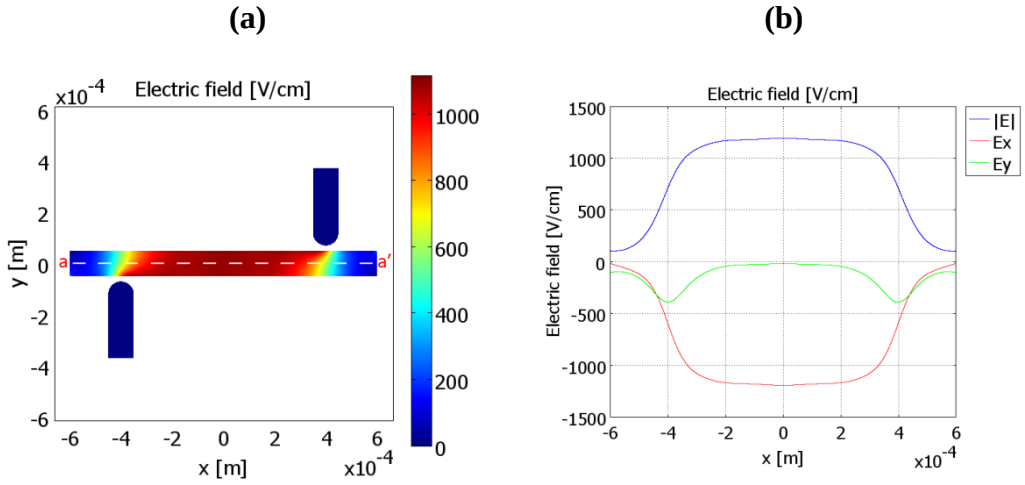

Figure 4.19 Electric field inside the electroporation microchannel when selected electrodes are connected to the voltage source. a) Electric field generated inside the microchannel. b) The electric field plotted along the axis of microchannel a-a'. The electric field is uniform in a region of the microchannel from x = -200 µm to 200 µm.

4.3 Conclusions of the Chapter

In conclusion, the proposed electroporation device is designed by taking into consideration the size of the cells, the voltage required to operate the device, the limitations of the equipment used in fabrication, and the results of the simulations. The electroporation microchannel with a width of 100 µm and a height of 50 µm is designed in order to allow the flow of cells through it without squeezing during electroporation. The electrode and the electroporation microchannels are separated by PDMS sidewalls with a width of ~15 µm in order to allow the fabrication of 3D electrodes by using the Autonomous Indium Injection Method. The separation between the two 3D electrodes of a same pair is ~130 µm, which will allow the device to perform electroporation using low voltage. An array of electrode pairs with circular tips is used to generate a uniform electric field focused inside the cross section of the electroporation microchannels for electroporation. The electrodes of neighboring electrode pairs are separated by a distance of 100 µm in order to isolate and control each electrode pair independently.

CHAPTER 5

FABRICATION OF HIGH YIELD ELECTROPORATION DEVICE

In the previous chapter, the design of the proposed electroporation device is described. In this chapter, the fabrication of the proposed electroporation device is discussed. The fabrication of the proposed device is divided into main three steps as shown in Figure 5.1. 1) Fabrication of the device with electroporation and electrode microchannels, 2) Fabrication of the 3D electrodes, and 3) Removal of the PDMS sidewalls between the 3D electrodes and the electroporation microchannel.

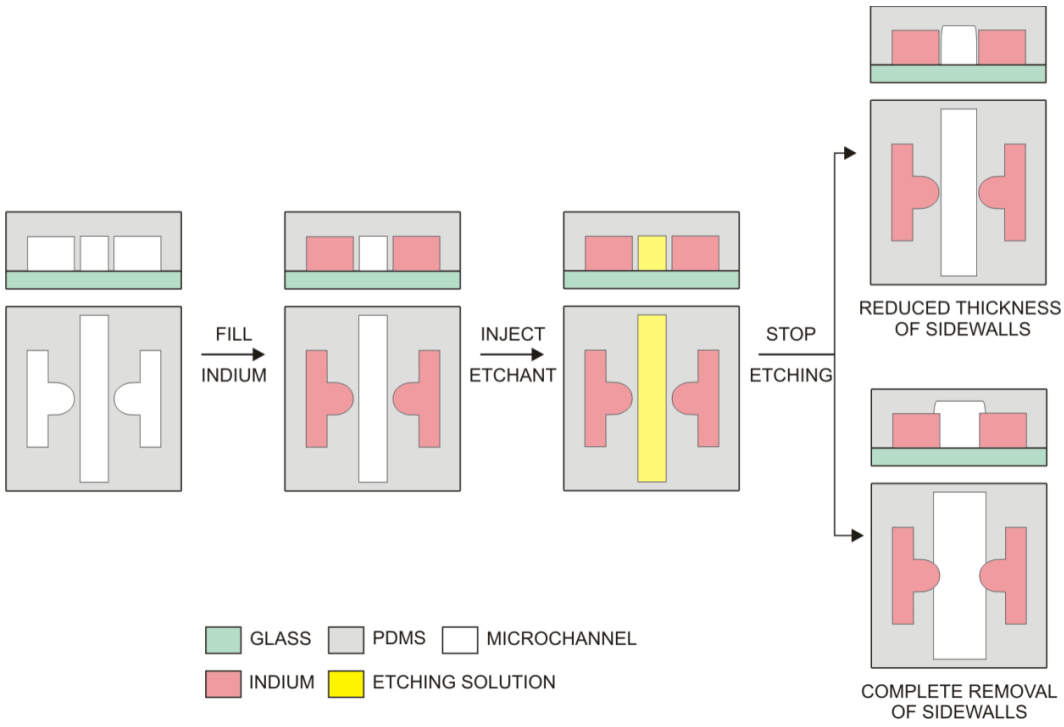

Figure 5.1 Flow chart to fabricate the high yield electroporation device. Molten indium is injected into the electrode microchannels of the soft-lithographically fabricated device. The tips of the indium electrodes are then exposed to the electroporation microchannel by wet etching the PDMS sidewalls. Etching is followed by thoroughly rinsing the microchannel before use.

First, the microchannel device is fabricated using soft lithography. This microchannel device consists of the electroporation and the electrode microchannels. The electrode microchannels are present on either side of the electroporation microchannel as shown in figure 5.1. Then, the electrode microchannels are filled with the molten indium. The electrode microchannels filled with indium act as 3D electrodes. The PDMS walls between the electroporation microchannel and the 3D electrodes are removed in order to expose the 3D electrodes in the electroporation microchannel. Finally, the electroporation microchannel is cleaned in order to avoid any damage to the cells due to chemical contamination.

All of the fabrication steps used to fabricate the proposed electroporation device are explained in detail in the following sections. First, the fabrication of the microchannel device using soft lithography is described. In this section, the fabrication of SU-8 50 master for the proposed electroporation device is described in detail, followed by the design of the photolithography mask. In addition, this section also explains the fabrication of an adhesive tape master that can be used to fabricate the microchannels of a width 250 μm and above without the use of a cleanroom. Then, the fabrication of the 3D electrodes by using Autonomous Indium Injection Method is described. Lastly, the PDMS sidewalls etching process is discussed in order to either remove or reduce the thickness of the PDMS sidewalls between the electroporation microchannel and the 3D electrodes.

5.1 Fabrication of Electroporation and Electrode Microchannels

Unlike the semiconductor microfabrication technologies, soft lithography is inexpensive, easy to learn, and accessible to a wide range of users. In soft lithography, the master is replicated by using thermally curable, transparent, and biocompatible polymer Poly(dimethylsiloxane) PDMS. The fabrication using soft lithography has two steps. 1) Fabrication of the master and 2) Replication of the master.

The master is a substrate with microscopic reliefs—for example, photoresist microstructures on the surface of a silicon wafer, as shown in Figure 5.2. The resulting microchannels will be the negative replicas of the micro reliefs. Two methods for the fabrication of masters for soft lithography are explained in the following sub-sections.

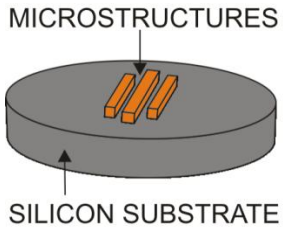

Figure 5.2 Illustration of a master for soft lithography. The pattern of photoresist is the negative replica of the microchannels on the silicon substrate fabricated using photolithography.

5.1.1 Fabrication of Master Using Negative Photoresist (SU-8)

Negative photoresist is a light sensitive polymer that cures when exposed to UV radiation. SU-8 is negative photoresist [78, 79] optimized to fabricate high-aspect-ratio microstructures with vertical sidewalls and is desirable in microchannel fabrication. The conventional photolithography is used to fabricate the master using the negative photoresist SU-8 50, as shown in Figure 5.3.

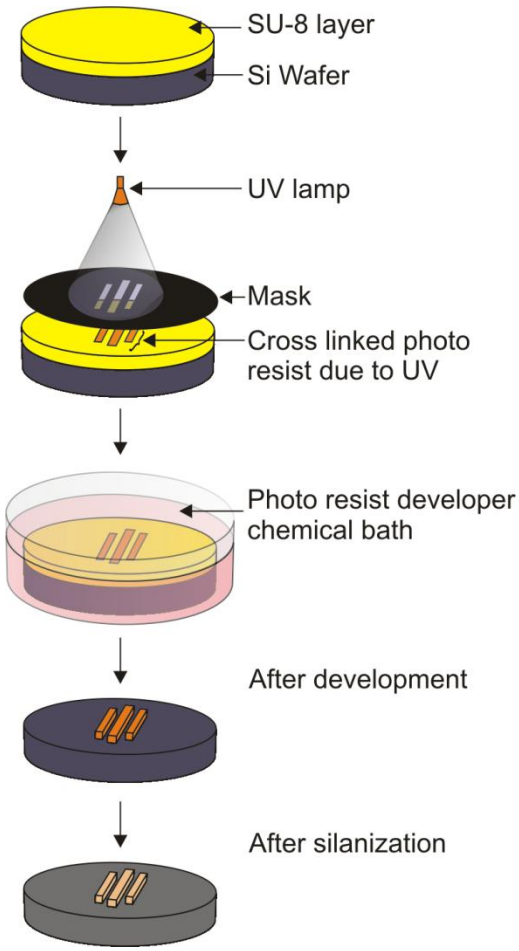

Figure 5.3 Fabrication of SU-8 50 photoresist master. The layer of negative photoresist SU-8 50 on a silicon wafer is patterned by using UV photolithography and then exposed to the vapors of the silane. The wafer with patterned SU-8 50 microstructures is used as a master to fabricate the microchannels.

This process first begins with a thin layer of negative photoresist SU-8 50 which is spun on a silicon wafer. The pre-exposure baking is applied to the photoresist layer in order to evaporate unnecessary solvent in the photoresist prior to the UV exposure. The photoresist is exposed to 365 nm UV light through the photolithography mask. The UV exposure is used to cross-link the photoresist in a region exposed to UV through the transparent region on the mask. The UV exposure is performed inside a cleanroom using the Karl Suss MA-6 with Backside Alignment exposure tool with UV exposure intensity

5 mW/cm^2. Then the post-exposure bake is applied to the photoresist for enhancing the adhesion between the cross-linked photoresist and the silicon substrate. The photoresist is developed in a solvent that dissolves the non cross-linked photoresist.

In this way, the negative replica of microchannels is obtained on the silicon substrate. Lastly, the micropattern on the wafer is exposed to the vapors of Tridecafluoro-1,1,2,2-Tetrahydrooctyl-1-Trichlorosilane in a vacuum for at least four hours. This process is called vapor phase silanization. It is necessary to avoid the sticking of the cured PDMS to the patterned features on the substrate during soft-lithographic replication.

The values of the process parameters such as photoresist spinning rate and time, pre-exposure and post-exposure baking time, and development time are obtained from the data sheet of photoresist SU-8 50 according to the thickness of SU-8 50. The UV exposure time to cure the designed thickness of SU-8 50 photoresist is calculated using the Equation 5.1.

$$Exposure\,Time = \frac{UV\ dose\ to\ cure\ the\ designed\ thickness\ of\ SU8-50\ (mJ/cm^2)}{UV\ Intensity\ of\ exposure\ tool\ (mW/cm^2)} \quad (5.1)$$

The photolithography mask is designed according to the layout of the microchannels on the proposed electroporation device, which will be explained later in the chapter. In addition to SU-8 master, a new method is also developed to fabricate the master using adhesive tape. In the following section, the fabrication of the adhesive tape master is described in detail.

5.1.2 Fabrication of Master Using Adhesive Tape

Often the fabrication of the microfluidic devices by using the soft lithography is restricted to those who have access to a cleanroom for the fabrication of the photoresist master. In an adhesive tape master, instead of the photoresist, the adhesive tape attached on the glass slide is patterned manually using a scalpel. This method requires tools and materials that are readily available in a resource-limited lab such as glass slides, adhesive tape, scalpel, Petri dish, tweezers, and oven or hot plate. The fabrication of an adhesive tape master is shown in Figure 5.2.

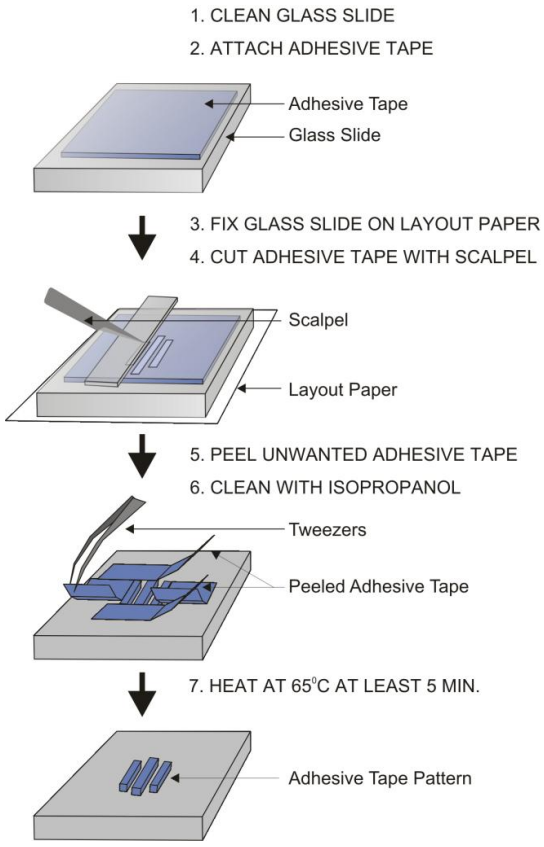

Figure 5.4 Fabrication of the adhesive tape master. The adhesive tape attached on the glass slide is cut according to the layout of the microchannels by using a scalpel. The glass slide with patterned adhesive tape structures without any chemical treatment is used as a master to fabricate the microchannels.

First, a strip of an adhesive tape (Scotch tape) is attached on a clean surface of the glass slide. The thickness of the adhesive tape determines the height of the microchannel. The height of the microchannels can be increased by attaching more than one layer of the adhesive tape as required. Next, the layout of the microchannels is printed on a regular paper using a printer and this layout page is then fixed on the flat surface. The glass slide with adhesive tape side facing up is aligned on the layout. The glass slide is fixed on the layout paper by attaching a piece of adhesive tape on the corners of the glass slide.

Then, the adhesive tape on the glass is cut according to the layout using a scalpel. Another glass slide is used as a ruler during cutting. The adhesive tape is removed from all regions of the glass slide except those in the layout of the microchannels. Lastly, the glass slide with the patterned adhesive tape is heated in an oven at 65°C for 5 minutes to improve the adhesion of the edges of the patterned adhesive tape to the glass substrate. At this point, the adhesive tape master is ready to be used as a master for soft-lithography without any further treatment.

Here, it is demonstrated that the patterned adhesive tape can be used (without the need of any chemical treatment) as a master for soft lithography yielding microfluidic devices with a uniform height of ~ 60 µm and width greater than 250 µm. Instead of manual scalpel cutting, a laser-cutting machine can be used to fabricate adhesive tape masters requiring higher precision. Adhesive tape masters have the following advantages:

- It is suitable to fabricate features above ~250 µm.
- It only requires bench top materials and tools.
- It does not require a cleanroom and photolithography.
- It is safe, as it does not use any chemical treatment.

- Unlike SU-8 master, the adhesive tape master is robust and reusable.
- This method is fast and extremely simple and inexpensive, costing $1 per device.

The adhesive tape master was helpful during the initial prototyping and evaluation in this research. It is a great educational tool and proven cell patterning technique.

5.1.3 Photolithography Mask for the Proposed Electroporation Device

In the previous chapter, the design of the proposed electroporation device is discussed based on the results of the simulation, the limit of the photolithography tool in use, the voltage required to operate the device and the requirements of the indium injection method. Accordingly, the mask is designed to fabricate the master for soft-lithography using the photolithography process described earlier in this chapter. The master is fabricated using the photolithography method since the proposed device has features less than 250 µm.

The layout of the photolithography mask for the proposed device is shown in Figure 5.5. This layout is drawn in a Corel Draw X4 graphics software and printed on the flexible transparent film using a high-resolution laser printer (outside vendor). Based on the results of the simulation, an array of five isolated electrode pairs with circular tips having radius of 50 µm and a width (E_w) of 100 µm is selected in this design. The neighboring electrode pairs are separated by a distance (g) of 100 µm. The electrodes and electroporation microchannels are separated by a distance of 15 µm.

The width of the electroporation microchannel (w) is 100 µm. This ensures that the cells are able to flow through the microchannel without experiencing the shear forces exerted by the microchannel walls. This mask is used to fabricate the proposed

electroporation device. According to this mask, the electrodes of the same pair are separated by a tip-to-tip distance (d) of 130 µm.

The master is fabricated using the process described Figure 5.6. This master has six identical layouts of the electroporation device shown in Figure 5.5. In three of the six layouts on the master, the separation between the electrodes of the neighboring electrode pairs is 50 µm, whereas it is 100 µm in the remaining three layouts. Two different separations between neighboring electrode pairs can be fabricated, which could be useful to study the effect of distance between neighboring pair of electrodes on electroporation of cells. Six layouts of the electroporation device on the master allow for the simultaneous fabrication of six devices, which decreases the fabrication time for the device.

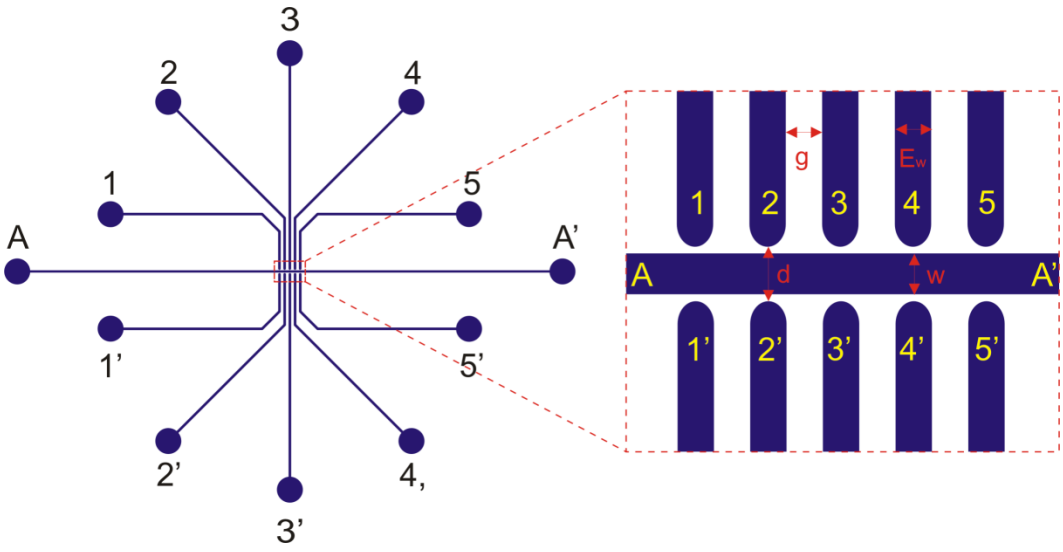

Figure 5.5 Photolithography mask of the proposed electroporation device. The proposed device has an electroporation microchannel A-A' with a width (w) of 100 µm and five pairs (1-1' to 5-5') of the circular tip electrodes with radius and width (E_w) of 100 µm. The separation between the neighboring electrodes pair is (g) 100 µm. The separation between the electroporation microchannel and electrodes (Pd) is 15 µm resulting in a total tip-to-tip separation (d) of 130 µm between the two electrodes of a same pair.

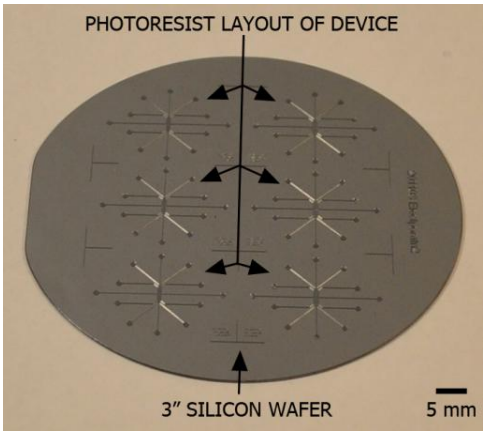

Figure 5.6 Master for soft lithography fabrication of the proposed device. Master has six identical layouts for the electroporation device. In three layouts, the separation between the neighboring electrode pairs (g) is 50 µm whereas it is 100 µm in the remaining three layouts. Six layouts allow for the simultaneous fabrication of six devices.

5.1.4 Fabrication of the Microchannel Device Using Soft Lithography.

The second step in the soft-lithography fabrication is the replication of the master by using a curable polymer. The thermally curable polymer Poly(dimethylsiloxane) PDMS is used to replicate the master. This polymer is transparent, biocompatible, easy to handle and hence widely used to fabricate the microfluidic devices for the cellular studies.

The step-by-step fabrication of a microchannel device using the soft-lithographic replication of the master (made of photoresist or adhesive tape) is shown in Figure 5.7. In this fabrication process, first the PDMS elastomer and its curing agent are mixed in 10:1 proportion by weight and degassed in a vacuum to obtain a bubble free mixture. This mixture is poured onto the master and again degassed in a vacuum to remove all the bubbles from the mixture poured onto the master.

The master covered with PDMS is then cured in an oven at 65˚C for 60 minutes since the high temperature accelerates the cross-linking rate in a PDMS polymer. After curing, the PDMS is peeled off the master. The peeled off PDMS with the microchannels

engraved on its surface is referred as the patterned PDMS stamp. The inlet holes are made using the suitable coring tool to the microchannels engraved in patterned PDMS stamp.

The patterned side of the PDMS stamp and the clean glass substrate are oxidized using air plasma and irreversibly sealed together. This seal is made strong by keeping the device in an oven at 65˚C for 10 minutes. The bonding method is simple and the seal in the PDMS/glass device is strong due to the bonding between two substrates without its features raised above the surface. As a result, the device can handle large pressure variation during the switching of the fluid flow inside the microchannels. In this way, a transparent microchannel device using biocompatible materials such as PDMS and glass is fabricated using the soft-lithography.

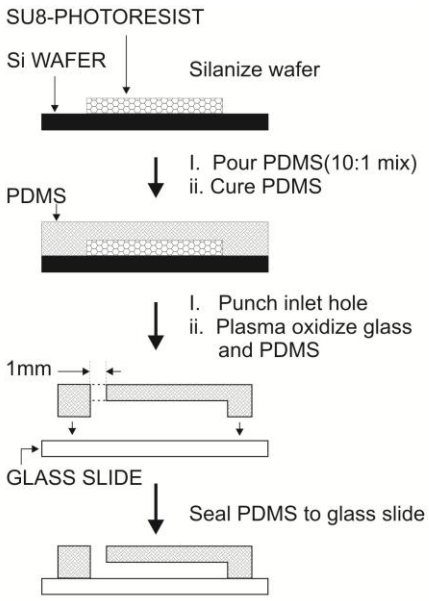

Figure 5.7 Fabrication of the microchannel device using soft-lithography. The master with a negative replica of the microchannels is replicated by thermally curable polymer PDMS. The patterned PDMS replica is bonded to the glass substrate after making the inlet and outlet holes. The PDMS glass device is transparent, biocompatible, and widely used in the study of cells.

5.2 Fabrication of 3D Electrodes

Unlike the conventional microfabrication approach, a new method is used to fabricate the microelectrodes integrated into the microfluidic device. In this new method, first the PDMS/glass device with high-aspect ratio microchannels is fabricated. In order to fabricate the high-aspect ratio 3D electrodes, the metal with a low melting point is injected inside the electrode microchannels of the device.

The PDMS is thermally stable below the temperature of 343°C [80]. Indium is selected as a metal to inject inside the electrode microchannels since it has a low melting point of 156˚C [81], which is below the temperature at which PDMS polymer degrades. In addition, the indium has a high conductivity [68] and is widely used as a solder metal.

The molten indium is injected inside the electrode microchannels by using the Autonomous Indium Injection Method discussed in the next chapter. The aspect-ratio of the fabricated 3D electrodes is the same as the aspect-ratio of the electrode microchannels. The electrode microchannels are fabricated by replicating a negative photoresist pattern on the master.

The negative photoresist SU-8 used in master fabrication is specially designed and optimized to allow the fabrication of a high aspect-ratio structure with vertical sidewalls. The injection of the molten indium inside the electrode microchannels does not depend on the aspect ratio of the electrode microchannels. As a result, the indium injection method makes it feasible to fabricate the high aspect ratio microstructure of the indium without using multistep photolithography and harmful chemicals. This method does not require an alignment of different layers.

5.2.1 Controlling the Thickness of PDMS Sidewalls

In order to fabricate the 3D electrodes using the Autonomous Indium Injection Method, electrode microchannels must be separated from the electroporation microchannel. This separation is essential to avoid the injection of the molten indium into the electroporation microchannel while it is being injected into the 3D electrode microchannels. Therefore, the electroporation microchannel in the proposed electroporation device is separated from the electrode microchannels present on either of its sides by the PDMS sidewalls with a width of ~15 μm.

In addition, the electrodes of the proposed electroporation device are made of indium which is a cytotoxic material. In the absence of PDMS sidewalls the electrodes will be exposed to the cell suspension inside the microchannel. After connecting to the voltage, indium electrodes will undergo reduction and oxidation reactions as the cell suspension act as electrolyte. As a result, the cell suspension will be contaminated by the indium ions released from the electrodes.

The exposure of cells to indium ions in the cell suspension can adversely affect the cell during electroporation. In the absence of PDMS sidewalls the exposure of cells to indium ions is inevitable. The PDMS sidewalls between the electrodes and electroporation microchannel prevent the contamination of the cell suspension with indium ions, and avoid exposure of cells to the indium ions. As a result, the PDMS sidewalls between the electrodes and electroporation microchannel are desirable. However, after fabrication of the electrodes by injecting the molten indium into the electrode microchannels, the PDMS sidewalls act as an insulator (dielectric constant ε_p

= 2.3) and attenuate the electric field before it reaches to the electroporation microchannel.

In order to understand the attenuation of the electric field inside the PDMS sidewalls, the proposed electroporation device with and without PDMS sidewalls between the electrodes and electroporation microchannel is modeled. In this modeling, the electric field generated by the 3D electrodes is observed using Finite Element Modeling (F.E.A.) tool COMSOL 3.5a. The electrodes of the device used in this modeling are separated by a distance of 130 μm and connected to 1V.

The schematic of the side view of the proposed device without PDMS sidewalls between electrodes and electroporation microchannel is shown in Figure 5.8a and the electric field generated inside the device is shown in Figure 5.8b. The schematic of the side view of the proposed device with PDMS sidewalls of thickness (P_d) 15 μm between electrodes and electroporation microchannel is shown in Figure 5.9a and the electric field generated inside the device is shown in Figure 5.9b. The comparison between Figure 5.8b and 5.9b shows that the electric field generated by electrodes inside the microchannel is decreased significantly due to the presence of PDMS sidewalls.

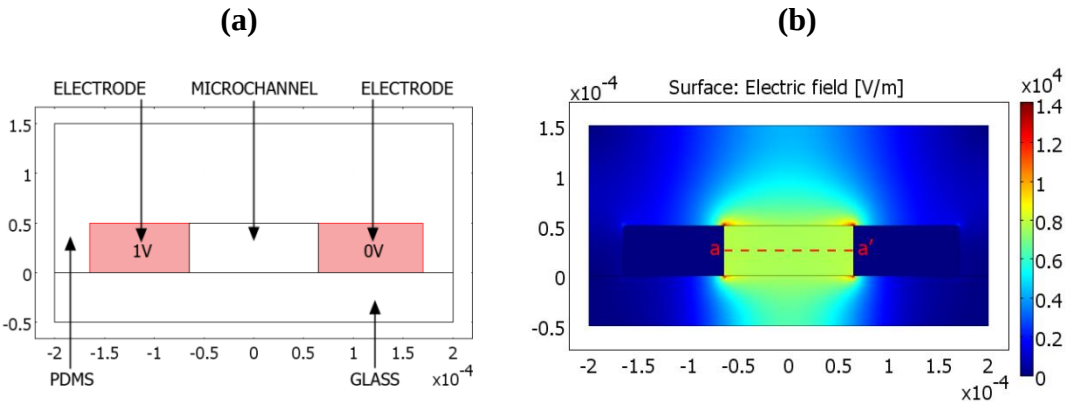

Figure 5.8 Electric field in device without PDMS sidewalls between electrodes and microchannel. a) The top view of the schematic of the electroporation device. b) Electric field generated inside the electroporation microchannel.

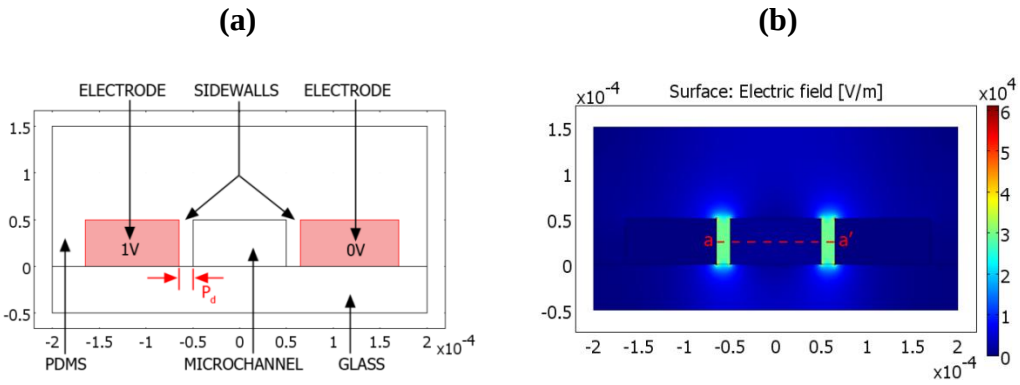

Figure 5.9 Electric field in device with PDMS sidewalls between electrodes and microchannel. a) The top view of the schematic of the electroporation device. b) Electric field generated inside the electroporation microchannel.

High voltage is required to generate the electric field for electroporation of cells in microchannel in the presence of PDMS sidewalls compared to no sidewalls. Therefore, the removal of the PDMS sidewalls is desirable in order to reduce the voltage required to operate the device. An attenuation of the voltage and the electric field inside the PDMS sidewalls depends on the thickness of the PDMS sidewalls.

In order to understand the dependence of the operating voltage on the thickness of the PDMS sidewalls, the relation between the voltage required and thickness of the PDMS sidewalls is derived as described below. During electroporation, the cells are suspended in either cell culture media or phosphate buffer solution having dielectric constants close to the dielectric constant of water 80 [82-84]. The cell suspension flows through the electroporation microchannels. Consequently, the space between the two electrodes consists of the PDMS sidewalls and/or cell suspension. In the proposed electroporation device, the electrodes are situated on either sides of the microchannel with a width W_c and separated from the microchannel by PDMS sidewalls with a thickness P_d. The separation between two electrodes (D_E) can be written as given in Equation 5.2.

$$D_E = 2P_d + W_c \tag{5.2}$$

In the absence of PDMS sidewalls (P_d = 0), the electric field generated by the electrodes propagates through the medium present inside the electroporation microchannel. The electric field generated by electrodes inside the microchannel when electrodes are connected to voltage (V_E) is given by Equation 5.3.

$$E_c = \frac{V_E}{D_E} = \frac{V_E}{W_c} \tag{5.3}$$

On the other hand, in the presence of PDMS sidewalls, the electric field generated by electrodes propagates in two mediums with different dielectric constants. These two mediums are the PDMS sidewalls with a dielectric constant (ε_p) of 2.3 and the medium present inside the electroporation microchannel with a dielectric constant (ε_c) of 80. In this case, the voltage applied between the two electrodes (V_E) is divided across the electroporation microchannel (V_c) and PDMS sidewalls (V_p) present on both the sides of electroporation microchannel. Therefore, the voltage applied to the electrodes can be written as given in Equation 5.4.

$$V_E = 2V_p + V_c \tag{5.4}$$

The electric field generated by electrodes inside the PDMS sidewalls and electroporation microchannel can be written as given in Equation 5.5.

$$E_p = \frac{V_p}{P_d} \quad \text{and} \quad E_c = \frac{V_c}{W_c} \tag{5.5}$$

At the boundary between the PDMS sidewalls and the electroporation microchannel, the electric field can be calculated by using the boundary condition of the electromagnetic field. Based on the electromagnetic field theory [85, 86], the relationship between the electric field generated by the 3D electrodes inside the electroporation microchannel (E_c) and the PDMS sidewalls (E_p) can be written as given in Equation 5.6.

$$\varepsilon_p E_p = \varepsilon_c E_c \tag{5.6}$$

After rearranging and substituting the parameters from Equation 5.5 in Equation 5.6, it can be written as given in Equation 5.7.

$$E_c = \frac{\varepsilon_p}{\varepsilon_c} E_p \qquad \Rightarrow \qquad V_c = \frac{\varepsilon_p}{\varepsilon_c} \frac{W_c}{P_d} V_p \tag{5.7}$$

After substituting the parameters from Equation 5.4 in Equation 5.7, it can be written as given in Equation 5.8.

$$V_c = \frac{\varepsilon_p W_c}{(2\varepsilon_c P_d + \varepsilon_p W_c)} V_E \qquad \text{and} \qquad V_p = \frac{\varepsilon_c P_d}{(2\varepsilon_c P_d + \varepsilon_p W_c)} V_E \tag{5.8}$$

The electric field inside the electroporation microchannel and the PDMS sidewalls can be written as given in Equation 5.9 by using Equations 5.5 and 5.8.

$$E_c = \frac{\varepsilon_p}{(2\varepsilon_c P_d + \varepsilon_p W_c)} V_E \qquad \text{and} \qquad E_p = \frac{\varepsilon_c}{(2\varepsilon_c P_d + \varepsilon_p W_c)} V_E \tag{5.9}$$

In order to verify above Equations 5.8 and 5.9, the proposed electroporation device with PDMS sidewalls of varying thickness is modeled using finite element analysis tool COMSOL 3.5a. In this modeling, a fixed distance of 130 μm between two electrodes is used and the thickness of the PDMS sidewalls (P_d) is increased from 0 μm to 15 μm in steps of 2.5 μm. As a result, the width of the electroporation microchannel (W_c) which is calculated using Equation 5.2 varies from 100 μm to 130 μm in steps of 5

μm. The height of the electroporation microchannel as well as the electrodes is 50 μm. The voltage across the PDMS sidewalls and microchannel when electrodes are connected to 1V calculated using Equation 5.8 and the simulation is given in Table 5.1. Similarly, the electric field generated by the electrodes inside the PDMS sidewalls and microchannel is calculated using Equation 5.9 and the simulation as shown in Table 5.2.

Table 5.1 Voltage across PDMS Sidewalls and the Electroporation Microchannel by Applying 1V Between the Electrodes of the Device

Thickness of PDMS sidewalls (μm)	**Voltage across PDMS sidewalls (V)**		**Voltage across channel (V)**	
	COMSOL	**Equation (5.9)**	**COMSOL**	**Equation (5.9)**
0	0	0	1.0	1.0
2.5	0.56	0.58	0.44	0.42
5	0.72	0.74	0.28	0.26
7.5	0.78	0.81	0.22	0.18
10	0.84	0.85	0.16	0.14
12.5	0.86	0.88	0.14	0.11
15	0.88	0.90	0.12	0.1

The dielectric constant of the cell suspension (ε_c=80) that flows in the microchannel during electroporation is ~34 times the dielectric constant of PDMS (ε_p = ~2.3). Equation 5.6 as well as Table 5.2 show that the electric field generated by the 3D electrodes inside the electroporation microchannel is ~34 times less than inside the PDMS sidewalls. The results of the simulation, Equation 5.8, and Equation 5.9, clearly show that PDMS sidewalls decrease the intensity of the electric field generated by electrodes inside the microchannel.

Table 5.2 The Intensity of an Electric Field Generated by Electrodes Inside PDMS Sidewalls and the Electroporation Microchannel by Applying 1 V Between the Electrodes of the Device

Thickness of PDMS sidewalls (μm)	Electric field in sidewalls (V/cm)		Electric field in channel (V/cm)	
	COMSOL	Equation (5.9)	COMSOL	Equation (5.9)
0			77	76.92
2.5	1118	1153.98	34	33.45
5	711	735.63	23	21.38
7.5	523	539.90	17	15.71
10	414	426.44	13	12.41
12.5	344	352.38	11	10.26
15	294	300.24	9	8.75

The voltage required to generate the same electric field inside the microchannel depends on the thickness of the PDMS sidewalls. Table 5.3 shows the voltage required to produce an electric field of intensity 1000 V/cm inside the electroporation microchannel by electrodes with 130 μm separation and the PDMS sidewalls of 0 to 15 μm on either sides of the microchannel. Thicker PDMS sidewalls require higher voltage than thin PDMS sidewalls. As a result, thinner PDMS sidewalls are desirable due to low operating voltage and isolation between cells and cytotoxic indium.

In the proposed electroporation device, given the limitation of the available photolithography tool for fabrication, the thickness of the PDMS sidewalls is selected ~15 μm. Therefore, the operating voltage requirement is 8.8 times the voltage required in the absence of the PDMS sidewalls. However, the operating voltage can be controlled after fabricating the electrodes by either complete removal or reduction in the thickness of the PDMS sidewalls. Instead of complete removal of the PDMS sidewalls after

fabrication of the electrodes, the thickness of the PDMS sidewalls can be controlled in order to decrease the operating voltage and prevent electrolysis of solution inside microchannel as well as the exposure of cells to the indium metal. The wet etching of the PDMS can be used to either remove or reduce the thickness of the PDMS sidewalls.

Table 5.3 Voltage Required to Generate Electric Field of 1000 V/cm Inside Microchannel Using Electrodes Separated by a Distance of 130 µm

Thickness of PDMS sidewalls (µm)	Voltage required to generates 1000 V/cm in microchannel (V)	Factor by which required voltage increased with PDMS sidewalls.
0	13	1
2.5	29.9	2.3
5	46.8	3.6
7.5	63.7	4.9
10	80.6	6.2
12.5	97.5	7.5
15	114.3	8.8

5.2.2 Wet Chemical Etching of PDMS Sidewalls

The high operating voltage of the electroporation device not only hinders the portability of the device but also increases the cost and the safety precautions. In order to operate the electroporation device with low voltage, it is necessary to either remove or reduce the thickness of the PDMS sidewalls after injecting the molten indium inside the electrodes microchannel. In this design, it is decided to remove or reduce the thickness of the PDMS sidewalls after the injection of the indium. The removal or reduction of thickness of the PDMS sidewalls is performed by using the wet chemical etching of the PDMS as explained in the following section.

The isotropic wet etching of PDMS [68, 87, 88] has been demonstrated by using a solution composed of tetrabutylammonium fluoride (TBAF) and N-methylpyrrolidinone (NMP) in a ratio of 1: 3 (v/v). It is important to note that the etching of the PDMS inside the microchannel is not feasible using any other process such as the dry etching of the PDMS [87] then wet etching. Wet chemical etching of the PDMS is used to remove or reduce the thickness of the PDMS sidewalls. This is performed by injecting the PDMS etching solution through the electroporation microchannel.

The etching solution is pumped through the electroporation microchannel with a flow rate of ~100 µl/min until the lateral PDMS sidewalls between the 3D electrodes and the microchannel disappear. It is experimentally determined that the flow rate of ~100 µl/min etches the PDMS sidewalls of the microchannel at a rate of ~3.4 µm/min. Immediately after the etching, the solution of N-MethylPyrrolidinone (NMP) is injected through the electroporation microchannel with the flow rate of ~10-50 µl/min. This is required to flush out the etching solution in order to stop the further etching of the PDMS. It also removes the partially etched PDMS along the sidewalls by dissolving it into the NMP solution.

The electroporation microchannel is cleaned to remove any contaminants before use. A 70% solution of ethanol in deionized (DI) water followed by pure DI water is then injected for 15 minutes in order to rinse and remove the leftover NMP solution from the microchannel. The complete electroporation device is also sterilized with the 70% ethanol solution followed by DI water before use.

CHAPTER 6

FABRICATION METHOD AND ITS CHARACTERIZATION

This chapter provides a detailed description of the Autonomous Indium Injection Method used to fabricate the 3D electrodes of the proposed electroporation device. First, the process of indium injection into the microchannel in order to fabricate the electrodes and the physics behind this process are explained. Then the characterization of indium injection method is discussed.

In characterization, the parameters that control the injection of indium into the microchannels are investigated. Numerous experiments are performed to study the effects of different process parameters such as magnitude and duration of the applied vacuum on the performance of the Autonomous Indium Injection Method. The results of these experiments are used to determine the optimum values of these process parameters necessary to fabricate the metal microstructures. Lastly, the fabrication of the metal as well as the polymer microstructures using the proposed injection method is demonstrated.

6.1 Autonomous Indium Injection Method

In the previous chapter, the fabrication of 3D electrodes for the high yield electroporation of cells by injecting the molten indium inside the high-aspect-ratio electrode microchannels is described in detail. The process by which the molten indium is injected into the microchannel using a vacuum is described with the help of a flowchart shown in Figure 6.1. This process requires the microchannel device to have an inlet to each electrode microchannel. The microchannel with only an inlet and no outlet is referred as a

dead end microchannel. The fabrication of this device is explained in the previous chapter.

In the indium injection method, the microchannel device with a single inlet to each microchannel is first placed on the flat surface of a hot plate. A piece of indium metal with a volume much larger than the volume of the microchannel that is to be filled is placed on the inlet in such a way that the indium covers the inlet completely. The device on the surface of the hotplate is covered with the vacuum enclosure. The vacuum enclosure is connected to the vacuum pump by using a hosepipe, and the vacuum pump is turned ON to apply the vacuum.

After 20 minutes, the hot plate is set to 170˚C without discontinuing the vacuum. The indium on the inlet of the microchannels is melted within 3-5 minutes after the hotplate has reached the set temperature. 30 minutes after applying the vacuum, the vacuum is released and the vacuum enclosure is removed to bring the device to atmospheric pressure. The molten indium on the inlet flowing inside the microchannels of the device is observed with the naked eye while the device is on the hotplate. The molten indium inside the microchannel is determined to cease flowing by visual confirmation. The device is removed from the hotplate as soon as the flow of indium inside the microchannels is found to have completely stopped. The molten indium filled device is allowed to cool to room temperature in order to solidify the indium. After cooling, the solidified excess indium on the inlet can be removed; if required.

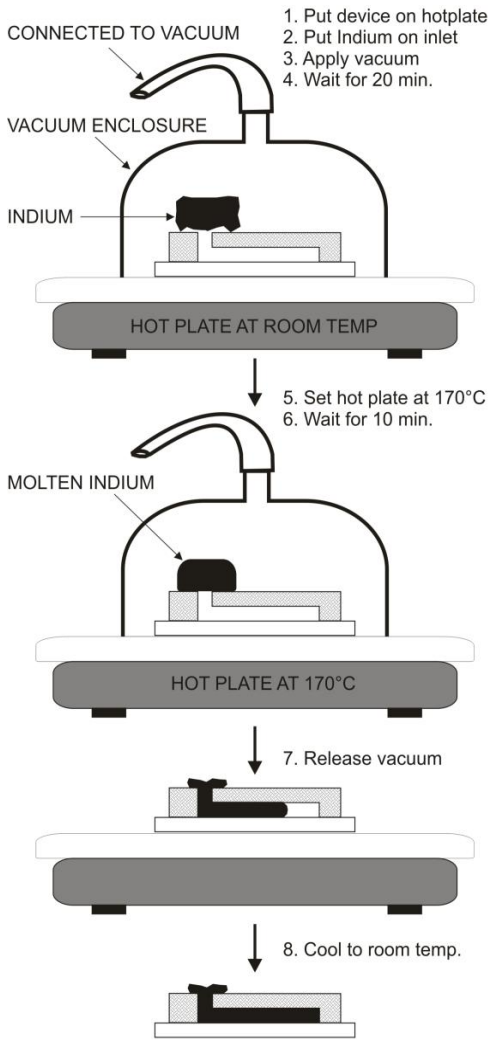

Figure 6.1 Schematic of the autonomous indium injection process. The molten indium flows autonomously inside the microchannel of the device when the vacuum is released. It uses a vacuum to inject the molten indium inside the dead microchannels until the end. The method is suitable to fabricate the high-aspect-ratio metallic microstructures integrated inside the PDMS devices.

Unlike the co-fabrication method explained in chapter 3, this method injects the molten indium inside the microchannels autonomously without the need for manual application of positive/negative pressure at the microchannel outlet. Therefore, we called this method the Autonomous Indium Injection Method.

This method is safe, as it does not require any chemical process to inject the molten indium. It is simple and can be performed in any resource-limited laboratory by the user regardless of their background and prior knowledge of the microfabrication process. It takes less than 35 minutes to inject the molten indium inside the microchannels regardless of their shapes and interconnection complexity. Therefore, the method is rapid and suitable for mass fabrication.

The method injects the molten indium inside the microchannels without outlets and hence is capable of filling indium in dead end microchannels. It is useful to fabricate the electroporation device with a high density of electrodes embedded into the PDMS device, which is desirable to decrease the electroporation time. In general, this method is suitable to fabricate high-density and high-aspect-ratio microstructures made of a low melting point metal embedded into the PDMS device.

6.2 Principle of Autonomous Indium Injection Method

The surface tension of the molten indium is ~560 dynes/cm [89], which is much higher than the surface tension of water ~72 dynes /cm [90]. As a result, an external force is required to push the molten indium inside the PDMS/glass microchannel. Also due to high surface tension, indium does not wet (stick to) the PDMS microchannel walls. The modification of the surface of the PDMS walls using chemical treatment called silanization is necessary in order to reduce the surface free energy of the PDMS walls and make them wettable to the molten indium. During the process of silanization, the surface of the PDMS microchannels is exposed to the vapors of (3-Mercaptopropyl) Trimethoxysilane inside the chamber under vacuum.

In the co-fabrication method [74, 75], the molten indium on the inlet is inserted inside the microchannel by applying the vacuum at the outlet, manually using a syringe. The co-fabrication method requires the silanization of the PDMS microchannels to make them wettable to the molten indium. The need for an inlet and outlet to the microchannel, silanization and manual application of negative pressure at the outlet of the microchannel by using a syringe are problems associated with the use of the co-fabrication method.

The permeability of a material is defined as the ability of a material to allow the passage or diffusion of other materials through it. The PDMS allows the passage or diffusion of a gas, while blocking vapors and liquids. This is a very remarkable property of the PDMS and is called gas permeability [91]. We used the gas permeability of the PDMS and the vacuum to overcome the problem associated with the currently used co-fabrication method.

In order to fabricate the 3D electrodes of our device using the Autonomous Indium Injection Method as previously described in Figure 6.1, the microchannel device is kept in the vacuum. The applied vacuum removes the air out of the device using two different mechanisms shown in Figure 6.2. The air inside the microchannel is first removed through the inlet as shown in Figure 6.2, using blue lines. Simultaneously, the air molecules inside the PDMS material are removed because of the gas permeability as shown in Figure 6.2, using red lines.

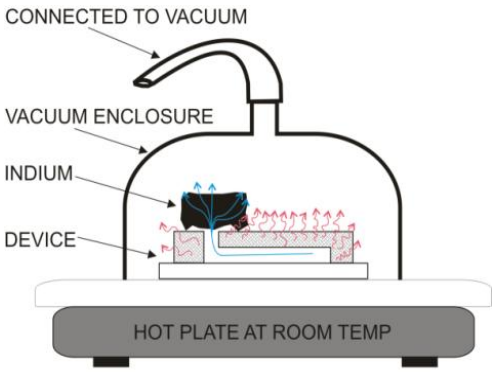

Figure 6.2 Illustration of the air molecules removed out of the PDMS microchannel device. The vacuum removes the air molecules from the microchannel (blue lines) as well as the PDMS sidewalls (red lines) due to the gas permeability of the PDMS and creates negative pressure inside both the microchannel and its walls.

The removal of air from the microchannel and the air molecules from the PDMS stops when the pressure inside the microchannel and PDMS becomes equal to the applied vacuum pressure. While the device is under vacuum, indium on the inlet of the microchannel melts and seals the microchannel completely. The molten indium on the inlet isolates the region inside the device (microchannel) from the region outside of the device (inside of the vacuum enclosure).

As long as the device is under vacuum, the pressure (vacuum) in both regions remains the same. When the vacuum is released, the region outside of the device is exposed to the atmospheric pressure but the region inside the device remains at vacuum pressure. The pressure gradient between the external atmospheric pressure and the internal vacuum pressure causes the flow of molten indium from higher to lower pressure. Therefore, the molten indium on the inlet of microchannel starts to flow inside the microchannel from the region of high pressure (inlet) to region of low pressure (inside microchannel).

As the molten indium flows inside the microchannel and fills it, the volume of the empty microchannel (V) decreases. In case the microchannel is made of a gas non-permeable material such as glass, the decrease in the volume of the empty microchannel (V) results in an increase in the pressure inside the empty microchannel (P) which can be explained by the ideal gas law as given in Equation 6.1.

$$PV = nRT = \text{Constant}_{\text{(at constant temperature of the gas } T\text{)}} \tag{6.1}$$

Therefore, in the case of a glass microchannel, indium flowing inside the microchannel stops when the pressure inside the microchannel becomes equal to the pressure outside of the device, i.e. atmospheric pressure. This is demonstrated with the help of an experiment in which a 64 mm long glass microchannel with a diameter 1.5 mm is filled with molten indium using the Autonomous Indium Injection Method. The result of filling the glass microchannel is shown in Figure 6.3 and clearly indicates that a microchannel made of gas non-permeable material cannot be filled to its end by using the Autonomous Indium Injection Method. On the other hand, due to the gas permeability of PDMS, the applied vacuum creates negative pressure not only inside the microchannels but also inside the walls of the PDMS microchannel. As a result, the ideal gas law given in Equation 6.1 is not applicable to the PDMS microchannel.

In the PDMS microchannel, the additional negative pressure inside the PDMS walls generates a pressure gradient between the inside and outside of the microchannel to maintain the flow of indium. Therefore, the molten indium continues to flow without stopping inside the microchannel until it reaches the other end of the microchannel. There the physical boundary wall of the microchannel stops the flow. This is verified with the

help of an experiment in which the molten indium is filled inside a 64 mm long PDMS microchannel with a width of 1.5 mm and height of 50 µm using the Autonomous Indium Injection Method. The result of this experiment as shown in Figure 6.4 clearly indicates that unlike the glass microchannel, the microchannel made of a gas permeable material such as PDMS can be filled to its end using the Autonomous Indium Injection Method.

In addition, the vacuum inside the PDMS walls holds the molten indium in place near the wall until it solidifies and retains its position. This avoids the need for surface modification by silanization. Eventually under atmospheric pressure, the air molecules removed from the PDMS diffuse back into it and PDMS comes back to an equilibrium state. Therefore, as soon as the indium flow stops the device is cooled to room temperature at atmospheric pressure before the air diffuses back into the PDMS. The solidification of indium before air molecules diffuse back into the PDMS is necessary in order to avoid space between solidified indium and walls of the microchannel.

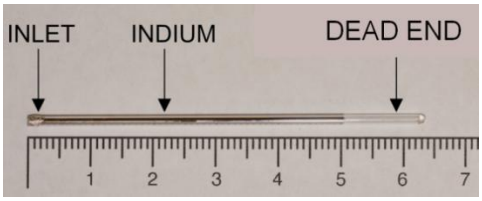

Figure 6.3 Glass microchannel (capillary) filled with the molten indium. The molten indium is filled inside a glass capillary with a diameter of 1.5 mm by applying a 16.93 kPa vacuum for 30 min. The indium does not fill the glass microchannel to its end, as glass is not permeable to gas.

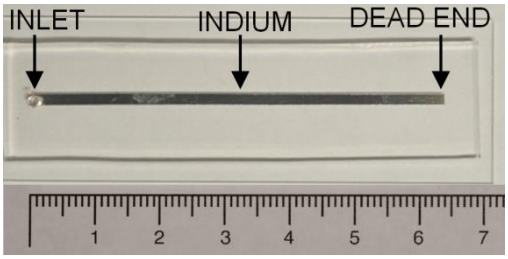

Figure 6.4 PDMS microchannel filled with the molten indium. The molten indium is filled in a PDMS microchannel of a width of 1.5 mm by applying a 16.93 kPa vacuum for 30 min. The indium is able to fill the PDMS microchannel to its end, as PDMS is permeable to gas.

The results of PDMS microchannel and glass capillary filling with indium, shown in Figure 6.3 and 6.4 indicates that the Autonomous Indium Injection Method relies on the gas permeability of the PDMS. The gas permeability of the PDMS plays a critical role in 1) filling the molten indium to the end of the channel and 2) preventing the creation of a void space between the solidified indium and walls of the microchannel without using silanization. This proves that the Autonomous Indium Injection Method cannot fill the molten indium inside the microchannel to its end, if the microchannels are not made of a gas permeable material such as PDMS.

6.3 Characterization of Autonomous Indium Injection Method

An important performance parameter of the Autonomous Indium Injection Method is the smallest width of a microchannel that can be filled with the molten indium using this method. This section describes the determination of the smallest width of a microchannel that can be filled with indium using the Autonomous Indium Injection Method and investigation of the factors that control the smallest width. The method uses a vacuum to overcome the high surface tension of the indium and inject it inside the microchannel by using the gas permeability of PDMS.

The molten indium on the inlet of the microchannel is subjected to atmospheric pressure upon releasing the vacuum. The negative pressure that is created inside the microchannel and PDMS walls by applied vacuum is less than the inlet pressure. As a result, the atmospheric pressure on the inlet causes the flow of indium inside the microchannel. This indicates that the applied vacuum is responsible for the flow of indium inside the microchannel.

In order to characterize the indium injection method, experiments are performed to find out how the magnitude and the duration of the applied vacuum affect the smallest width of the microchannel that the method can fill. In these experiments, the molten indium is injected into two different types of the microchannels present on the same device: 1) Fixed width microchannels and 2) Varying width microchannels.

The width of a rectangular microchannel is fixed from end to end. These microchannels have dimensions: length 11.6 mm, height ~23um, and width varying from 20um to 1000um. The various widths of these rectangular microchannels are 20, 40, 60, 80, 100, 150, 200, 250, 300, 400, 500, 600, 700, 800 and 1000 μm.

The width of the triangular microchannel linearly decreases from its wide end to the sharp end. The triangular microchannels shown in Figure 6.5 are used as the varying width microchannels. The molten indium is injected simultaneously into all the microchannels through an inlet hole of 1 mm made at one end of each microchannel. The inlet hole is made at the broad width end of the triangular microchannels. A vacuum of 16.93 kPa is applied for 30 minutes to inject the molten indium into the microchannel.

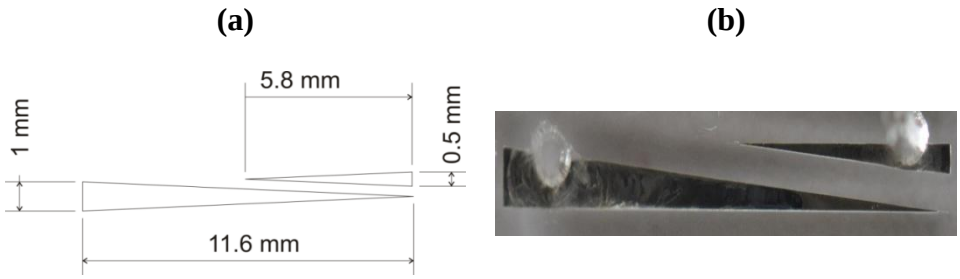

Figure 6.5 Variable width triangular microchannels. a) Layout of triangular microchannels with a width that vary from one end to the other. b) Triangular microchannels filled with the molten indium through a single inlet at the broad end using the Autonomous Indium Injection Method.

The results of this experiment show that the PDMS microchannels with a width of 40 µm and above are completely filled as shown in Figure 6.6. The rectangular microchannels filled with the indium are observed under the microscope and no empty spaces are found anywhere inside the microchannels. This experiment is repeated at least 5 times to test reproducibility of the indium injection. The indium filling is found consistent and reproducible in all the experiments.

However, the microchannel with a width of 20 µm always remained unfilled, as the indium does not flow in it. In addition, the sharp ends of the triangular microchannels are found empty when observed under a microscope. The results of this experiment prove that the Autonomous Indium Injection Method can fill microchannels with a width of 40 µm and above with 100% reproducibility. This experiment also revealed that the smallest width of the microchannel that can be filled using our method is somewhere between 20 µm to 40 µm. The experiments discussed in the following section are used to further determine how the magnitude and the duration of the applied vacuum affect the smallest width of the microchannel that method can fill.

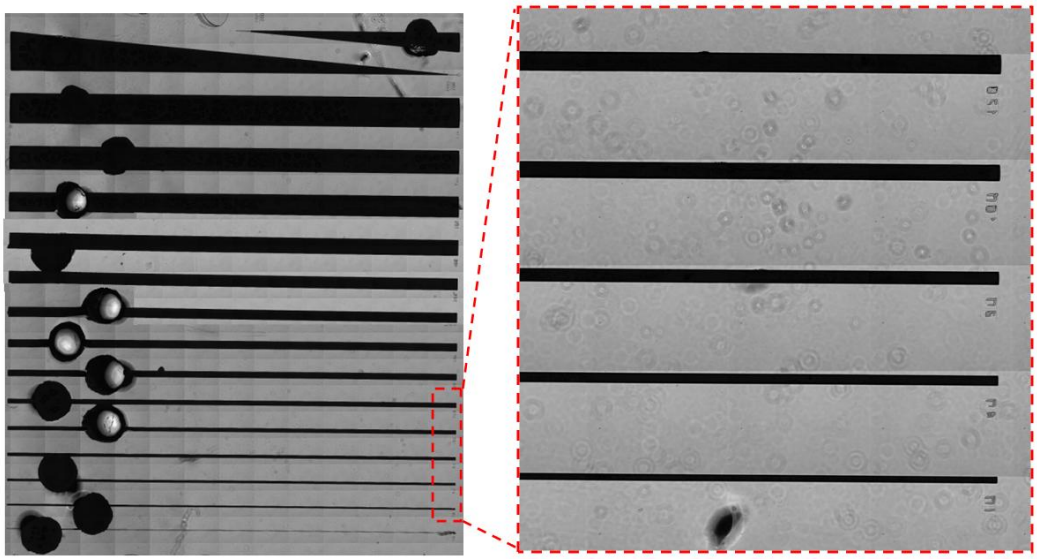

Figure 6.6 Rectangular microchannels filled with the molten indium. The molten indium is filled inside the microchannels with widths varying from 20 µm to 1000 µm, through the inlet of each microchannel by applying a 16.93 kPa vacuum for 30 min. The method repeatedly fills the indium in a microchannel with a width of 40 µm and above, without any empty space.

6.3.1 Dependence on Magnitude of Applied Vacuum

In this section, the experiments used to find the relation between the width up to which the indium can be filled in the triangular microchannel and the magnitude of the applied vacuum is discussed. In this experiment, the molten indium is injected inside the triangular microchannels by applying a vacuum with two different magnitudes for 20 min.

The first set of three identical triangular microchannels are filled with indium by applying 16.93 kPa vacuum for 30 minutes. Then, the second set of three similar microchannels is filled with the molten indium by applying a 33.86 kPa vacuum for 20 minutes. The ends of the indium filled triangular microchannels are observed under the microscope and the width of the triangular microchannel where the indium has stopped is measured using a microscope. Indium filled triangular microchannels, one from each set

of microchannels filled by applying a 16.93 kPa and 33.86 kPa vacuum, are shown in Figure 6.7 along with their magnified sharp ends.

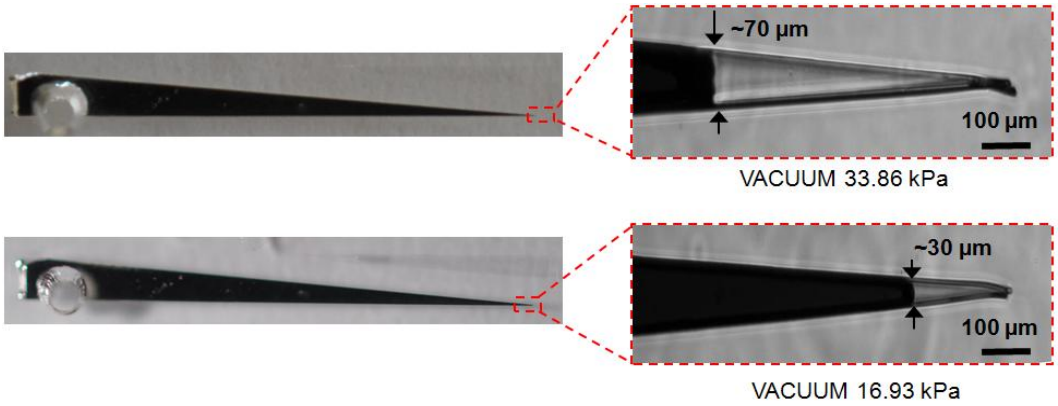

Figure 6.7 Triangular microchannels filled with indium using vacuums of different magnitudes. The high vacuum (16.93 kPa) injected indium inside the microchannel to a width of ~30 µm, whereas the low vacuum (33.86 kPa) injected indium inside the microchannel to a width of ~70 µm. The high vacuum injects the molten indium inside the microchannel to a narrower width than the low vacuum.

Figure 6.7 shows that neither the 16.93 kPa nor the 33.86 kPa magnitude of the vacuum filled the molten indium inside the microchannel completely to its end. However, the 16.93 kPa (high) vacuum filled the microchannel to a width of ~30 µm, which is narrower than the width ~70 µm filled by the 33.86 kPa (low) vacuum. This experiment shows that the high vacuum is able to inject the indium inside the narrower microchannel further than the low vacuum. It is clear that the magnitude of the applied vacuum decides the width of the microchannel up to which the molten indium can be injected by using the Autonomous Indium Injection Method. The strong vacuum is necessary to fill the molten indium inside the narrow microchannels. Consequently, we used a 16.93 kPa vacuum to fabricate the 3D microelectrodes.

6.3.2 Dependence on Duration of Applied Vacuum

In the previous experiment, it is observed that the indium could not flow inside a triangular microchannel beyond a certain width depending upon the magnitude of the applied vacuum. The width of the triangular microchannel where the indium flow stops in the triangular microchannel is referred to as the limiting width for the applied magnitude of the vacuum. The experiments are performed to test whether the width of the microchannel where the molten indium stops depends on the duration for which the vacuum of a certain magnitude is applied. In these experiments, triangular microchannels are filled with the molten indium by applying a 16.93 kPa vacuum for varying durations of 1 to 60 minutes. The end of the indium filled triangular microchannels is observed under a microscope, and the width where the indium stopped inside the microchannel is measured.

In each experiment, a set of three triangular microchannels are filled with indium by using the same magnitude and duration of the applied vacuum. The average width is obtained by averaging the width where indium stopped in three microchannels of a given set. This process is repeated for the other sets of the microchannels by changing the duration of the applied vacuum from 1 to 60 minutes. The average width where indium stops inside the triangular microchannel filled by applying a 16.93 kPa vacuum for varying durations of 1 to 60 minutes are measured and given in Table 6.1.

The relationship between the average width where the indium stops in the triangular microchannel and the duration of the applied vacuum is plotted in Figure 6.8. This plot shows that the average unfilled length and hence the limiting width remains almost constant when the vacuum is applied for more than or equal to 20 minutes. The

plot also shows that the average width of the microchannel filled by applying a 16.93 kPa vacuum for 3 minutes is 48.4 µm, which is higher than the average width of microchannels filled by applying a vacuum for any other duration in the range of 1 to 60 minutes. This might have occurred due to a change in the magnitude of the applied vacuum without notice.

From this experiment, it is clear that the width where the indium flow stops in a triangular microchannel is independent of the duration of the applied vacuum. The results of this experiment also suggest that a minimum 20-30 minutes application of the vacuum is desirable to inject the molten indium in a microchannel up to the limiting width of the applied vacuum of 16.93 kPa.

Table 6.1 Average Width Where Indium Stops Inside the Triangular Microchannel Filled by Applying a 16.93 kPa Vacuum for Varying Durations (the width where the indium stops in each of three microchannels of one set is measured and the average of the three widths from the same set is called average width of that set)

Duration of applied vacuum (min)	Avg. width of three triangular microchannels where indium stops (µm)
1	38.1
3	48.4
5	30.1
9	31.8
15	32.1
20	30.5
28	32.9
41	32.2
50	30.4
60	30.0

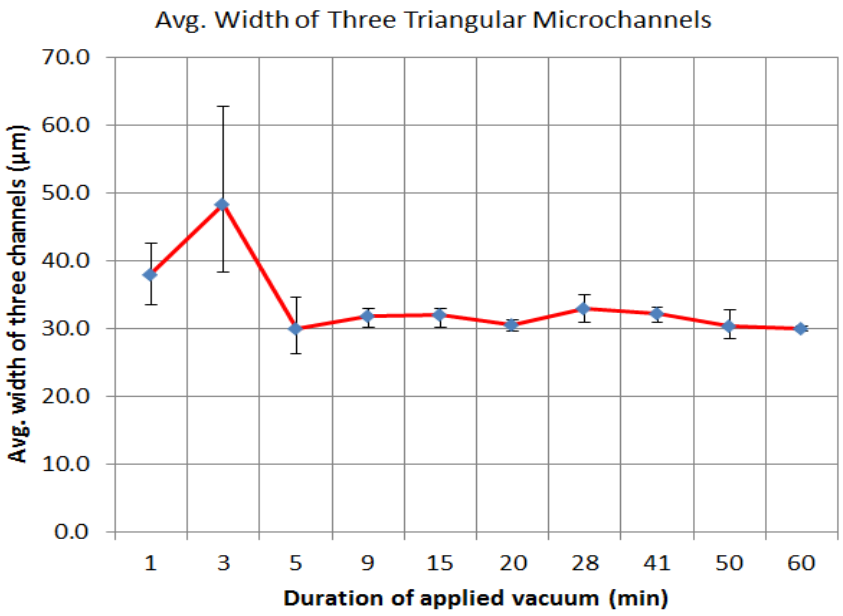

Figure 6.8 Relationship between the duration of the applied vacuum and the average width where indium stops in the triangular microchannel. The molten indium is injected in a set of three microchannels by applying a 16.93 kPa vacuum for a duration varying from 1 to 60 min. The variation in the average width is small when indium is injected by applying the vacuum for 20 min and above. Errors are calculated by subtracting average width of three microchannels from the lowest and the highest width from that respective set of three microchannels.

6.3.3 Dependence on Surface Tension of Microchannel Walls

In the Autonomous Indium Injection Method, the applied vacuum causes the indium to flow inside the microchannel despite its high surface tension. Therefore, the effect of the surface tension and width of the microchannel where indium stops in the triangular microchannel is investigated with the help of experiments. The experiments are performed to fill the triangular microchannels of low and high surface tension with molten indium using the Autonomous Indium Injection Method. The triangular microchannels are silanized by exposing them to the vapors of (3-Mercaptopropyl) Trimethoxysilane in vacuum in order to reduce the surface tension between the PDMS and the indium. The silanized microchannels are referred to as low surface tension

microchannels. On the other hand, the triangular microchannels without any silanization are referred to as high surface tension microchannels.

The molten indium is injected inside the low and high surface tension microchannels by applying a vacuum of 16.93 kPa for 30 minutes. The experiments are repeated with a set of three low surface tension and three high surface tension triangular microchannels to confirm the reproducibility. One microchannel filled with indium from the set of low and high surface tension microchannels along with the magnified view of the unfilled ends is shown in Figure 6.9. The results of these experiments given in Figure 6.9 shows that the width where the molten indium stopped in the microchannels with low and high surface tension is ~30 µm. This indicates that indium injection in the microchannel using the Autonomous Indium Injection Method is not affected by change in the surface tension of the microchannel. Consequently, the molten indium stopped at approximately the same width in both low and high surface tension microchannels.

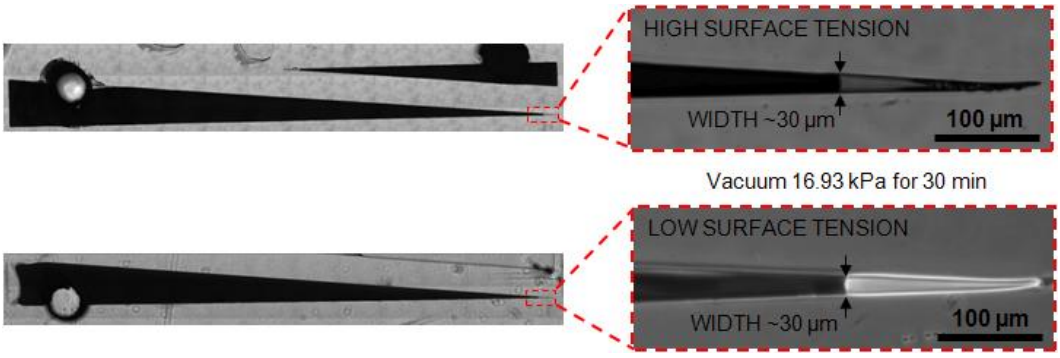

Figure 6.9 Triangular microchannels with low and high surface tension filled with the molten indium. Molten indium is injected up to a width of ~30 µm in both the microchannels by applying a 16.93 kPa vacuum for 30 min. Meniscus of indium inside the microchannel with low surface tension is different from the microchannel with high surface tension due to the modification in surface tension between the indium and the PDMS. Silanization does not improve the injection of the indium in the microchannels.

It is important to note that the meniscus of the indium filled in the microchannel with low surface tension is different from that of the microchannel with the high surface tension due to differences in surface tension. This experiment shows that silanization modifies the surface tension but it does not improve the molten indium injection inside the microchannels using the Autonomous Indium Injection Method. It can therefore be concluded that the performance of the Autonomous Indium Injection Method is unaffected by silanization. As a result, unlike the current co-fabrication method, the Autonomous Indium Injection Method does not require silanization and thus avoids the use of hazardous chemicals.

6.3.4 Dependence on Long Term Vacuum

So far, the characterization experiments revealed that the Autonomous Indium Injection Method can inject the molten indium up to a width of ~30 μm in the triangular microchannels by applying a 16.93 kPa vacuum for durations of 30 minutes. The duration of the applied vacuum as well as the modification in the surface tension by silanization, independently, cannot inject the molten indium inside the microchannels of a width less than 30 μm. An experiment is performed in order to examine the possibility of injecting the molten indium beyond the limiting width of ~30 μm in the triangular microchannels.

In this experiment, the molten indium is injected inside the silanized and unsilanized triangular microchannels by applying a 16.93 kPa vacuum for durations of 30 minutes, 6 hours, and 24 hours. In this way, the combined effects of using a long-term duration vacuum and modification surface tension on the injection of the indium inside

the microchannels is studied simultaneously. The experiment is repeated at least three times to confirm all the observations.

The results of these experiments are given in Figure 6.10, which shows the magnified view of the ends of the triangular microchannels filled with the molten indium. The limiting width where the indium flow stopped inside the triangular microchannel is measured by observing the ends of the microchannel under microscope. Figure 6.10 shows that the method injects the indium in unsilanized triangular microchannels up to a width of 30 to 34 μm by applying the vacuum for 30 minutes, 6 hours, and 24 hours. This indicates that the injection of molten indium inside the unsilanized triangular microchannels is independent of the duration of the applied vacuum. Figure 6.9 shows that the molten indium is injected in silanized triangular microchannels up to a width of ~23 μm by applying 16.93 kPa for duration of 24 hours. This suggests that the injection of the molten indium in the triangular microchannels is improved by simultaneously applying silanization and long-term vacuum.

However, the improvement in the minimum width that can be filled is very small compared to the efforts required in silanization and the time required for filling the microchannel. The performance of the proposed method using 30 minutes of the vacuum without silanization is better than the long-term vacuum with silanization. In conclusion, neither long-term vacuum, nor silanization significantly improves the indium filling inside the microchannels compared to short-term vacuum without silanization. The use of a 16.93 kPa vacuum for 30 minutes is optimal for injecting the molten indium in the microchannel using the Autonomous Indium Injection Method. Finally, we conclude that

the Autonomous Indium Injection Method can be used to inject the molten indium inside the PDMS microchannels with widths of ~30 μm and above reproducibly.

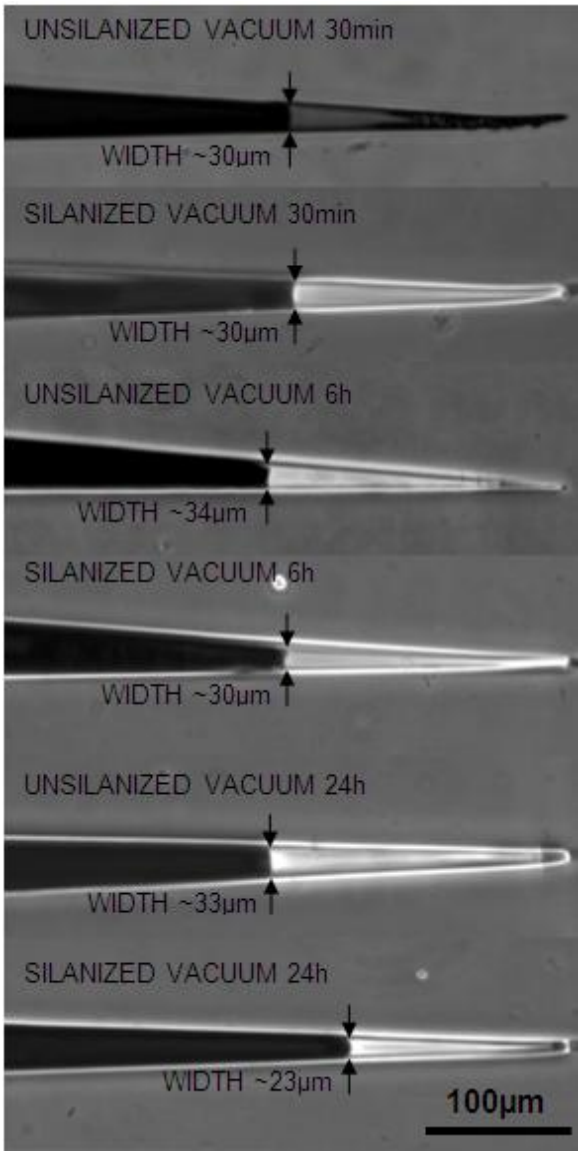

Figure 6.10 Triangular microchannels filled with indium by applying the short and long term vacuum. The proposed method is used to inject the molten indium in silanized and unsilanized microchannels by applying a 16.93 kPa vacuum for durations of 30 min, 6 hrs, and 24 hrs. Long-term duration vacuum does not significantly affect the indium injection in the silanized or unsilanized microchannels.

6.4 Fabrication of Complex Microstructure of Metal and Polymer

The current co-fabrication method is not suitable to inject the molten indium in a complex network of microchannels and dead end microchannels. It is important to note that in all the experiments discussed so far, the molten indium is injected in dead end microchannels through the inlet of the microchannel. In addition to this the ability of the Autonomous Indium Injection Method to inject the molten indium in a complex network of interconnected dead end microchannels is accessed in the following experiments.

The proposed method is used to inject indium in a device having a complex network of interconnected dead-end microchannels of widths 45 µm. The microchannel device with indium filled in complex interconnected network of dead-end microchannels is shown in Figure 6.11.

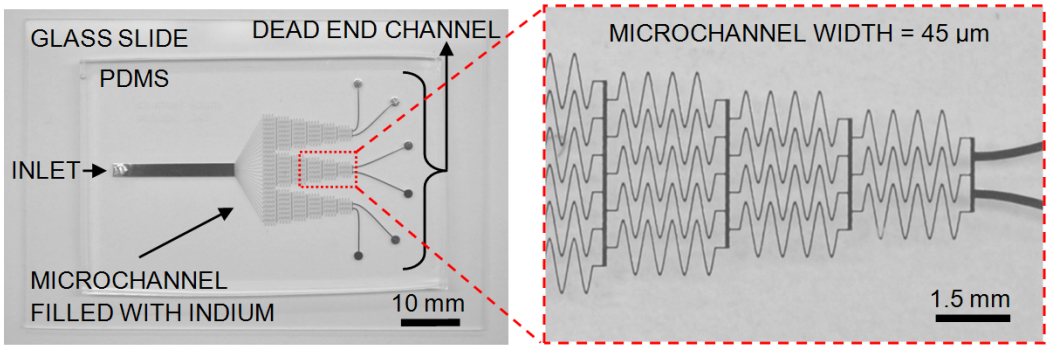

Figure 6.11 PDMS microchannel device filled with indium. Molten indium is injected into a complex interconnected network of microchannels with dead ends by using the proposed method. Dead end microchannels are filled completely without empty spaces by applying a 16.93 kPa vacuum applied for 30 min.

The observation of the device under the microscope shows that the indium is filled in all the microchannels without empty space anywhere as can be seen in a magnified view of Figure 6.11. This demonstrates that the proposed method injects the

molten indium in not only a complex network of interconnected microchannels but also in any dead end microchannels of a width greater than or equal to 30 μm using only the inlet.

In cell culture studies, it is often required and desirable to inject the viscous liquid such as a gel inside the microchannel or capillary [92]. Injecting high viscous liquid inside the microchannel is difficult due to a high capillary pressure inside the microchannel or capillary. In addition to molten indium, the Autonomous Indium Injection Method is also compatible with other viscous as well as non-viscous liquids. This is demonstrated with the help of an experiment in which both low viscous liquids such as water ink and high viscous liquids such as liquid PDMS are injected inside the complex network of interconnected dead-end microchannels.

The PDMS microchannel device filled with red PDMS in a complex interconnected network of dead-end microchannels is shown in Figure 6.12. Similarly, the microchannels of the same device are also filled with water ink, which are not shown here. The observation of red PDMS filled microchannels under the microscope showed that the red PDMS is filled in all the microchannels without any empty space to be found anywhere in the microchannels, as can be seen in the magnified view in Figure 6.12. This shows that the proposed method can also be used to fill the microchannel with other materials, which either are in liquid form or can be brought to liquid form by applying a temperature less than 300˚C. These materials include but are not limited to viscous liquid PDMS, water ink, indium, metal and alloys with melting points less than 300˚C. Unlike the indium, other materials such as water ink or color PDMS are in liquid form and do

not require heating to melt them as they are already in liquid form. This further simplifies the proposed method by replacing the hot plate with a flat top surface.

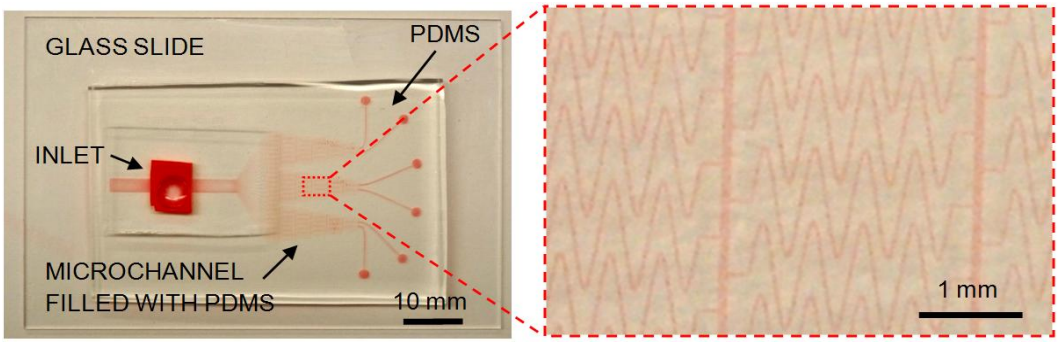

Figure 6.12 PDMS microchannel device filled with color PDMS. Highly viscous material such as the PDMS mixed with red oil color is injected in the complex interconnected network of microchannels with dead ends by using the proposed method. Dead end microchannels are filled completely without empty spaces by applying a 16.93 kPa vacuum applied for 30 min. The proposed method is compatible with other materials such as viscous color PDMS.

6.5 Theory Behind the Results of Characterization

Based on the Young-Laplace Equation [93, 94], the capillary pressure which is defined as the pressure difference at the meniscus of liquid flowing inside the rectangular microchannel is given by Equation 6.2. In this equation, σ is the surface tension of the liquid, θ is the contact angle between the walls of the microchannel and the curvature of the meniscus of the liquid, w is the width and h is the height of the rectangular microchannel as shown in Figure 6.13. Equation 6.2 shows that the capillary pressure inside the microchannel depends on the dimension of the microchannel and the surface tension between the liquid and walls of the microchannel.

$$P_c = 2\sigma \cos\theta \left(\frac{1}{w} + \frac{1}{h} \right) \tag{6.2}$$

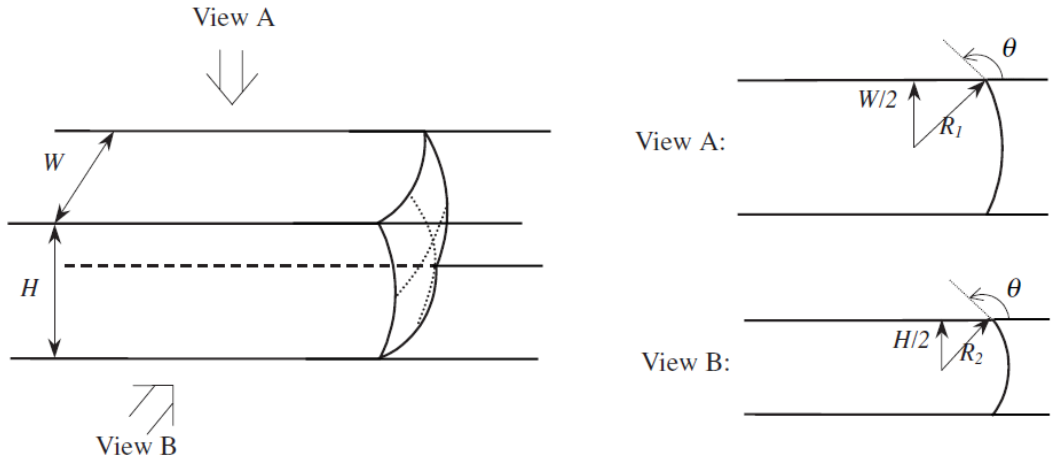

Figure 6.13 Schematic of the meniscus of liquid flowing inside the rectangular microchannel [93]. Top view A shows the curvature of the meniscus in terms of the contact angle and the width and side view B shows the curvature of the meniscus in terms of the contact angle and the height of the microchannel.

In order for the liquid to flow inside the microchannel, the pressure acting on the liquid at the inlet must be greater than the capillary pressure inside the microchannel [95] that opposes flow. When the pressure acting on liquid at the inlet of the microchannel is greater than capillary pressure, it pushes the liquid through the microchannel towards the low pressure region [93, 95, 96]. This results in the flow of liquid through the microchannel from high to low pressure ends. As a result, there is a threshold pressure gradient [93, 95] required in order to flow liquid through the microchannel from the higher pressure end to the lower pressure end. This threshold pressure gradient is equal to the capillary pressure inside the microchannel.

It is clear from Equation 6.2 that the capillary pressure increases with a decrease in the width of the microchannel if the surface tension, contact angle and height of the

microchannel are constant. This indicates that a higher pressure gradient is required to allow the flow of liquid in a narrower microchannel than a wider microchannel.

In characterization experiments, it is found that the flow of indium inside the microchannel stops before it reaches the end of the microchannel. The flow of indium inside microchannels filled by applying vacuums of magnitude 33.86kPa and 16.93 kPa stops at ~70 µm and ~30 µm width of the triangular microchannels respectively. This shows that the width of the triangular microchannel where indium stops inside the microchannel depends on the magnitude of the vacuum used to fill the microchannel.

In all experiments, the molten indium on the inlet is exposed to atmospheric pressure (P_{inlet}) equal to 101 kPa when the vacuum is released. The threshold pressure gradient required to inject the molten indium in dead-end microchannels is created by applying a vacuum as given by Equation 6.3.

$$\begin{aligned} \Delta P &= P_{inlet} - P_{microchannel} = P_{inlet} - Vacuum \\ \Delta P &= (P_{inlet} - Vacuum) \geq P_c \qquad \Rightarrow \qquad Vacuum < P_c \end{aligned} \tag{6.3}$$

The capillary pressure, threshold pressure gradient, and pressure inside the microchannel required for injecting the molten indium inside the microchannel of a width of 30 µm and 70 µm is calculated using Equation 6.2 and 6.3. In this calculation the contact angle is assumed to be zero for simplification. The analytical values of the vacuum required to inject the molten indium inside the microchannels are compared with the experimental values as shown in Table 6.2 and graphically shown in Figure 6.14.

Table 6.2 Vacuum Required to Inject Molten Indium Inside Triangular Microchannels of Different Widths

w **(μm)**	h **(μm)**	σ **(mN/m)**	P_c **(kPa)**	ΔP **(kPa)**	P_{inlet} **(kPa)**	$P_{microchannel} = Vacuum$ **(kPa)**	
						$P_{inlet} - P_c$	**Experiment**
30	23	0.56	88.24	88.24	101	12.76	16.93
70	23	0.56	66.90	66.90	101	34.01	33.86

Table 6.2 shows that the theoretical magnitudes of the vacuum required to inject the molten indium inside the microchannel of a width of 30 μm and 70 μm are close to experimental values. In all the experiments performed during characterization, the measurements of width of microchannels, height of microchannels and applied vacuum are not free of error. The difference between experimental and theoretical values in Table 6.2 can be justified by considering the 10 % errors in all measurements.

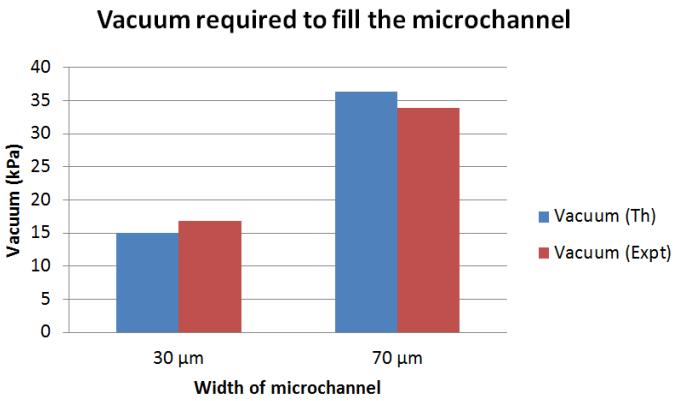

Figure 6.14 Vacuum required for filling microchannels of different widths. Experimental and theoretical magnitudes of vacuum required for injecting the molten indium inside the microchannel up to a width of 30 μm and 70 μm differs by a small magnitude.

In characterization experiments, it is also found that the width where indium stops in triangular microchannels is not affected by modification of the surface tension of indium. However, Equation 6.2 and 6.3 show that the width where indium stops in triangular microchannels depends on the surface tension of indium. So far, the exact amount by which surface tension of indium is modified by using silanization process is unknown.

Therefore, there exist two possibilities for discrepancy in theoretical and experimental observation related to surface tension. First, the change in surface tension due to silanization is very small and causes small change of width which cannot be measured. Second, the difference in width where indium stops in the microchannel due to modification of surface tension is less than the error in measurement of width. In this way, characterization results suggest that after considering the experimental as well as measurement errors, the injection of molten indium using the Autonomous Indium Injection Method can be explained by the Young-Laplace equation.

6.6 Conclusions of the Chapter

In conclusion, the Autonomous Indium Injection Method injects the molten indium in a microchannel irrespective of their aspect ratio by using a vacuum. The method uses the gas permeability of PDMS material and traps the vacuum to pull the molten indium inside the microchannel to its end. This method does not require silanization and can inject the molten indium in a microchannel fabricated by using a gas permeable material such as PDMS. The smallest width of a microchannel in which the molten indium can be injected using the proposed method depends on the magnitude of the applied vacuum. It

is independent of the duration of the applied vacuum and surface tension of the microchannel walls. The method can inject indium in a microchannel up to a width of ~30 μm and above by applying a vacuum of 16.93 kPa for 30 minutes.

The method is also compatible with other materials that can be converted to the liquid phase by melting so long as their melting point is less than 300˚C. The method is autonomous, inexpensive, and simple to adapt by biologists or other researchers without prior knowledge of microfabrication since it only requires a hotplate and vacuum source. It is safe, fast, inexpensive and suitable for mass fabrication of disposable and portable electroporation devices. The method can be used to fabricate the flexible electronic circuits, flexible interconnections and 3D metallic microstructure used as MEMS components. The method can also be used to fabricate 3D patterns of biopolymers for tissue engineering and cell biology applications.

CHAPTER 7

EVALUATION OF PROPOSED DEVICE

In this chapter, the proposed electroporation device is tested in order to estimate its usability to be used as an electroporation device. Chapter 5 explains in detail the need for removal of the PDMS sidewalls. In this chapter, the fabricated device is first tested for the removal of the PDMS sidewalls. Next, the effect of an applied electric field on the cell is studied with the help of finite element modeling. Lastly, the effects of storage conditions on the device and its electrodes are studied in order to determine the expiration time for the device.

7.1 Testing of Removal of PDMS Sidewalls of the Device

The high yield electroporation device fabricated using the method described in the above sections is shown in Figure 7.1. This device has five pairs of 3D electrodes with circular tips exposed in an electroporation microchannel. The electroporation microchannel on the device has an inlet and an outlet in order to inject the cell suspension during electroporation of cells. Indium solidified on the inlet after filling microchannels will be used as a connection pad to connect the voltage supply to the 3D electrodes.

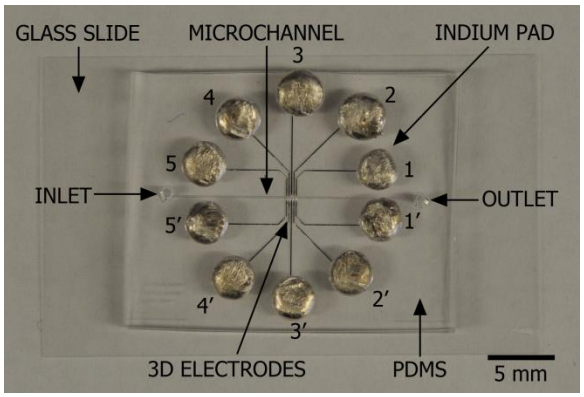

Figure 7.1 The fabricated proposed electroporation device. PDMS/glass device has five isolated 3D electrode pairs (1-1' to 5-5') and a microchannel with an inlet and an outlet to inject the cell suspension for electroporation. 3D electrodes can be connected to the voltage supply using indium pads.

In order to perform the evaluation of the fabricated device, the continuity between the two electrodes of a pair is verified. In this evaluation, 3D electrode pair 3-3' is connected to the voltage source in series with a light emitting diode (LED) as shown in Figure 7.2a. The voltage supply is set at 2 V and phosphate buffer solution (PBS) is injected through the electroporation microchannel. The phosphate buffer acts as a conducting solution and connects the two electrodes of the 3D electrode pair 3-3' inside the microchannel. As a result, the current flows though the circuit shown in Figure 7.2a.

The light emitting diode becomes a forward bias and glows as shown in Figure 7.2b, which indicates that the circuit is closed and current flows through the phosphate buffer solution. This is only possible if the PDMS sidewall between the electrodes and electroporation channel is completely removed, exposing the electrodes inside the microchannel. The presence of PBS solution between the electrodes connects the two electrodes and closes the path for current to flow inside the circuit.

Similarly, the continuity between other electrode pairs is also verified by connecting the LED to other electrode pairs one by one. In this way, it is verified that the

electrodes are exposed inside the electroporation microchannel and there exists continuity between them when the microchannel is filled with conducting solution such as the PBS. This proves that the device is working and the 3D electrodes will generate an electric field inside the microchannel when the electrodes are connected to a voltage supply during the process of electroporation.

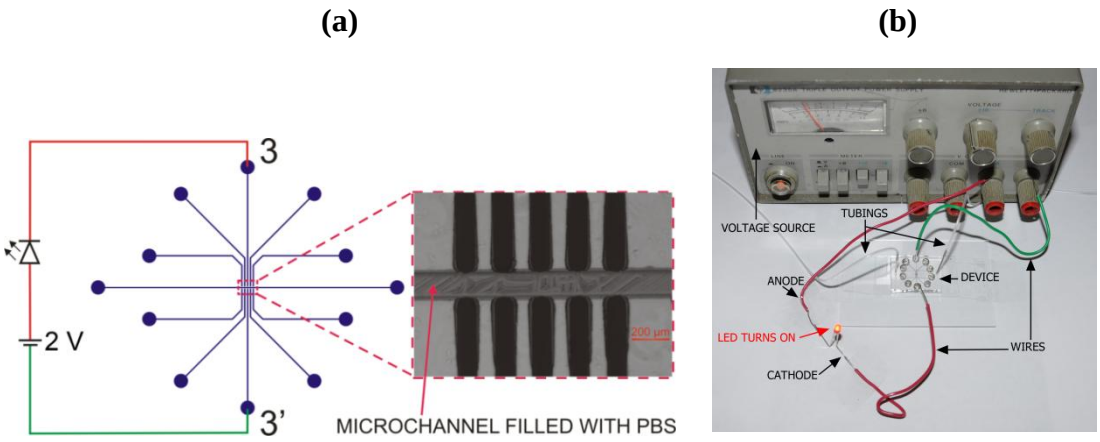

Figure 7.2 Testing of high yield electroporation device. a) Schematic showing the connection between voltage source, electrode pair (3-3'), and LED. b) High yield electroporation device is connected to voltage source showing the continuity between two 3D electrodes of a pair (3-3'). The phosphate buffer solution is injected through the microchannel. PBS connects two electrodes of a pair (3-3') and current flows in a closed circuit through PBS solution. LED is ON showing that the 3D electrodes are exposed in PBS solution and generate electric field when connected to the voltage source.

7.2 Modeling of the Cell in the Proposed Electroporation Device

The modeling of the proposed electroporation device containing a single cell in the electroporation region is performed in order to verify the interaction between biological cells and the electric field generated by electrodes of the proposed device. This modeling is limited to two dimensions (2D) and is performed by using finite element analysis COMSOL 3.5a. In order to simplify the modeling, the portion of the proposed

electroporation device having a pair of circular tip electrodes with a radius 50 µm is used in this modeling.

Figure 7.3 shows the top view schematic of the proposed device used in this study. In this device, the electrodes are present on either side of the 100 µm wide electroporation microchannel separated by 5 µm thick PDMS sidewalls. The cell is present inside the electroporation microchannel as shown in Figure 7.3. The circular shape of the biological cell is assumed to further simplify the modeling of the cell. The radius of the cell is assumed to be 10 µm whereas the thickness of the cell membrane is assumed to be 10 nm. Other electrical parameters of the cell are assumed as mentioned in Table 1 [97-99].

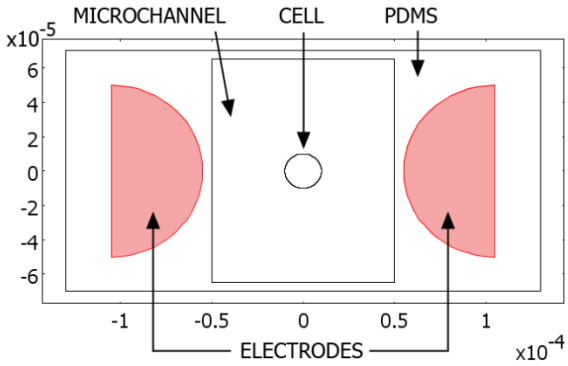

Figure 7.3 Schematic of the top view of the electroporation device with cell. The cell with a radius 10 µm and membrane thickness 10 nm is present inside the 100 µm wide microchannel. The 15 µm thick PDMS sidewalls separate the circular tip electrodes with a radius 50 µm from the electroporation microchannel.

Table 7.1 Electrical Parameters of the Cell Used in Order to Model the Effects of an Electric Field on the Living Cell Inside the Microchannel of the Proposed Electroporation Device

Electrical parameter of biological cell	**Assumed Value**
Radius of cell	10 μm
Thickness of the cell membrane	10 nm
Permittivity of region inside the cell	60
Permittivity of region outside the cell	80
Permittivity of cell membrane	7
Conductivity of the cytoplasm	0.3 S/m
Conductivity of the cell membrane	3×10^{-7} S/m
Conductivity of extracellular solution	5.5×10^{-6} S/m
Charge density on membrane surface inside the cell	-2×10^{-4} C/m^2
Charge density on membrane surface outside the cell	2×10^{-4} C/m^2

The concentration of ions such as Na^+, K^+ and Ca^+ inside the cell is different from their concentration outside of the cell. In this model of the cell, the difference between concentrations of ions inside and outside of the cell is mimicked by applying a suitable boundary condition on the inner and outer surfaces of the cell membrane. A surface charge density of magnitude -2×10^{-4} C/m^2 on the inner side and 2×10^{-4} C/m^2 on the outer side of the cell membrane is assigned to represent the difference in concentration of ions inside and outside the cell. The difference between concentrations of ions is responsible for setting up the transmembrane potential across the thin cell membrane [100]. The transmembrane potential generates an electric field across the cell membrane. In this study, the device is first modeled without applying any external potential to the electrodes. The results of this modeling are shown in Figure 7.4a-c.

(a) **(b)** **(c)**

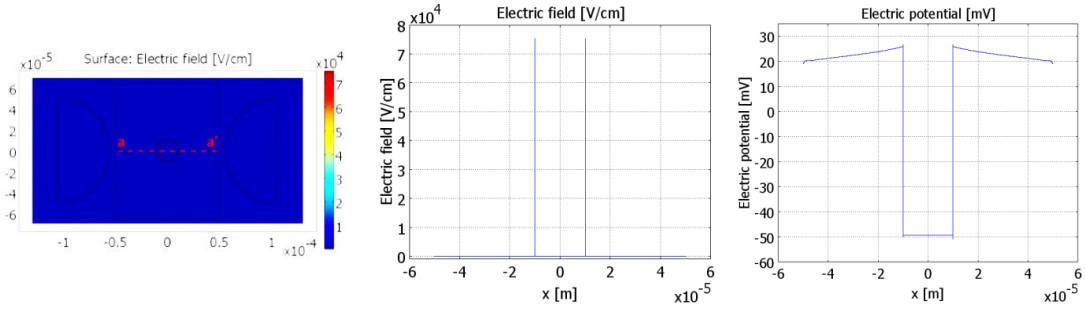

Figure 7.4 Electric field inside device with cell before applying external voltage to the electrodes. a) Electric field inside the device b) Electric field across the cell membrane along the red dotted line a-a' c) Voltage across the cell membrane along the red dotted line a-a'.

Figure 7.4a shows the electric field inside the device. In the absence of external voltage, the electric field is found to be zero everywhere except across the cell membrane, which is not visible in Figure 7.4a due to its small dimension of 10 nm. The plot of electric potential and electric field across the cell membrane along the red color dotted line a-a' is shown in Figure 7.4b and Figure 7.4c. These figures show that in the absence of an external potential, the cell has its own transmembrane potential of magnitude ~75 mV. This transmembrane potential sets up an electric field of magnitude 7.5x 10^4 V/cm as shown in Figure 7.4c.

These modeling results match with conventional values for the transmembrane potential and the electric field across the cell membrane [101]. Next, an external voltage with a magnitude 65 V is applied to the electrodes of the electroporation device and again performed in the same study. The electrode on the left in Figure 7.3 is connected to 65 V, whereas the electrode on the right is connected to the ground potential. The applied external potential generates an electric field inside the device as shown in Figure 7.5a. An

external electric field generated by electrodes interacts with the cell and modifies the electric field as well as the transmembrane potential across the cell from their values in the absence of an external electric field.

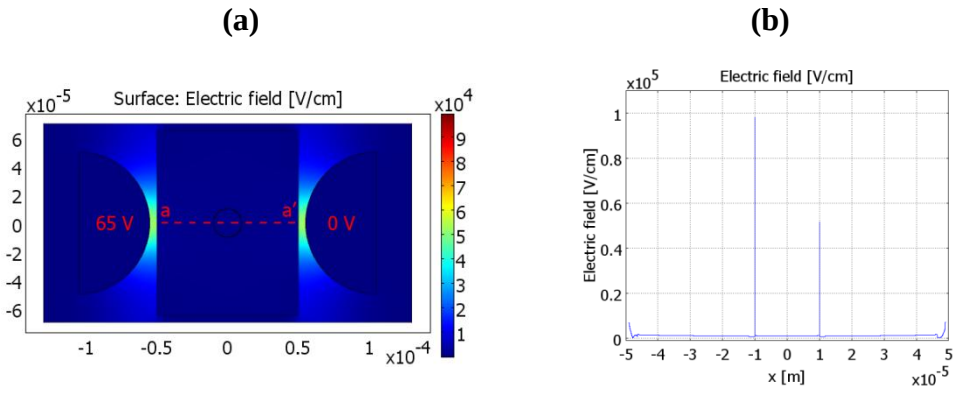

Figure 7.5 Electric field inside the device with cell after applying an external voltage to the electrodes. a) Electric field inside the device b) Electric field across the cell membrane along the dotted line a-a' shown in red color.

Figure 7.5b shows the modification of the electric field across the cell membrane due to the external electric field [45]. The electric field across the cell membrane close to the positive electrode is increased from 7.5 x 10^4 V/cm to 9.8 x 10^4 V/cm. On the other hand the electric field inside the cell membrane close to the ground electrode is decreased from its value 7.5 x 10^4 V/cm to 5.2 x 10^4 V/cm. These results show that the external electric field modifies the electric field across the cell membrane by a magnitude of 2.3 x 10^4 V/cm.

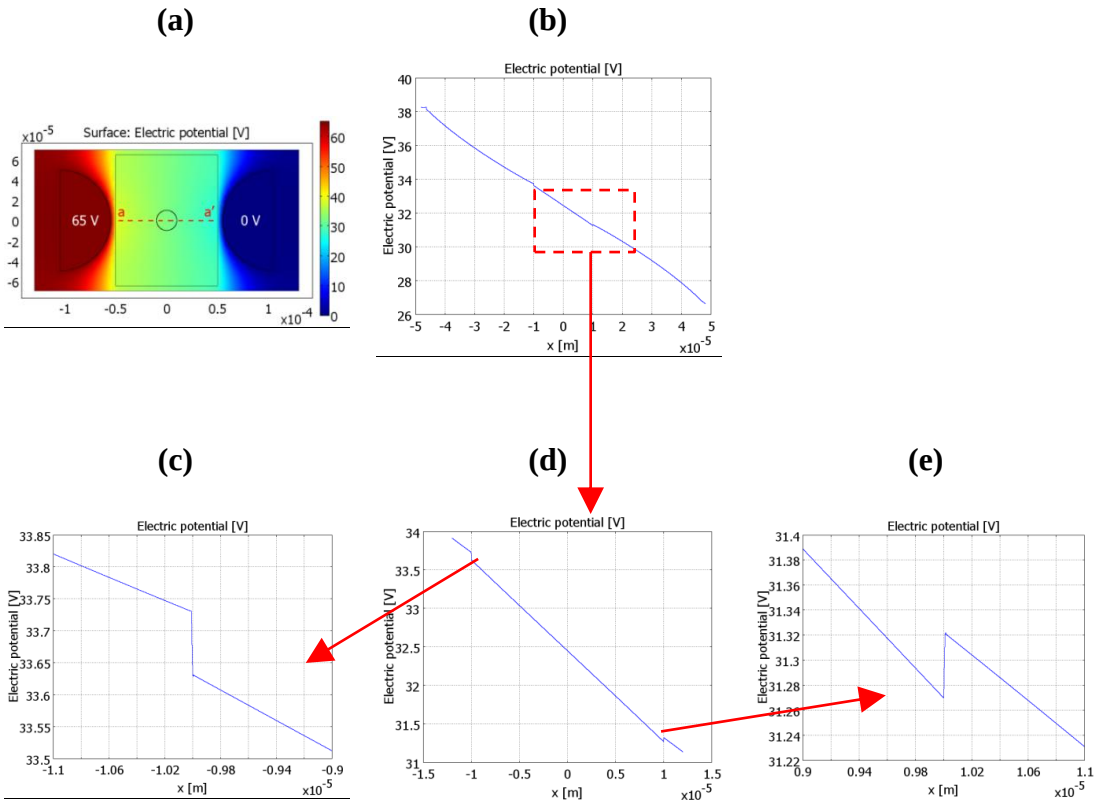

Figure 7.6 Voltage distribution inside the device and cell after applying external voltage to the electrodes. a) Voltage distribution inside the device. b) Voltage plotted along red dotted line a-a'. c) Voltage plotted across the cell membrane inside the region close to the electrode connected to positive terminal (65 V). d) Voltage plotted across the cell inside the device. e) Voltage plotted across the cell membrane inside the region close to the electrode connected to negative terminal (0 V).

The interaction between the cell and the electric field generated by electrodes inside the microchannel of the device also modify the transmembrane potential [45] across the cell membrane, as shown in Figure 7.6(a-e). Figure 7.6a shows the distribution of voltage inside the device and the cell. The voltage distribution inside the microchannel and the cell along the red dotted line a-a' is plotted in Figure 7.6b. This plot shows that the voltage inside the microchannel as well as the cell varies linearly between the electrodes. The region of plot in Figure 7.6b indicated by red dotted rectangle is magnified and shown in Figure 7.6d which shows the discontinuity in voltage distribution

inside the cell membrane. The voltage across the cell membrane close to the electrode connected to the 65 V and 0 V is further magnified and shown in Figure 7.6c and Figure 7.6e, indicated by the respective red arrows. Figure 7.6c shows that the voltage difference across the membrane towards the electrode connected to 65 V is changed from 75 mV to 100 mV.

On the other hand, Figure 7.6e shows that the voltage difference across the membrane towards the electrode connected to 0 V is changed from 75 mV to 50 mV. These plots show that the voltage across the cell membrane is modified by a magnitude of 25 mV due to an interaction between the cell and the electric field generated by the electrodes inside the microchannel of the proposed device. This indicates that the proposed device is capable of modifying the transmembrane potential of the cell located inside the microchannel of the device. The result of the above modeling shows that the proposed device is capable of modifying the electric field, and hence the transmembrane potential across the cell membrane by means of external voltage connected to the electrodes of the device. As a result, this device is capable of performing the electroporation of the cell by applying external voltage.

7.3 Expiration Testing of Fabricated Device

The 3D electrodes of the proposed electroporation device are embedded inside the PDMS polymer. The electrodes are made of indium metal. The device will be exposed to the environmental storage conditions before use. In order to understand the effect of storage conditions on the device and its electrodes, the expiration testing of the device is performed. In this experiment, it is assumed that the devices before use will be stored at

room temperature and in sealed form. As a result, the devices will be subjected to the pressure inside the packaging and room temperature.

In this testing experiment, a vacuum of magnitude 33.86 kPa and a temperature of 100 °C are used to mimic the aggravated storage conditions. For this test, three devices are fabricated simultaneously and their combined weight is measured. Their combined weight is found to be 14.7162 g, which is measured using the weighing scale (Devon Instrument) capable of measuring weights as low as 0.0001 g. A picture of these devices, 30 minutes after fabrication and before the start of experiment is shown in Figure 7.7a. Inside the electroporation microchannel, the cell will be close to the electrodes of the device in the electroporation region between the electrode pairs. Therefore, the electrodes of the device in the electroporation region are carefully observed under a microscope during the expiration experiment.

The electrodes in the electroporation region of one of the three devices under test are shown in Figure 7.8a. After imaging, within 30 minutes of fabrication, all devices are kept on a hot plate at 100 °C. The devices on the hotplate are covered with a sealed enclosure connected to a vacuum of magnitude 33.86 kPa. The devices are kept on the hot plate without disturbing the applied vacuum and the temperature for seven days. After seven days, the vacuum is released and all of the devices are removed from the hotplate. The devices are kept at room temperature for 15 minutes in order to cool them, and then weighted once more. The combined weight of the three devices after the experiment is found to be 14.7162 g. The combined weight of the devices before and after the experiment is found to be the same. This indicates that the aggravated storage condition used during the expiration experiment did not affect the devices for seven days.

To further examine the effect of the aggravated storage conditions on the devices under test, pictures of all devices in these experiments are taken, as shown in Figure 7.7b. A careful observation of Figure 7.7a and Figure 7.7b shows that the devices under testing conditions remained unaffected by the aggravated storage conditions mimicked during the experiment. Similarly, after seven days under aggravated storage conditions, the electrodes in the electroporation regions of all of the devices under test are carefully observed under a microscope.

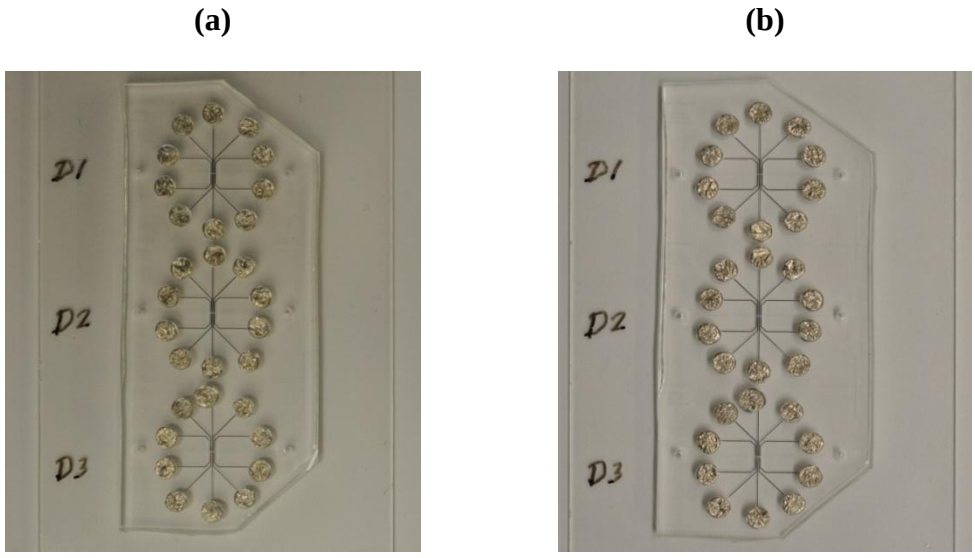

Figure 7.7 Expiration testing of the fabricated electroporation devices. a) Three devices before applying the expiration test. b) Same three devices after the expiration test. The visual inspection of devices before and after expiration testing shows no change.

The electrodes in the electroporation region of the device are shown in Figure 7.8a. Figure 7.8b shows the same electrodes after seven days in experiment. The visual inspection of Figure 7.8a and Figure 7.8b shows that the electrodes in the electroporation region of the device are not affected by the aggravated storage conditions. The results of the expiration testing experiments show that the weights of the devices as well as the

electrodes in the electroporation region of the devices are not affected by storage conditions. Therefore, long term storage of the proposed electroporation devices before use is possible without causing any damage to the electrodes of the device.

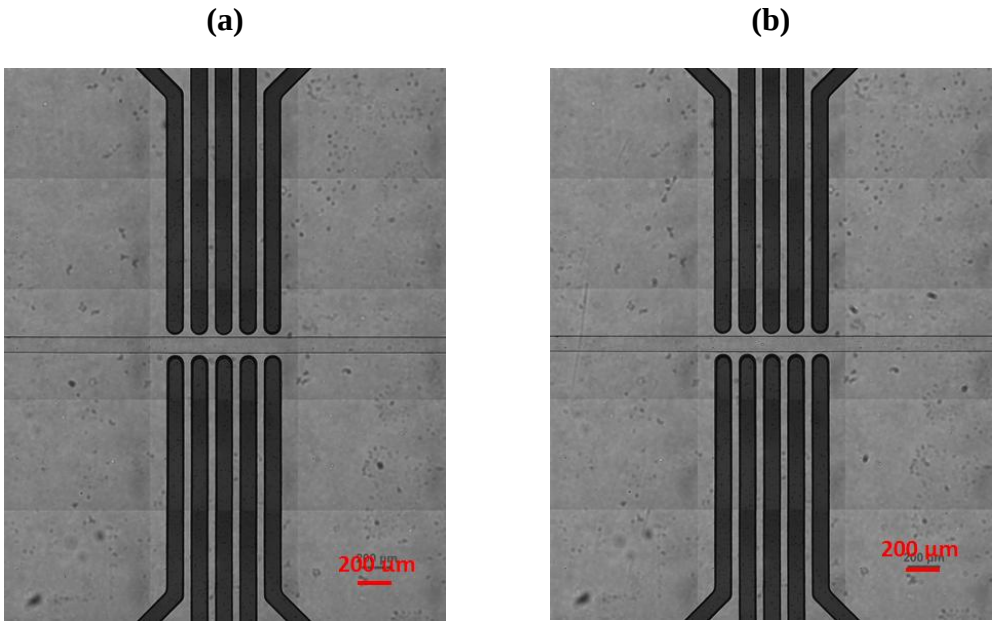

Figure 7.8 Electrodes of the proposed electroporation device under expiration testing observed under microscope. a) One of the three devices before applying the expiration test. b) Same device after the expiration test. The microscopic inspection of electrodes and electroporation region of the device before and after expiration also confirms that the electrodes remain unaffected by experimental conditions during expiration testing.

7.4 Conclusions of the Chapter

In this chapter, the removal of the PDMS sidewalls by using the wet chemical etching of the PDMS is verified. The change in the electrical conductivity between the two electrodes of the pair indicated that the PDMS sidewalls are completely removed by etching. As a result, the proposed electroporation device will require a low voltage for electroporation.

The effects of an external voltage applied to the electrodes on the cell inside the electroporation microchannel of the proposed device are modeled. This modeling revealed that the electric field and the voltage across the cell membrane of the cell inside the electroporation microchannel can be modified by applying an external voltage to the electrodes of the proposed device. It also shows that the device is capable of increasing the transmembrane potential of the cell in order to perform its electroporation. Consequently, the proposed device is able to perform the electroporation of the cells inside the electroporation microchannel.

The effects of the storage conditions on the proposed device and its electrodes are examined. The devices are found to be unaffected by aggravated storage conditions such as high temperature (100°C) and low pressure (33.86kPa) for seven days. Therefore, the proposed device and its electrodes are robust and can be stored for a long time before use under standard storage conditions such as room temperature and atmospheric pressure. In this way, this research demonstrated that the proposed electroporation device is robust and capable of performing the electroporation of the cells using the uniform electric field generated by the 3D electrodes.

CHAPTER 8

ELECTROPORATION USING THE PROPOSED DEVICE

In this chapter, the use of the proposed electroporation device with 3D electrodes to perform the electroporation of fibroblast cells is discussed. In chapter 5, the merits and demerits of the proposed device with and without PDMS sidewalls between the electrodes and microchannel as well as their fabrication is explained in detail. In this chapter, an experimental evaluation of both devices is performed first in order to determine the maximum voltage that can be applied to them during electroporation. Next electroporation of fibroblast cells using the device with PDMS sidewalls is explained in detail. The chapter is concluded by summarizing the results of the experimental evaluation of devices and the electroporation of fibroblast cells using the device with PDMS sidewalls.

8.1 Determination of Operating Voltage Limits for the Proposed Device

In a device without PDMS sidewalls between the electrodes and the electroporation microchannel, the electrodes are exposed inside the microchannel. As a result, these electrodes come in direct contact with the solution present inside the electroporation microchannel. When these electrodes are connected to the voltage, a current flows between the electrodes through the solution which causes the electrolysis of the solution [102, 103]. During the electrolysis process, when the voltage applied between the electrodes exceeds threshold, bubbles are generated inside the solution near the electrode and solution interface due to the release of hydrogen gas [102]. The formation of bubbles

during electroporation can be detrimental to the cells being electroporated [46, 104]. To prevent cell damage due to bubbles during electroporation, it is necessary to select a voltage to be applied between the electrodes of the device that is less than the threshold voltage, which results in the formation of bubbles in the solution inside the electroporation microchannel.

An experiment is performed to determine the maximum voltage that can be safely applied to the electrodes exposed inside the microchannel without creating bubbles during electroporation. This experiment is performed by using a device without PDMS sidewalls between the electrodes and the electroporation microchannel. The electroporation microchannel of the device is filled with fibroblast cell culture media. Fibroblast cell culture media is composed of a high glucose DMEM (Dulbecco's modified Eagle's medium) media, 10% (v/v) horse serum, and 1% (v/v) antibiotics (penicillin/streptomyocin).

After filling culture media inside the microchannel, the device is then fixed onto a microscope stage in order to observe the formation of bubbles in the electroporation region. The electrodes of the device are connected to a DC voltage supply. All of the electrodes on one side of the microchannel are connected to a positive terminal, whereas all of the electrodes on the other side of microchannel are connected to the negative terminal of the DC voltage source, as shown in Figure 8.1.

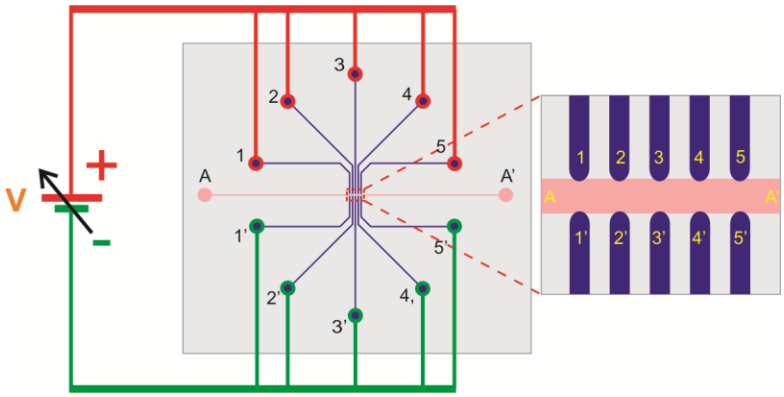

Figure 8.1 Schematic used to determine the voltage that generates bubbles inside the microchannel. The electrodes are connected to the DC voltage supply, which is varied until the formation of bubbles in solution inside the microchannel is observed under microscope.

The electroporation region of the device before applying the voltage to the electrodes is shown in Figure 8.2a. The electroporation region of the device is continuously observed under a microscope. The DC voltage applied to the electrodes is simultaneously increased from zero in steps of 0.1 V until the formation of bubbles in the solution inside the microchannel is observed under a microscope. The experiment is repeated using three identical devices to confirm the observation. The lowest voltage, at which the formation of bubbles is observed in the solution inside the microchannel, is 1.67 V. The electroporation regions, after formation of bubbles inside the microchannel by applying the voltage with a magnitude of 1.67 V between the electrodes of the device, are shown in Figure 8. 2b.

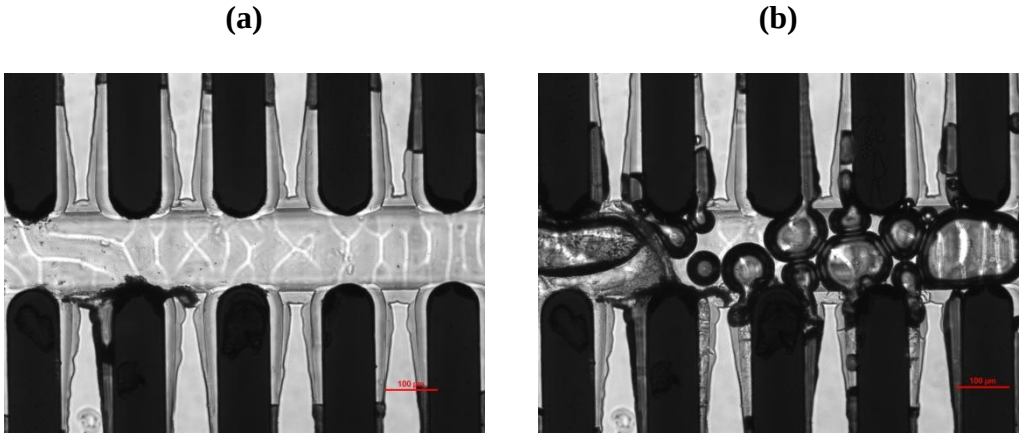

Figure 8.2 Electroporation region of the device without PDMS sidewalls under microscope. a) Device before applying the voltage to the electrodes. b) Device after applying 1.67 V to the electrodes. The formation of bubbles in solution inside the electroporation microchannel started at 1.67 V.

The result of this experiment revealed that the maximum voltage that can be applied to the electrodes of the device without PDMS sidewalls without forming bubbles in the solution inside the microchannel is 1.67 V. It is important to note that this voltage is insufficient to generate an electric field inside the microchannel for the electroporation of the cell. This indicates that the proposed device without PDMS sidewalls between the electrodes and the electroporation microchannel is not suitable for electroporation.

The electroporation device with PDMS sidewalls requires a higher voltage than the device without PDMS sidewalls. However, in a device with PDMS sidewalls between the electrodes and the electroporation microchannel, the electrodes do not make contact with the solution inside the microchannel. This prevents electrolysis, and hence the formation of bubbles in the solution inside the microchannel. The electrodes of the device with PDMS sidewalls can be connected to high voltage in order to generate an electric field for the electroporation of cells. As a result, the device with PDMS sidewalls is

desirable for electroporation as it prevents electrolysis, bubbles, and cell damage due to the exposure of cytotoxic indium ions, which is explained in detail in chapter 4.

The maximum voltage that can be connected between the electrodes of the device with PDMS sidewalls is limited by the electrical breakdown of the PDMS polymer. The electrical breakdown of cured PDMS polymer occurs when it is subjected to an electric field with an intensity above ~2 x 10^5 V/cm [105-107]. The voltage across PDMS at which breakdown occurs depends on its thickness. In the proposed device, the thickness of the PDMS sidewalls between the electrodes and the electroporation microchannel is ~15 μm. As a result, the electrical breakdown of the PDMS sidewalls of the proposed device will start at a voltage above ~300 V across each PDMS sidewall.

The maximum voltage that can be applied between the electrodes of the device with PDMS sidewalls without causing the electrical breakdown of the PDMS sidewalls is determined experimentally. In this experiment, the electroporation microchannel of the device with PDMS sidewalls is filled with fibroblast culture media since it will be used during electroporation later on. The electrodes of the device are connected to the output of the low to high voltage DC converter as shown in Figure 8.3, in order to apply high voltage (0 to 1000 V) until the breakdown of PDMS sidewalls occurs. The device before applying the voltage to the electrodes is shown in Figure 8.4a.

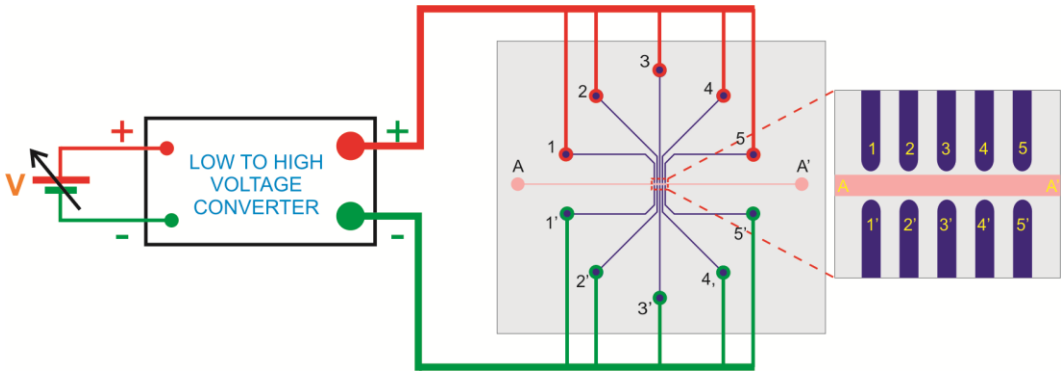

Figure 8.3 Schematic used to determine the breakdown voltage of PDMS sidewalls. The electrodes are connected to high voltage, which is varied until the breakdown of the PDMS sidewalls is observed under microscope.

The input voltage applied to the voltage converter using a DC power supply is varied from zero onward in steps of 0.1 V in order to generate high voltage for the electrodes. The electroporation region of the device is continuously observed under a microscope while gradually increasing the voltage applied to the electrodes. The electrical breakdown of PDMS sidewalls is observed under a microscope at 763 V between the electrodes of the device corresponding to 2.31 V applied by the DC power supply. The device after the breakdown of the PDMS sidewalls due to an excessive electric field across the PDMS sidewalls is shown Figure 8.4b.

The experiment is repeated with three identical devices in order to confirm the results. In addition, it is observed during the experiment that the electrical breakdown destroys the PDMS sidewalls and exposes electrodes to the solution inside the microchannel. As a result, high current flows between the electrodes due to high voltage, which causes a spark between them and destroys the microchannel in the electroporation region. The results of this experiment show that the maximum voltage that can be applied to the device with PDMS sidewalls without damaging the device is 763 V. The device with PDMS sidewalls allows application of a higher voltage (i.e. up to 763 V) than the

device without PDMS sidewalls (i.e. up to 1.67 V), and is able to generate an electric field up to 8.8 kV/cm (found using F.E.M. COMSOL 3.5a).

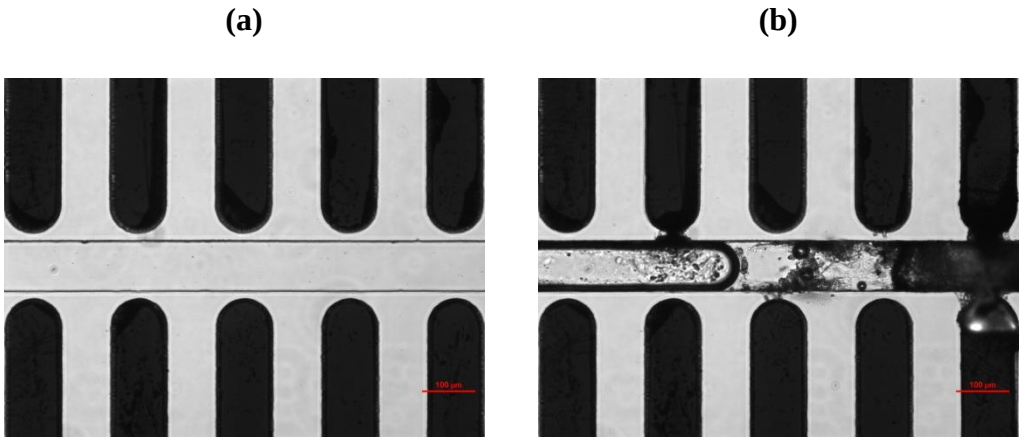

Figure 8.4 Electrical breakdown of PDMS sidewalls between electrodes and microchannel of the device. a) Device before applying the voltage to the electrodes. b) Device after the breakdown of PDMS due to application of 763 V obtained by applying 2.31 V from the DC power supply. PDMS sidewalls breakdown due to excessive electric field generated by high voltage and destroys the electrodes due to the high current flowing between them.

The ability of the device with PDMS sidewalls to withstand high voltage allows the generation of an electric field with an intensity (above 700 V/cm) necessary for the electroporation of cells. As a result, the device with PDMS sidewalls is decided to be used for the electroporation. It is also important to note that the high voltage (up to 763 V) required for the device with PDMS sidewalls is obtained from low voltage (up to 2.31 V) using the low to high voltage converter. The current flowing between the electrodes in the presence of PDMS sidewalls is zero due to the high resistivity (~10^{14} Ω.cm) of PDMS [108].

8.2 Electroporation (Lysis) of Fibroblast Cells Using Proposed Device

In this research, it is hypothesized that the uniform electric field generated by high aspect ratio 3D electrodes can be used to perform the electroporation of cells. To test this hypothesis, the electroporation of fibroblast cells is performed by using the proposed device with ~15 μm thin PDMS sidewalls between the 3D electrodes and the electroporation microchannel. This device has an array of five electrode pairs situated along the sidewalls of the microchannel. The cells in the electroporation region between the two electrodes of the electrode pair are subjected to a uniform electric field generated between the electrodes. The electric field induces the formation of pores on the cell membrane and performs the electroporation of the cells, which is explained in detail in chapter 1.

Fibroblasts are the most common cells of the connective tissue in animals and humans. Fibroblast cells synthesize the extracellular matrix, the structural framework (stroma) for tissues, and play a critical role in wound healing [109, 110]. The main function of fibroblasts is to maintain the structural integrity of connective tissues by continuously secreting precursors of the extracellular matrix. In this research, fibroblast cells are used in order to perform the electro-lysis experiments.

In this research, electroporation is performed by applying 500 V between the electrodes of the device for 1 minute. In order to prevent the destruction of the device and the cell during electroporation, the voltage used for electroporation is selected below the maximum voltage at which the PDMS sidewalls of the device breakdown. The high voltage used for electroporation is obtained by applying 1.65 V as an input to the low to high voltage converter. This is clearly in agreement with the claim of this research, which

is to fabricate a device that performs electroporation using low voltage. The use of low voltage (1.65 V) to perform electroporation satisfies the requirement for a portable device to do electroporation of cells.

8.2.1 Preparation of the Fabricated Device for Electroporation

The electroporation experiments in this research are aimed to kill selected fibroblast cells, which are present in electroporation regions of the device. The flow chart for electroporation using the proposed device is shown in Figure 8.5. DC power supply (0-3 V) is used as the electroporation power supply. In order to simplify the experiments, the same voltage is applied between all of the electrode pairs of the device. As a result, all of the electrodes on one side of the electroporation microchannel are connected to the positive terminal, and all electrodes on the other side are connected to the negative terminal of the low to high voltage converter, as indicated in step 4 of Figure 8.5.

The cleaning of the fabricated electroporation device is important in order to make it suitable for cells. The device is cleaned by using a conventional sterilization process. First, the electroporation microchannel of the device is flushed by injecting 100% ethanol solution from the inlet of the microchannel and aspirated from the outlet of the same microchannel. The complete device is then washed by spraying 70 % ethanol solution (by v/v in DI water) on it and allowing to dry in an oven at 65°C for 10 minutes. The sterilized device is transferred to the cell culture hood where it is then allowed to cool at room temperature for 5 minutes before injecting the cells into its microchannel.

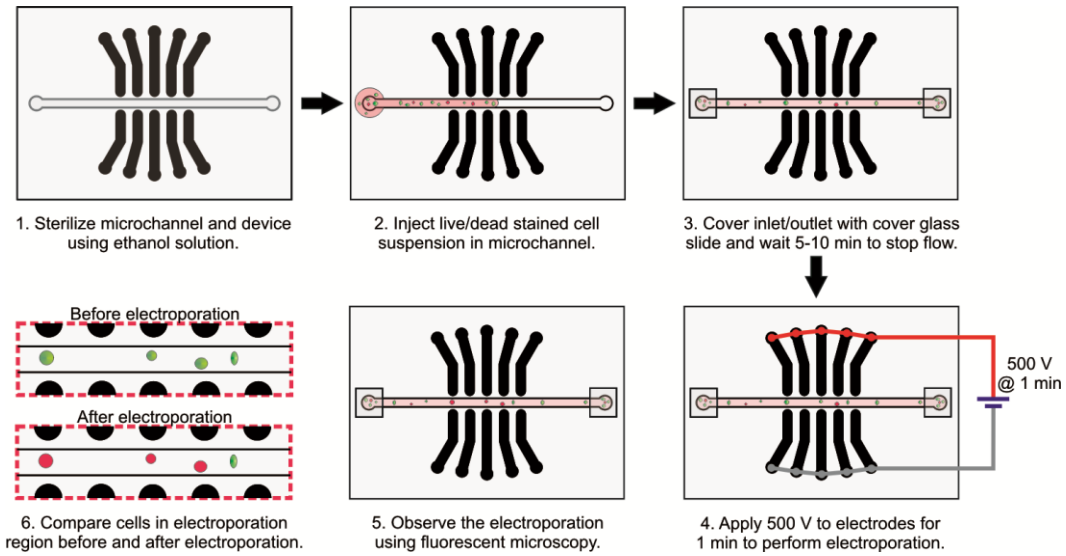

Figure 8.5 Schematic of the electroporation process using the proposed device. After the cell suspension flow in microchannel is stopped, 500 V is applied for 1 min between the electrodes. The cells in the electroporation regions are observed before and after applying electric field and compared to study the electroporation of cells.

The cell suspension with a volume of 6 µl is taken in a pipette and injected inside the electroporation microchannel through an inlet until it comes out of the outlet of the electroporation microchannel. The inlet and outlet of the electroporation microchannel are covered with a sterilized cover glass slip (5 mm x 5mm x 0.15 mm) in order to stop the flow of cell suspension in the microchannel. Covering the inlet and outlet with a glass slide not only helped in stabilizing the flow of the suspension but also prevented the evaporation of suspension during the experiment.

The device is then fixed on the microscope stage and ~5-10 minutes is allowed to pass so that the cell suspension can stop flowing inside the microchannel. Meanwhile, the electrodes of the device are connected to the output of the low to high DC voltage converter (EMCO High Voltage Corporation, model no. F121 , Sutter Creek, CA 95685). The experimental set-up showing the equipment used in electroporation using the proposed device is shown in Figure 8.6.

(a) **(b)**

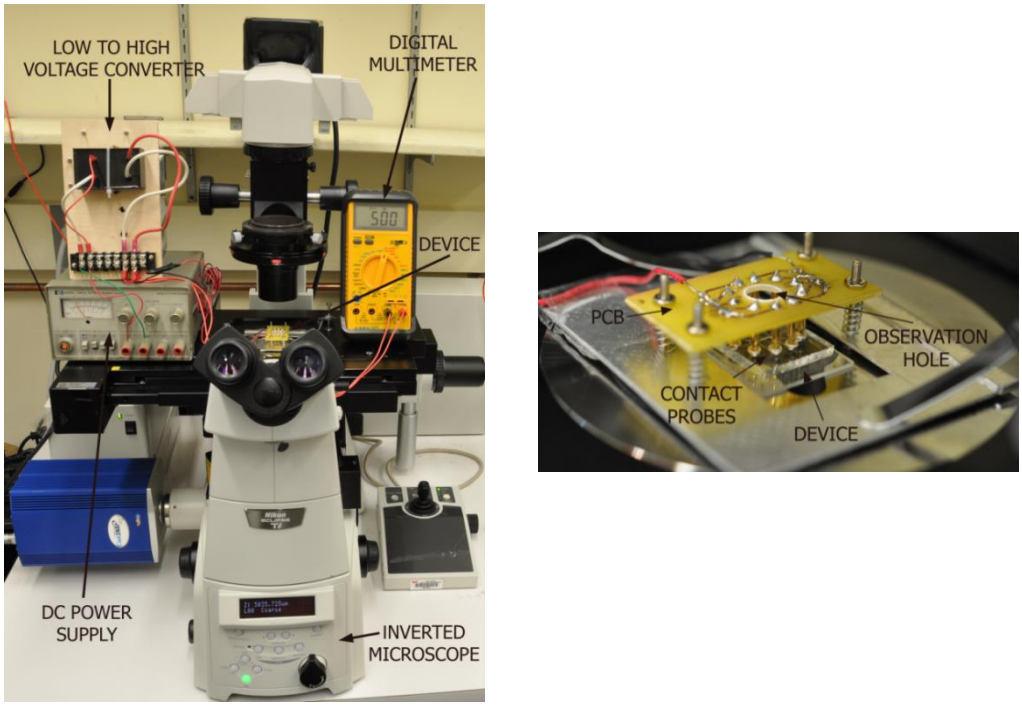

Figure 8.6 Experimental setup to perform electroporation using the proposed device. a) Complete set up b) Device on stage of microscope. After injecting cell suspension in microchannel, the device is fixed on microscope stage and its electrodes are conneted to low to high voltage converter to obtain high voltage for electroporation using low voltage DC power supply.

Once the cell flow inside the electroporation microchannel stops, time is marked as t=0 minutes and a picture of the device in electroporation region is taken using the phase contrast and the fluorescent microscope. After 5 minutes, 1.65 V is applied to the low to high voltage converter for 1 minute to generate 500 V between the electrodes of the device in order to apply an electric field for the electroporation of the cells. Phase contrast, green fluorescent protein (GFP), and Texas Red images of the electroporation regions are captured at t=0 minutes, 5 minutes (i.e. before electroporation), 6 minutes (i.e. after electroporation), 10 minutes, 15 minutes and 20 minutes. The observations of the

electroporation regions of the device before and after applying an electric field are compared to study the results of the electroporation experiments.

8.2.2 Preparation of Cell Suspension for Electroporation

The fibroblast cells used for electroporation using the fabricated device are the 3T3-J2 cell line. These fibroblasts are specific for the liver and should not be confused for the popular 3T3-NIH cell line. The fibroblast cell culture is maintained in a high glucose DMEM (Dulbecco's modified Eagle's medium) media containing 10% horse serum, and 1% antibiotics (penicillin/streptomyocin) in a 60 mm tissue culture dish. The media is changed twice a week until the observed cell population is confluent.

The determination of live and dead cells using fluorescent molecules is called the Live/Dead cell assay. The fluorescent molecule Calcein AM penetrates through the cell membrane of live cells. After entering the live cells, Calcein AM is converted to a green-fluorescent Calcein, which allows the cells to fluoresce green. As a result, the Calcein AM is used to detect the live cells during electroporation. Unlike Calcein AM, molecules of Ethidium homodimer cannot penetrate through the cell membrane of the live cells and can only enter inside the cells when the cell membrane is ruptured and the cells are dead. The dead cells fluoresce red as Ethidium homodimer binds with the DNA of the dead cells, and then emits red fluorescent light. As a result, Ethidium homodimer is used to detect the dead cells during the electroporation process.

The electroporation experiments in this research are aimed at killing the live cells present in the electroporation region. The killing of cells due to the application of an electric field during electroporation can be visualized by providing molecules of Ethidium homodimer around the cells. These molecules will enter inside the cells which

have died due to electroporation and then will cause those dead cells to fluoresce red. As a result, in order to visualize the killing of live cells due to the application of an electric field, the cells are first stained with Calcein AM and Ethidium homodimer. The stained cell suspension is then washed in order to remove the excess Calcein AM from the suspension. The cell suspension for the electroporation experiments is then prepared by mixing stained live/dead cells and a solution of Ethidium homodimer. This is done in order to make available the molecules of Ethidium homodimer around the cells for entering into the newly dead cells during electroporation. The cell suspension is prepared 30 minutes before the electroporation experiment. The flow chart of the process used to prepare the cell suspension is shown in Figure 8.7.

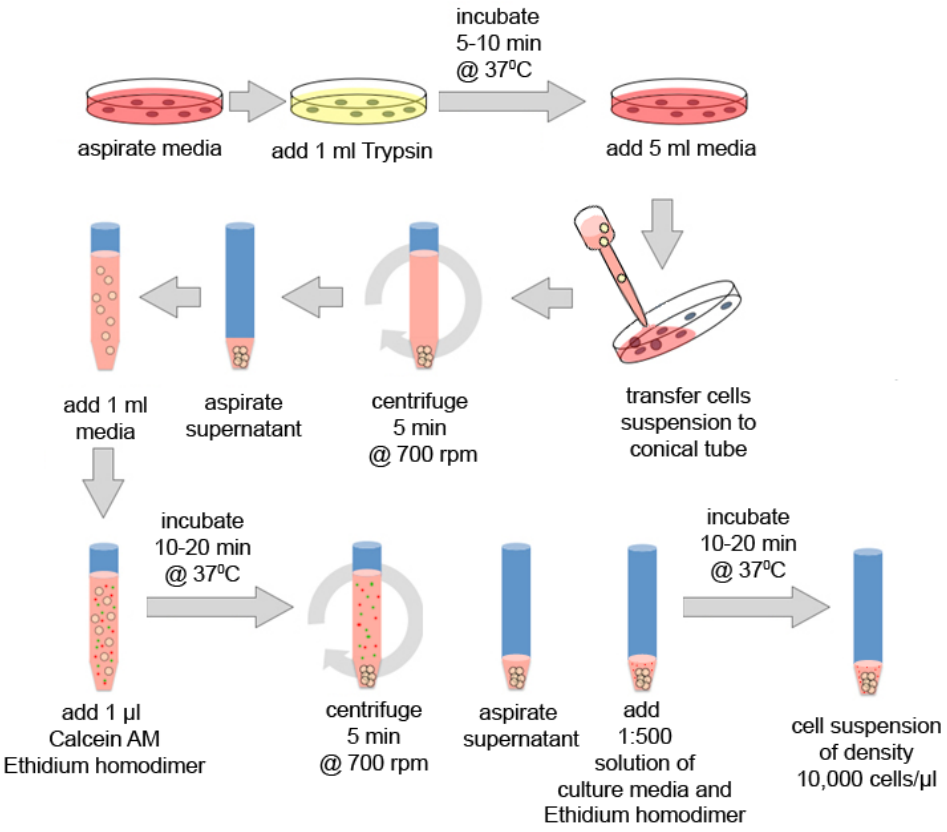

Figure 8.7 Flow chart of process used to prepare the cell suspension for electroporation. The suspension consisting of Ethidium homodimer, culture media and cells stained with Calcein AM and Ethidium homodimer is prepared with cell density ~10,000 cells / µl.

In this process the tissue culture dish, which was incubated for 3-5 days, is removed and cells are washed 2-3 times with a phosphate buffer solution in a cell culture hood after aspirating the media. The cells are detached from the bottom of the tissue culture dish by adding 1 ml of trypsin to the culture dish and incubating it at 37°C for 5-10 minutes. Then 5 ml of cell culture media is added to the culture dish and cells suspension is transferred to a conical tube and centrifuged at 700 rpm for 5 minutes. After centrifugation, the supernatant is aspirated from the conical tube and 1 ml of fresh cell culture media is added to the conical tube. The number of total cells present in the conical tube is counted by using a hemocytometer since it is necessary to prepare the cell suspension with cell density ~10,000 cells / µl.

The live and dead cells are stained in order to determine the live and dead cells before performing the electroporation experiments. In order to stain the live cells with Calcein AM and the dead cells with Ethidium homodimer fluorescent molecules, 1 µl of each Calcein AM and Ethidium homodimer is added to the cell suspension and incubated at 37°C for 10-20 minutes. The excess Calcein AM and Ethidium homodimer is then washed from the solution by centrifuging the cell suspension at 700 rpm for 5 minutes and aspirating the supernatant. The cell suspension for the electroporation experiments using the proposed electroporation device is prepared by adding 1:500 (v/v) solutions of Ethidium homodimer and cell culture media in the cell pallet.

In order to ensure that there are sufficient numbers of cells in the electroporation regions of the device during electroporation, the density of cells in cell suspension is selected as ~10,000 cells / µl. The volume of Ethidium homodimer solution added to the cell pallet is selected to obtain a cell density of ~10,000 cells / µl using the knowledge of

the total number from the hemocytometer. In this way a cell suspension in which live cells stained with Calcein AM, dead cells stained with Ethidium homodimer, and cells surrounded by additional molecules of Ethidium homodimer, is prepared for the electroporation experiment to be performed using the proposed electroporation device.

8.2.3 Electroporation of Fibroblast Cells

In order to demonstrate electroporation by using the fabricated electroporation device, the control experiment is performed to establish a reference for comparing the results of electroporation. The control experiment is performed by injecting the prepared cell suspension in the electroporation microchannel without applying voltage between the electrodes of the device. During the experiment, the cells are observed at regular intervals of 5 minutes after the cell suspension flow in the microchannel is stopped completely. The state of cells at time t=0 minutes is compared with their state at time t=5 minutes, 10 minutes, 15 minutes and 20 minutes. The results of the control experiments are shown in Figure 8.8.

The image of the electroporation regions at t=0 minutes shows the presence of live (green dots) as well as dead cells (red dots) inside the microchannel. This is common and expected since some cells die during the process of preparing the cell suspension. The images of the electroporation regions at t=5 minutes, 10 minutes, 15 minutes and 20 minutes shows that the cells which are alive at time t=0 minutes remained alive until the end of the experiment. In these images, no green dot (which represent live cell) changes from t=0 minutes to t=20 minutes indicating that no cells died during the interval of 20 minutes while the cells are in the microchannel of the device. The results of this control

experiment show that the cells remain unchanged in the microchannel of the device during the 20 minutes period. The control experiment is repeated using three identical devices in order to confirm the observation.

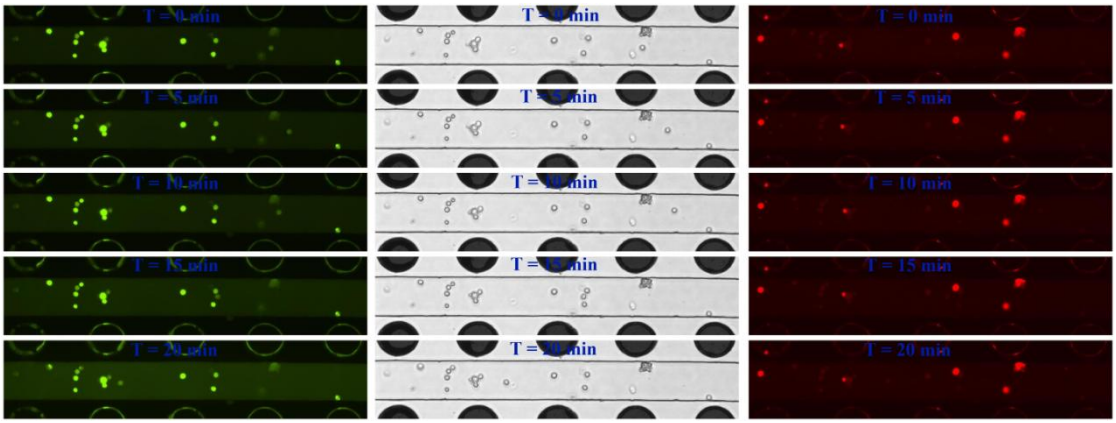

Figure 8.8 Results of control experiments. The electroporation region of the device with PDMS sidewalls is observed at t = 0 min, 5 min, 10 min, 15 min, and 20 min. fluorescent images of live cells (green), dead cells (red) and phase contrast image confirms that the cells are unchanged from t=0 min to t=20 min.

Once it is confirmed that the cells remain unchanged in the microchannel of the proposed device over a period of 20 minutes, electroporation experiments are performed. Electroporation experiments are performed by using the same setup, devices, and cell suspension used in the control experiments. Similar to the control experiments, during electroporation, the electroporation microchannel of the device is first filled with a cell suspension with a cell density of ~10,000 cells / µl. The inlet and outlet of the microchannel are covered with a glass cover slide and 5-10 minutes are allowed to pass in order to completely stop the flow of suspension in the microchannel. The recording of observations of electroporation experiments is started after confirming the stopping of flow in the microchannel, which is marked as time t=0 minutes.

The electroporation region of the device is observed at t=0 minutes using phase contrast and a fluorescent microscope in order to capture the initial state of the cells in the microchannel. The region is again observed at t=5 minutes to record the state of the cells just before applying the electric field for the electroporation of the cells. After 5 minutes (at t= 5 minutes), voltage with a magnitude of 1.65 V is applied for 1 minute to the input of the low to high voltage converter in order to generate 500 V at its output, which is connected between the electrodes of the proposed device.

The 500 V applied between the electrodes of the device generates an electric field of 5.7 kV/cm (measured using F.E.M in COMSOL 3.5a) which is higher than the threshold electric field (700 V/cm) required for the irreversible electroporation of cells [77]. The electroporation region of the device is again observed at t=6 minutes, i.e. immediately after applying electric field for the electroporation of cells. The observation is continued at t=10 minutes, 15 minutes and 20 minutes using phase contrast and a fluorescent microscope. The results of the electroporation experiments recorded at time t= 0 minutes, 5 minutes (before electroporation), 6 minutes (after electroporation), 10 minutes, 15 minutes and 20 minutes are shown in Figure 8.9.

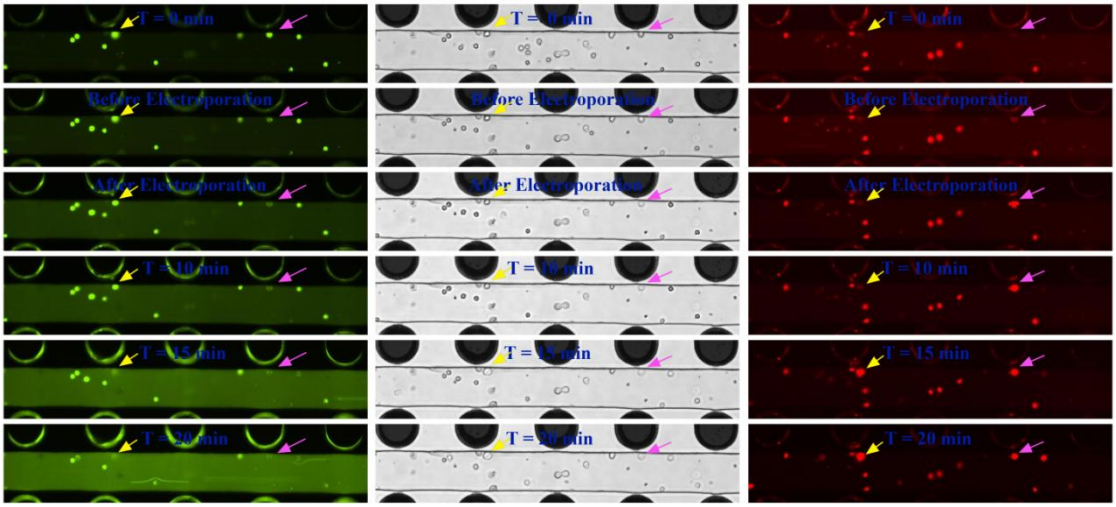

Figure 8.9 Results of electroporation experiments. The electroporation region is observed at 0 min, 5 min (before electroporation), 6 min (after electroporation), 10 min, 15 min, and 20 min. Live cells (green), dead cells (red) and phase contrast images show that the cells, indicated using yellow and pink arrows are alive at t= 0 min and completely died after electroporation at t=20 min due to applied electric field.

Figure 8.9 shows that the two cells present in the electroporation region and indicated by the yellow and pink arrows are successfully electroporated. The red dot corresponding to the cell indicated by the magenta arrow is absent before applying an electric field for electroporation and appears bright red after electroporation. The green dot associated with the same cell is present from t= 0 minutes until before electroporation indicating the cell was alive before electroporation. After electroporation, the intensity of the green dot corresponding to the same cell gradually decreases until t=20 minutes. This observation clearly indicates that the cell, pointed by the magenta arrow, was alive before electroporation and died after electroporation due to the electric field in the electroporation region.

The yellow arrow indicates the second cell, which is successfully electroporated. The presence of the green and absence of the red dot corresponding to the second cell pointed by the yellow arrow indicates that this cell was alive until t=10 minutes (i.e. until

4 minutes after electroporation). This cell is then dead at t=15 minutes which is indicated by the presence of the red dot and absence of the green dot corresponding to the cell after t= 15 minutes. The second cell dies after 4 minutes from the application of the electric field. This can be explained by the fact that the formation of pores can take from seconds to several minutes after application of the electric field [45, 111].

Other cells which are not in the electroporation regions remained unaffected, as the proposed device is designed to generate the electric field in a region other than the electroporation region, is insufficient to electroporate the cell. The electroporation results of the cells pointed to by the yellow arrow is in good agreement with the ability of the proposed electroporation device to perform the selective electroporation of cells (cells in the electroporation regions) using circular electrodes.

The results of the electroporation clearly show that the cells are dead after the application of the electric field in the electroporation region. On the other hand, the results of the control experiments revealed earlier that the cells remain unaffected in the microchannel of the device without applying voltage. A comparison between the results of the control and the electroporation experiments makes it clear that the proposed electroporation device with PDMS sidewalls has successfully killed (electroporated) selected cells in the electroporation regions without affecting the neighboring cells. The electroporation experiment is repeated using three identical devices in order to test the reproducibility of electroporation using the proposed device. The results of all three devices are found to be consistent, and are in agreement with each other, which confirmed the reproducibility of electroporation using the proposed device.

8.3 Conclusions of the Chapter

In this chapter, the operating voltage limits for the fabricated electroporation device with and without the PDMS sidewalls between the electrodes and microchannel is first determined experimentally. It is found that the device without the PDMS sidewalls is not suitable to use above 1.67 V due to the formation of bubbles in the solution inside the microchannel of the device. The device without the PDMS sidewalls is not selected to demonstrate the electroporation of cells in this research as it cannot generate a sufficient electric field for the electroporation of cells due to low limits of maximum operating voltage.

The operating voltage limits for the device with PDMS sidewalls between the electrodes and microchannel is then determined experimentally. Maximum voltage limit for the device with PDMS sidewalls is found to be 763 V, which is much larger than the device without PDMS sidewalls and is capable of generating an electric field up to 8.8 kV/cm for electroporation. As a result, the device with PDMS sidewalls is selected to demonstrate the electroporation of cells.

The electroporation of fibroblast cells filled in a microchannel of the device with PDMS sidewalls is performed by applying 500 V for 1 minute between the electrodes of the device. The control experiments are also performed using the experimental setup similar to the electroproation experiments, but without applying voltage to the device in order to obtain a reference to compare with the results of electroporation. The results of the electroporation of fibroblast cells show that the cells in the electroporation regions of the device with PDMS sidewalls are successfully electroporated (killed) due to the

applied electric field. These results prove the ability of the proposed device to perform the selective electroporation of cells (cells in the electroporation regions).

Although a high voltage of magnitude 500 V is applied to the electrodes, the proposed device performed the electroporation by actually using 1.65 V due to the use of a low to high voltage converter. The device, voltage converter, and voltage requirement to perform electroporation using the proposed device support the portability of the complete electroporation setup. In this way, this research demonstrated the selective electroporation of fibroblast cells by applying low voltage (1.65 V @ 60 mA) to the proposed device.

CHAPTER 9

CONCLUSIONS

In conclusion, this research studied the conventional microfluidic electroporation process and devices. The conventional electroporation devices use planar electrodes situated at the bottom of the electroporation microchannel. In this research, the electric field generated by the planar electrodes inside the electroporation microchannel is modeled using the Finite Elements Modeling tool COMSOL 3.5a. It is found that the planar electrodes are easy to fabricate. However, they generate a nonuniform electric field inside the electroporation microchannel. The nonuniform electric field is responsible for the low yield of electroporation using conventional microfluidic devices with planar electrodes.

This research hypothesized and later proved with the help of a simulation, that electrodes thicker than planar electrodes are capable of generating a uniform electric field inside the electroporation microchannel. As a result, this research proposes a thick electrode situated along the sidewalls of the electroporation microchannel called 3D electrode to perform the electroporation of the cells. In this research, the electric field generated by 3D electrodes with different shaped tips is simulated. It is found in simulation that the 3D electrodes with circular tips generate a uniform electric field inside the cross section of the microchannel in the selected region using low voltage.

The electric field generated by 3D electrodes is focused between two electrodes and gradually decreases away from the electrodes, which is desirable for electroporation. As a result, 3D electrodes with circular tips are considered as the optimal electrodes to generate the electric field that increases the yield of the electroporation of the cells. This

research successfully designed the microfluidic electroporation device with an array of five 3D electrode pairs to produce a uniform electric field for electroporation using low voltage.

The proposed electroporation device uses the electrodes of a height above ~50 µm. Standard silicon technologies can only fabricate a planar electrode up to a height of ~5µm. However, these techniques do not support the fabrication of 3D electrodes due to their high aspect ratio. This research hypothesizes that the injection of the molten indium can be used to fabricate high aspect ratio metallic microstructures. Based on this hypothesis, a new fabrication approach is proposed in order to fabricate the proposed electroporation device with 3D electrodes. This research developed a novel technique that can autonomously inject the molten indium inside the dead end and complex network of the interconnected microchannels without chemical processing.

To fabricate the electroporation device with 3D electrodes, the proposed fabrication process uses the Autonomous Indium Injection Method in order to inject the molten indium inside the electrode microchannels of the microfluidic device fabricated using soft-lithography. Unlike the current co-fabrication method, the Autonomous Indium Injection Method uses PDMS gas permeability and a vacuum to inject the molten indium inside the microchannel until the end.

The new fabrication method was characterized and it was found that the magnitude of the applied vacuum controls the smallest width of the microchannel that can be filled using this method. A stronger vacuum is capable of injecting the molten indium inside a narrower channel than a weaker vacuum. This suggests that the magnitude of applied vacuum control the smallest feature fabricated by Autonomous

Indium Injection Method. In this research, it is recorded that the Autonomous Indium Injection Method is capable of fabricating microstructures made of indium metal to a feature size of ~23 μm and above by applying a 16.93 kPa vacuum for 30 minutes.

This method is suitable for fabrication of high aspect ratio microstructures without using a multistep process or hazardous chemicals, and is compatible with the transparent polymer PDMS. The Autonomous Indium Injection Method is compatible with other materials such as high viscous liquid PDMS polymer. In this research, the high aspect ratio 3D electrodes embedded into microfluidic devices using the Autonomous Indium Injection Method are successfully fabricated.

In addition, this research also developed a method to fabricate masters for soft-lithography using adhesive tape. The research demonstrated the fabrication of the adhesive tape master with feature size 300 μm and above by using the adhesive tape, glass slide, scalpel, hot plate and tweezers. The adhesive tape master is used to fabricate the microfluidic devices to pattern the biological cells. The adhesive tape masters are also used in classroom education in order to provide hands-on experience to the students on the fabrication of the microfluidic devices. This technology is functional in resource limited microfluidics laboratories and research. The technology is also compatible to various users regardless of their background and knowledge of conventional cleanroom microfabrication.

In this research, the proposed devices with and without PDMS sidewalls between the electrodes and microchannel are fabricated. The device without PDMS sidewalls is fabricated from the device with PDMS sidewalls by using wet chemical etching to remove the PDMS sidewalls. The proposed devices are made of transparent polymer

PDMS and hence suitable for study of electroporation using phase contrast microscopy. PDMS is biocompatible and used in cell culture, hence the fabricated device is biocompatible and suitable to use with live cells without causing any adverse effects on them. The device without PDMS sidewalls has the ability to generate an electric field higher than the device with PDMS sidewalls using the same voltage due to prevention of loss of electric field in PDMS sidewalls. However, in spite of a high voltage requirement, the device with PDMS sidewalls is capable of preventing the direct exposure of cells to the electrodes, avoiding the contamination of cells during electroporation.

This research also modeled the effects of an external voltage applied to the electrodes of the device on the cell inside the microchannel of the proposed device. This modeling revealed that the electric field and the voltage across the cell membrane of the cell inside the microchannel can be modified by applying an external voltage to the electrodes of the proposed device. Consequently, the modeling confirmed that the proposed device is able to perform the electroporation of the cells inside the electroporation microchannel.

It is certain that the device will be exposed to storage conditions before its use for electroporation. Therefore, the effects of the storage conditions on the proposed device and its electrodes are examined. The devices are found unaffected by aggravated storage conditions such as high temperature (100°C) and low pressure (33.86kPa) for seven days. This observation confirmed that the proposed device and its electrodes are robust and can be stored for a long time before use and under standard storage conditions such as room temperature and atmospheric pressure.

This research hypothesized that a uniform electric field can be used to perform the electroporation of cells. To prove this hypothesis, the electroporation device with 3D electrodes is fabricated and the electroporation of fibroblast cells injected into the electroporation microchannel of the device is demonstrated. The device used in order to demonstrate the electroporation is selected based on the ability of the device to generate the electric field necessary for electroporation. Therefore, the maximum voltage that can be applied to the proposed device with and without PDMS sidewalls is determined.

The device without PDMS sidewalls is found unsuitable to use above 1.67 V due to the formation of bubbles in the solution inside the microchannel of the device. On the other hand, the device with PDMS sidewalls allows the application of voltage up to 763 V and is capable of generating an electric field of up to 8.8 kV/cm inside the microchannel without PDMS breakdown. As a result, the device with PDMS sidewalls is used in demonstrating electroporation of cells in this research.

The electroporation of fibroblast cells filled in the microchannel of the device is performed after the flow of cells in the microchannel is completely stopped by applying 500 V for 1 minute between the electrodes of the device. The high voltage (500 V) used for electroporation is obtained by applying a low voltage (1.65 V) to the low to high voltage converter. A reference to compare with the results of the electroporation experiments is obtained by performing control experiments using an experimental setup similar to the electroporation experiments, but without applying voltage to the device. The results of the electroporation of fibroblast cells show that the cells in the electroporation regions of the device with PDMS sidewalls are successfully electroporated (killed) due to an applied electric field. These results prove the ability of

the proposed device to perform the selective electroporation of cells (cells in electroporation regions). Although high voltage of magnitude 500 V is applied to the electrodes, the proposed device performed the electroporation by actually using 1.65 V due to use of a low to high voltage converter.

In this way, this research has demonstrated that the proposed electroporation device is robust and capable of performing the electroporation of the cells using a uniform electric field generated between the 3D electrodes. The proposed device performs the electroporation of cells using low voltage (1.65 V @ 60 mA), and is promising to maximize the yield of electroporation due to the use of a uniform electric field generated by the 3D electrodes. The fabricated electroporation device is safe, portable, and inexpensive. The device has a long storage life. In addition, the proposed fabrication method is simple, inexpensive, supports mass fabrication and is suitable to fabricate hybrid devices for Micro Total Analysis System (μTAS).

REFERENCES

[1] C. Stephen. (2006, December 20). Cell Structure: Diagram of a eukaryotic cell. Available: http://scienceaid.co.uk/biology/cell/structure.html.

[2] R. Tyzio, A. Ivanov, et al., "Membrane Potential of CA3 Hippocampal Pyramidal Cells During Postnatal Development," Journal of Neurophysiology, vol. 90, pp. 2964-2972, November 1, 2003 2003.

[3] R. Franco, C. D. Bortner, et al., "Potential Roles of Electrogenic Ion Transport and Plasma Membrane Depolarization in Apoptosis," Journal of Membrane Biology, vol. 209, pp. 43-58, 2006.

[4] D. X. Zhang, C. M. Owens, et al., "Intracellular study of electrophysiological features of primate spinothalamic tract neurons and their responses to afferent inputs," Journal of Neurophysiology, vol. 65, pp. 1554-1566, June 1, 1991 1991.

[5] S. Chaiyarit and V. Thongboonkerd, "Comparative analyses of cell disruption methods for mitochondrial isolation in high-throughput proteomics study," Anal Biochem, vol. 394, pp. 249-58, Nov 15 2009.

[6] M. Yalvac, M. Ramazanoglu, et al., "Comparison and Optimisation of Transfection of Human Dental Follicle Cells, a Novel Source of Stem Cells, with Different Chemical Methods and Electro-poration," Neurochemical Research, vol. 34, pp. 1272-1277, 2009.

[7] M. Yamada, J. Kobayashi, et al., "Millisecond treatment of cells using microfluidic devices via two-step carrier-medium exchange," Lab on a Chip, vol. 8, pp. 772-778, 2008.

[8] A. S. Waldman and B. C. Waldman, "Stable transfection of mammalian cells by syringe-mediated mechanical loading of DNA," Analytical Biochemistry, vol. 258, pp. 216-22, May 1 1998.

[9] J. K. Valley, S. Neale, et al., "Parallel single-cell light-induced electroporation and dielectrophoretic manipulation," Lab on a Chip, vol. 9, pp. 1714-1720, 2009.

[10] L. Raptis and K. L. Firth, "Electrode Assemblies Used for Electroporation of Cultured Cells," in Electroporation Protocols. vol. 423, S. Li, Ed., ed: Humana Press, 2008, pp. 61-76.

[11] Y. Huang and B. Rubinsky, "Microfabricated electroporation chip for single cell membrane permeabilization," Sensors and Actuators A: Physical, vol. 89, pp. 242-249, 2001.

[12] S. Movahed and D. Li, "Microfluidics cell electroporation," Microfluidics and Nanofluidics, pp. 1-32, 2010.

[13] F. Yamauchi, K. Kato, et al., "Spatially and temporally controlled gene transfer by electroporation into adherent cells on plasmid DNA-loaded electrodes," Nucleic Acids Research, vol. 32, p. e187, January 1, 2004 2004.

[14] H. Y. Wang and C. Lu, "Microfluidic electroporation for delivery of small molecules and genes into cells using a common DC power supply," Biotechnoly and Bioengineering, vol. 100, pp. 579-86, Jun 15 2008.

[15] Y. Okahata, S. Hachiya, et al., "The formation of stable transient pores across bilayer-coated capsule membranes by external electric fields," Journal of the Chemical Society, Chemical Communications, pp. 1377-1379, 1984.

[16] E. Neumann, S. Kakorin, et al., "Fundamentals of electroporative delivery of drugs and genes," Bioelectrochemistry and Bioenergetics, vol. 48, pp. 3-16, 1999.

[17] A. Le Saux, J.-M. Ruysschaert, et al., "Membrane Molecule Reorientation in an Electric Field Recorded by Attenuated Total Reflection Fourier-Transform Infrared Spectroscopy," Biophysical journal, vol. 80, pp. 324-330, 2001.

[18] H. He, D. C. Chang, et al., "Nonlinear current response of micro electroporation and resealing dynamics for human cancer cells," Bioelectrochemistry, vol. 72, pp. 161-168, 2008.

[19] C. Chen, J. A. Evans, et al., "Measurement of the efficiency of cell membrane electroporation using pulsed ac fields," Physics in Medicine and Biology, vol. 53, p. 4747, 2008.

[20] T. R. Gowrishankar, U. Pliquett, et al., "Dynamics of membrane sealing in transient electropermeabilization of skeletal," Annals of the New York Academy of Sciences, vol. 888, pp. 195-210, 1999.

[21] F. Aguel, K. A. Debrutn, et al., "Effects of Electroporation on the Transmembrane Potential Distribution in a Two-Dimensional Bidomain Model of Cardiac Tissue," Journal of Cardiovascular Electrophysiology, vol. 10, pp. 701-714, 1999.

[22] R. Wheeler, “A diagram of the main components of an electroporator with cuvette,” loaded, Available:http://en.wikipedia.org/wiki/File:Electroporation_Diagram.png #filelinks, 2007, December 20.

[23] M. Wang, O. Orwar, et al., "Single-cell electroporation," Analytical and Bioanalytical Chemistry, vol. 397, pp. 3235-3248, 2010.

[24] M. Khine, A. Lau, et al., "A single cell electroporation chip," Lab on a Chip, vol. 5, pp. 38-43, 2005.

[25] R. I. Mahato, A. Rolland, et al., "Cationic Lipid-Based Gene Delivery Systems: Pharmaceutical Perspectives," Pharmaceutical Research, vol. 14, pp. 853-859, 1997.

[26] S. M. Elbashir, J. Harborth, et al., "Analysis of gene function in somatic mammalian cells using small interfering RNAs," Methods, vol. 26, pp. 199-213, 2002.

[27] S. Mansouri, P. Lavigne, et al., "Chitosan-DNA nanoparticles as non-viral vectors in gene therapy: strategies to improve transfection efficacy," European Journal of Pharmaceutics and Biopharmaceutics, vol. 57, pp. 1-8, 2004.

[28] T. Niidome and L. Huang, "Gene therapy progress and prospects: nonviral vectors," Gene Therapy, vol. 9, pp. 1647-52, 2002.

[29] G. Romano, C. Pacilio, et al., "Gene transfer technology in therapy: current applications and future goals," Stem Cells, vol. 17, pp. 191-202, 1999.

[30] T. Ishii, Y. Okahata, et al., "Mechanism of cell transfection with plasmid/chitosan complexes," Biochimica et Biophysica Acta (BBA) - Biomembranes, vol. 1514, pp. 51-64, 2001.

[31] P. Palese, H. Zheng, et al., "Negative-strand RNA viruses: genetic engineering and applications," Proceedings of the National Academy of Sciences of the United States of America, vol. 93, pp. 11354-8, 1996.

[32] F. S. Wu and T. Y. Feng, "Delivery of plasmid DNA into intact plant cells by electroporation of plasmolyzed cells," Plant Cell Reports, vol. 18, pp. 381-386, 1999.

[33] S. L. Van Wert and J. A. Saunders, "Electrofusion and electroporation of plants," Plant Physiology, vol. 99, pp. 365-7, Jun 1992.

[34] L. Frelin, A. Brass, et al., "Electroporation: a promising method for the nonviral delivery of DNA vaccines in," Drug News Perspect, vol. 23, pp. 647-53, 2010.

[35] S. B. Dev, D. P. Rabussay, et al., "Medical applications of electroporation," Plasma Science, IEEE Transactions on, vol. 28, pp. 206-223, 2000.

[36] M. Belehradek, C. Domenge, et al., "Electrochemotherapy, a new antitumor treatment. First clinical phase I-II trial," Cancer, vol. 72, pp. 3694-3700, 1993.

[37] M. Marty, G. Sersa, et al., "Electrochemotherapy – An easy, highly effective and safe treatment of cutaneous and subcutaneous metastases: Results of ESOPE (European Standard Operating Procedures of Electrochemotherapy) study," European Journal of Cancer Supplements, vol. 4, pp. 3-13, 2006.

[38] A. Gothelf, L. M. Mir, et al., "Electrochemotherapy: results of cancer treatment using enhanced delivery of bleomycin by electroporation," Cancer Treatment Reviews, vol. 29, pp. 371-387, 2003.

[39] K. Huang and J. Wang, "Designs of pulsed electric fields treatment chambers for liquid foods pasteurization process: A review," Journal of Food Engineering, vol. 95, pp. 227-239, 2009.

[40] M. Selbach, B. Schwanhausser, et al., "Widespread changes in protein synthesis induced by microRNAs," Nature, vol. 455, pp. 58-63, 2008.

[41] (December 20). Electroporation Cuvettes. Available: http://www.midsci.com/lp/Electroporation_cuvettes.html.

[42] T. Y. Tsong, "Electroporation of cell membranes," Biophysical journal, vol. 60, pp. 297-306, 1991.

[43] J. A. Nickoloff, "Electroporation," in eLS, ed: John Wiley & Sons, Ltd, 2001.

[44] J. A. Nickoloff, Electroporation Protocols for Microorganisms, 1 ed. vol. 47: Springer-Verlag New York, LLC.

[45] J. Gehl, "Electroporation: theory and methods, perspectives for drug delivery, gene therapy and research," Acta Physiologica Scandinavica, vol. 177, pp. 437-447, 2003.

[46] M. B. Fox, D. C. Esveld, et al., "Electroporation of cells in microfluidic devices: A review," Analytical and Bioanalytical Chemistry, vol. 385, pp. 474-485, 2006.

[47] M. Khine, A. Lau, et al., "A single-cell electroporation device with integrated perfusion channels for efficient intracellular delivery," in Microtechnology in Medicine and Biology, 2005. 3rd IEEE/EMBS Special Topic Conference on, 2005, pp. 225-228.

[48] G. D. Troszak and B. Rubinsky, "A primary current distribution model of a novel micro-electroporation channel configuration," Biomedical Microdevices: BioMEMS and Biomedical Nanotechnology, vol. 12, 2010.

[49] J. A. Kim, K. Cho, et al., "A novel electroporation method using a capillary and wire-type electrode," Biosensors and Bioelectronics, vol. 23, pp. 1353-60, Apr 15 2008.

[50] W. G. Lee, U. Demirci, et al., "Microscale electroporation: challenges and perspectives for clinical applications," Integrative biology (Camb), vol. 1, pp. 242-51, Mar 2009.

[51] Y. Huang and B. Rubinsky, "Flow-through micro-electroporation chip for high efficiency single-cell genetic manipulation," Sensors and Actuators A: Physical, vol. 104, pp. 205-212, 2003.

[52] H.-Y. Wang, A. K. Bhunia, et al., "A microfluidic flow-through device for high throughput electrical lysis of bacterial cells based on continuous dc voltage," Biosensors and Bioelectronics, vol. 22, pp. 582-588, 2006.

[53] S. Vassanelli, L. Bandiera, et al., "Space and time-resolved gene expression experiments on cultured mammalian cells by a single-cell electroporation microarray," New Biotechnology, vol. 25, pp. 55-67, Jun 2008.

[54] H. Song, J. D. Tice, et al., "A microfluidic system for controlling reaction networks in time," Angewandte Chemie International Edition in English, vol. 42, pp. 768-72, 2003.

[55] D. J. Beebe, G. A. Mensing, et al., "Physics and applications of microfluidics in biology," Annual Review of Biomedical Engineering, vol. 4, pp. 261-286, 2002.

[56] S. K. Sia and G. M. Whitesides, "Microfluidic devices fabricated in Poly(dimethylsiloxane) for biological studies," Electrophoresis, vol. 24, pp. 3563-3576, 2003.

[57] R. M. McCormick, R. J. Nelson, et al., "Microchannel Electrophoretic Separations of DNA in Injection-Molded Plastic Substrates," Analytical Chemistry, vol. 69, pp. 2626-2630, 1997.

[58] J. S. Mellors, K. Jorabchi, et al., "Integrated Microfluidic Device for Automated Single Cell Analysis Using Electrophoretic Separation and Electrospray Ionization Mass Spectrometry," Analytical Chemistry, vol. 82, pp. 967-973, 2010.

[59] J. Gao, X.-F. Yin, et al., "Integration of single cell injection, cell lysis, separation and detection of intracellular constituents on a microfluidic chip," Lab on a Chip, vol. 4, pp. 47-52, 2004.

[60] H. Park, D. Kim, et al., "Single-cell manipulation on microfluidic chip by dielectrophoretic actuation and impedance detection," Sensors and Actuators B: Chemical, vol. 150, pp. 167-173, 2010.

[61] X. B. Wang, Y. Huang, et al., "Dielectrophoretic manipulation of cells with spiral electrodes," Biophysical journal, vol. 72, pp. 1887-1899, 1997.

[62] T. B. Jones, "Basic theory of dielectrophoresis and electrorotation," Engineering in Medicine and Biology Magazine, IEEE, vol. 22, pp. 33-42, 2003.

[63] H. He, D. C. Chang, et al., "Using a micro electroporation chip to determine the optimal physical parameters in the uptake of biomolecules in HeLa cells," Bioelectrochemistry, vol. 70, pp. 363-368, 2007.

[64] K. Y. Lu, A. M. Wo, et al., "Three dimensional electrode array for cell lysis via electroporation," Biosensors and Bioelectronics, vol. 22, pp. 568-574, 2006.

[65] V. P. Nikolski, A. T. Sambelashvili, et al., "Effects of electroporation on optically recorded transmembrane potential responses to high-intensity electrical shocks," American Journal of Physiology - Heart and Circulatory Physiology, vol. 286, pp. H412-H418, January 1, 2004 2004.

[66] Y. Xia and G. M. Whitesides, "Soft lithography," Annual Review of Materials Science, vol. 28, pp. 153-184, 1998.

[67] O. Larsson, O. Ohman, et al., "Silicon based replication technology of 3D-microstructures by conventional CD-injection molding techniques," in Solid State Sensors and Actuators, 1997. TRANSDUCERS '97 Chicago., 1997 International Conference on, 1997, pp. 1415-1418 vol.2.

[68] A. C. Siegel, D. A. Bruzewicz, et al., "Microsolidics: Fabrication of three-dimensional metallic microstructures in poly(dimethylsiloxane)," Advanced Materials, vol. 19, pp. 727-733, 2007.

[69] E. Lennon, V. Senez, et al., "Integration of three-dimensional microelectrodes in microfluidic biochip for electric field based processing of biological species: Application to electrical impedance spectroscopy," Seoul, 2005, pp. 1724-1727.

[70] E. T. Jordan, M. Collins, et al., "Optimizing electroporation conditions in primary and other difficult-to-transfect cells," J Biomol Tech, vol. 19, pp. 328-34, Dec 2008.

[71] R. A. Rae Jl Fau - Levis and R. A. Levis, "Single-cell electroporation," Pflugers Arch, vol. 443, pp. 664-70, 2002.

[72] M. Wallace, B. Evans, et al., "Tolerability of Two Sequential Electroporation Treatments Using MedPulser DNA Delivery System (DDS) in Healthy Adults," Mol Ther, vol. 17, pp. 922-928, 2009.

[73] H. Lu, M. A. Schmidt, et al., "A microfluidic electroporation device for cell lysis," Lab on a Chip - Miniaturisation for Chemistry and Biology, vol. 5, pp. 23-29, 2005.

[74] A. C. Siegel, S. K. Y. Tang, et al., "Cofabrication: A strategy for building multicomponent microsystems," Accounts of Chemical Research, vol. 43, pp. 518-528, 2010.

[75] A. C. Siegel, S. S. Shevkoplyas, et al., "Cofabrication of electromagnets and microfluidic systems in poly(dimethylsiloxane)," Angewandte Chemie - International Edition, vol. 45, pp. 6877-6882, 2006.

[76] J.-W. Wang, M.-H. Wang, et al., "Effects of electrode geometry and cell location on single-cell impedance measurement," Biosensors and Bioelectronics, vol. 25, pp. 1271-1276, 2010.

[77] R. V. Davalos, I. L. Mir, et al., "Tissue ablation with irreversible electroporation," Ann Biomed Eng, vol. 33, pp. 223-31, Feb 2005.

[78] G. Liu, Y. Tian, et al., "Fabrication of high-aspect-ratio microstructures using SU8 photoresist," Microsystem Technologies, vol. 11, pp. 343-346, 2005.

[79] A. d. Campo and C. Greiner, "SU-8: a photoresist for high-aspect-ratio and 3D submicron lithography," Journal of Micromechanics and Microengineering, vol. 17, p. R81, 2007.

[80] N. Grassie and I. G. Macfarlane, "The thermal degradation of polysiloxanes—I. Poly(dimethylsiloxane)," European Polymer Journal, vol. 14, pp. 875-884, 1978.

[81] P. Gondi, R. Montanari, et al., "X-ray characterization of indium during melting," Advances in Space Research, vol. 29, pp. 521-525, 2002.

[82] H. P. Schwan, S. Takashima, et al., "Electrical Properties of Phospholipid Vesicles," Biophysical Journal, vol. 10, pp. 1102-1119, 1970.

[83] Y. Huang, X. B. Wang, et al., "Introducing dielectrophoresis as a new force field for field-flow fractionation," Biophys J, vol. 73, pp. 1118-29, Aug 1997.

[84] M. T. Chen, C. Jiang, et al., "Two-dimensional nanosecond electric field mapping based on cell electropermeabilization," PMC Biophys, vol. 2, p. 9, 2009.

[85] M. Zahn, Electromagnetic Field Theory: A Problem Solving Approach: Malabar, FL: Krieger Publishing Company, 2003.

[86] D. Gerlach, N. Alleborn, et al., "Numerical simulations of pulsed electric fields for food preservation: A review," Innovative Food Science & Emerging Technologies, vol. 9, pp. 408-417, 2008.

[87] B. Balakrisnan, S. Patil, et al., "Patterning PDMS using a combination of wet and dry etching," Journal of Micromechanics and Microengineering, vol. 19, p. 047002, 2009.

[88] S. Takayama, E. Ostuni, et al., "Topographical Micropatterning of Poly(dimethylsiloxane) Using Laminar Flows of Liquids in Capillaries," Advanced Materials, vol. 13, pp. 570-574, 2001.

[89] D. White, "The surface tensions of indium and cadmium," Metallurgical and Materials Transactions B, vol. 3, pp. 1933-1936, 1972.

[90] J. A. Caskey and W. B. Barlage, "Experimental Evidence that Water Has No Time-Dependent Dynamic Surface Tension," Industrial & Engineering Chemistry Fundamentals, vol. 9, pp. 495-497, 1970/08/01 1970.

[91] M. Sadrzadeh, K. Shahidi, et al., "Synthesis and gas permeation properties of a single layer PDMS membrane," Journal of Applied Polymer Science, vol. 117, pp. 33-48, 2010.

[92] M. Bauer, G. Su, et al., "3D microchannel co-culture: method and biological validation," Integrative Biology, vol. 2, pp. 371-378, 2010.

[93] D. S. Kim, K.-C. Lee, et al., "Micro-channel filling flow considering surface tension effect," Journal of Micromechanics and Microengineering, vol. 12, p. 236, 2002.

[94] N. Ichikawa, K. Hosokawa, et al., "Interface motion of capillary-driven flow in rectangular microchannel," Journal of Colloid and Interface Science, vol. 280, pp. 155-164, 2004.

[95] L. Li, M. A. Karymov, et al., "Dead-End Filling of SlipChip Evaluated Theoretically and Experimentally as a Function of the Surface Chemistry and the Gap Size between the Plates for Lubricated and Dry SlipChips," Langmuir, vol. 26, pp. 12465-12471, 2010/07/20 2010.

[96] G. Hetsroni, A. Mosyak, et al., "Fluid flow in micro-channels," International Journal of Heat and Mass Transfer, vol. 48, pp. 1982-1998, 2005.

[97] I. Meny, N. Burais, et al., "Finite Element Modeling of Cell Exposed To Harmonic and Transient Electric Fields," in Electromagnetic Field Computation, 2006 12th Biennial IEEE Conference on, 2006, pp. 310-310.

[98] T. Sun, N. G. Green, et al., "Analytical and numerical modeling methods for impedance analysis of single cells on-chip," Nano, vol. 3, pp. 55-63, 2008.

[99] B. Mossop, R. Barr, et al., "Electric Fields around and within Single Cells during Electroporation—A Model Study," Annals of Biomedical Engineering, vol. 35, pp. 1264-1275, 2007/07/01 2007.

[100] C. H. Johnson, Y. Nakaoka, et al., "The effects of altering extracellular potassium ion concentration on the membrane potential and circadian clock of Paramecium bursaria," Journal of Experimental Biology, vol. 197, pp. 295-308, December 1, 1994 1994.

[101] B. Valič, M. Golzio, et al., "Effect of electric field induced transmembrane potential on spheroidal cells: theory and experiment," European Biophysics Journal, vol. 32, pp. 519-528, 2003.

[102] R. Ziv, Y. Steinhardt, et al., "Micro-electroporation of mesenchymal stem cells with alternating electrical current pulses," Biomedical Microdevices, vol. 11, pp. 95-101, 2009.

[103] S.-H. Yoon, J. Chang, et al., "A biological breadboard platform for cell adhesion and detachment studies," Lab on a Chip, vol. 11, pp. 3555-3562, 2011.

[104] S. Wang, X. Zhang, et al., "Semicontinuous Flow Electroporation Chip for High-Throughput Transfection on Mammalian Cells," Analytical Chemistry, vol. 81, pp. 4414-4421, 2009/06/01 2009.

[105] J. C. McDonald and G. M. Whitesides, "Poly(dimethylsiloxane) as a Material for Fabricating Microfluidic Devices," Accounts of Chemical Research, vol. 35, pp. 491-499, 2002/07/01 2002.

[106] L. L. Yeshaiahu Fainman, Demetri Psaltis, Changhuei Yang, Optofluidics: Fundamentals, Devices, and Applications, 01 ed.: McGraw-Hill Prof Med/Tech, 2009.

[107] J.-T. Feng and Y.-P. Zhao, "Experimental observation of electrical instability of droplets on dielectric layer," Journal of Physics D: Applied Physics, vol. 41, p. 052004, 2008.

[108] W. J. Xu, M. Kranz, et al., "Micropatternable elastic electrets based on a PDMS/carbon nanotube composite," Journal of Micromechanics and Microengineering, vol. 20, p. 104003, 2010.

[109] G. Tettamanti, A. Grimaldi, et al., "The multifunctional role of fibroblasts during wound healing in Hirudo medicinalis (Annelida, Hirudinea)," Biol Cell, vol. 96, pp. 443-55, Aug 2004.

[110] S. McDougall, J. Dallon, et al., "Fibroblast migration and collagen deposition during dermal wound healing: mathematical modelling and clinical implications," Philosophical Transactions of the Royal Society A: Mathematical, Physical and Engineering Sciences, vol. 364, pp. 1385-1405, June 15, 2006 2006.

[111] J. C. Weaver and Y. A. Chizmadzhev, "Theory of electroporation: A review," Bioelectrochemistry and Bioenergetics, vol. 41, pp. 135-160, 1996.